Spring 1-1-2020

Identification of Motion Controllers In Human Standing And Walking

Huawei Wang
Cleveland State University

IDENTIFICATION OF MOTION CONTROLLERS IN HUMAN STANDING AND WALKING

HUAWEI WANG

Master of Science in Aeronautical Engineering

Beihang University

January 2015

Bachelor of Science in Aeronautical Engineering

Civil Aviation University of China

June 2012

Submitted in partial fulfillment of requirement for the degree

DOCTOR OF PHILOSOPHY IN MECHANICAL ENGINEERING

at

CLEVELAND STATE UNIVERSITY

MAY 2020

We hereby approve the dissertation of
HUAWEI WANG
Candidate for the Doctor of Philosophy in Engineering degree.

This dissertation has been approved for the specialization of
Mechanical Engineering, Ph.D.
and CLEVELAND STATE UNIVERSITY'S
College of Graduate Studies by

Dr. Antonie van den Bogert
Committee Chairperson
Department of Mechanical Engineering

Dr. Anne Su
Committee Member
Department of Health Sciences

Dr. Hanz Richter
Committee Member
Department of Mechanical Engineering

Dr. Dan Simon
Committee Member
Department of the Electrical Engineering

Dr. Eric Schearer
Committee Member
Department of Mechanical Engineering

April 10, 2020
Student's Date of Defense

This student has fulfilled all requirements for the Doctor of Philosophy in Engineering degree.

Chandra Kothapalli, Doctoral Program Director

ACKNOWLEDGMENTS

There are many many people that I want to thank for their priceless help through out my doctoral study and life in Cleveland. First of all, I would like to thank my advisor, Dr. Ton van den Bogert, for giving me the opportunity to get into this interesting research field. Thank you for your patience and trust to allow me exploring different research topics and at the same time consistently providing insightful discussions. Over the past four and half years, with the knowledge and social graces that learned from you, I am truly ready and confident to handle future challenges.

I also would like to thank my committee members: Dr. Hanz Richter, Dr. Dan Simon, Dr. Eric Schearer, and Dr. Anne Su, for providing me valuable comments. Thank you for making this dissertation in a good shape.

This dissertation study was supported by National Science Foundation under Grant No.1344954 and 1544702. I would like to thank both of them for providing me with the necessary funding to finish this research. I also want to say thanks to the Parker Hannifin Corporation for loaning the Indego to us and to Ryan Farris and Skyler Dalley for helping us in all of our questions regarding the Indego.

This research is based on the fundamental work that was conducted by Dr. Jason Moore when he was doing postdoc in the Human Motion & Control Lab. He also developed and contributed to several useful toolboxes. Without his efforts in this field, this research would be very hard to come out as it is now.

Without doubt, I should thank the amazing lab-mates for making the graduate school so much fun: Sandy, Anne, Hala, Farzad, Roemer, Nicole, Farbod, Milad, Dana, Sai, and Micheal. Thank you all for including me in those fun stuffs.

I also would like to thank the center of human machine system (CHMS) for providing me a warm space to study. Thank all the faculty and student members for forming a united and diverse group. I will miss you all and will surely visit back sometime.

Great thanks to my family (my parents, my sister, and my brother) who always be

supportive to the dreams that I want to catch. I am very lucky to be one unit of it.

My wife, Jing, played an important role in finishing this degree. Thank you for coming with me to a foreign country which is on the other side of the earth. In this four and half years, you also found your interests and started your career. I am proud of you! Credits should be given to our puppy 'Q' also, who made the home isolation and the dissertation writing less suffering.

At the end, I would like to thank myself for making the right choice to study abroad in four and half years ago. You did a good job and keep it up!

IDENTIFICATION OF MOTION CONTROLLERS IN

HUMAN STANDING AND WALKING

HUAWEI WANG

ABSTRACT

The method of trajectory optimization with direct collocation has the potential to extract generalized and realistic motion controllers from long duration movement data without requiring extensive measurement equipment. Knowing motion controllers not only can improve clinic assessments on locomotor disabilities, but also can inspire the control of powered exoskeletons and prostheses for better performance. Three aims were included in this dissertation.

Aim 1 was to apply and validate the trajectory optimization for identification of the postural controllers in standing balance. The trajectory optimization approach was first validated on the simulated standing balance data and demonstrated that it can extract the correct postural control parameters. Then, six types of postural feedback controllers, from simple linear to complex nonlinear, were identified on six young adults' motion data that was collected in a standing balance experiment. Results indicated that nonlinear controllers with multiple time delay paths can best explain their balance motions. A stochastic trajectory optimization approach was proposed that can help finding practically stable controllers in the identification process.

Aim 2 focused on the foot placement control in walking. Foot placement controllers were successfully identified through the trajectory optimization method on nine young adults' perturbed walking motions. It was shown that a linear controller with pelvis position and velocity feedback, suggested by the linear inverted pendulum model, was not sufficient to explain their foot placement among multiple walking speeds. Nonlinear controllers or more feedback signals, such as pelvis acceleration, are needed. Foot placement control was applied on a powered leg exoskeleton to control its legs' swing motion. Two healthy participants were able to achieve stable walking with the controlled exoskeleton.

Results suggested that the foot placement controller helped decelerate the swing motion at late swing.

In Aim 3, the trajectory optimization method was used to identify joint impedance properties in walking. Results of the synthetic study showed that relatively close impedance parameters can be identified. Then, a preliminary study was done to identify the ankle joint impedance properties of two participants at two walking speeds. The identified impedance properties were close to previous studies and consistent between different participants and walking speeds.

TABLE OF CONTENTS

LIST OF TABLES

LIST OF FIGURES

CHAPTER I

INTRODUCTION

Locomotor disabilities can be caused by spinal cord injury (SCI), stroke, and lower limb loss. In just the United States, about 17,730 new SCI cases, 795,000 new stroke cases, and 185,000 new lower extremity amputations occur each year. [1–3]. People with disabilities in locomotion have difficulties moving from one place to another which has largely limited their community participation and reduced the quality of their life. Powered exoskeletons [4–7] and prosthetic/orthotics (P/O) devices [8–12] have been designed and developed in the past several decades that intend to help these individuals regain the abilities to stand up, walk, and even run, as illustrated in Figure 1. Unlike passive devices, powered devices can offer more assistance in locomotion so that better motion patterns can be generated which provide a more comfortable wearing experience. It has been established that powered prostheses can reduce the metabolic cost of amputees which as a result encouraged them walk longer distances and reach a wider community[13].

Powered exoskeletons and P/O devices share similar design ideas in which electrical motors are used to replace or assist the lost/nonfunctional joints. Even though the hardware design has become compact and elegant, the performance of current devices requires improvement. For instance, the motion of current exoskeletons is often jerky, and crutches are always needed to keep balance. The performance of current P/O devices largely depends on the experience of clinicians to manually tune the control parameters through many trials

Figure 1: Currently existing powered exoskeletons and P/O devices: a. Mina v2 (ihmc); b. C-Leg (Ottobock); c. Bionic Leg (MIT); d. ReWalk Personal 6.0 (ReWalk) e. Prosthetic Leg (Standford); f. ReStore™ Soft Exo-Suit (ReWalk); g. PHOENIX Medical Exoskeleton (SuitX); h. Open-source Bionic Leg (UMich); i. Indego (Parker Hannifin); j. REX (RexBionics).

of walking tests [14]. These unpleasant facts are mainly caused by the control algorithms that are currently used in these devices. For example, powered exoskeletons commonly use fixed reference trajectories for each joint which lack the ability to react to walking pattern changes and external perturbations [4–6]. Quasi-stiffness of lower limb joints in healthy humans' locomotion is typically used as the starting point to tune the prostheses controller, which are usually far from the the actual suitable parameters [10].

While improving the performance of exoskeletons and P/O devices through the improvements in control theory or researchers' experience has led to limited advances, a more promising approach is to better understand how healthy humans control their motions. Exoskeletons and P/O devices are normally designed with similar structure and shape as human limbs; therefore, control information learned from healthy humans' movement can be used or can provide a good reference for these devices to mimic the behavior of healthy humans. In general, it is good for people with locomotor disabilities to move like healthy humans because they can participate more actively in their community without drawing

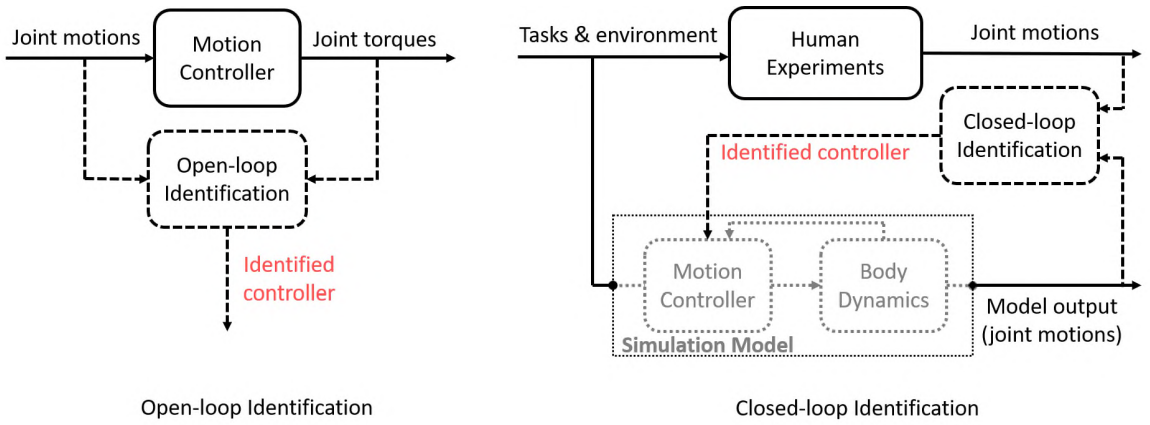

Figure 2: Open-loop and closed loop controller identification approaches.

attention to their disability.

Studies have extracted the motion controllers of healthy humans in different activities, e.g. standing balance, walking, and running [10, 15–20]. These controllers were identified from movement data that mathematically mapped the motion control process. In general, two main approaches have been used to identify motion controllers: open-loop (direct) identification and closed loop (indirect) identification (Figure 2).

In the open-loop identification approach, only the controller input and output are used to identify the control parameters [18–20]. This ignores the closed loop connection between the controller and the plant. Thus, the identified controller might be the inverse of the plant dynamics, instead of the motion controllers. Studies on synthetic data have shown that the direct identification can cause bias in identifying the postural controllers of human standing balance, while the closed loop identification can provide correct results [21, 22]. In the closed loop identification approach, a simulation model is needed to represent the closed loop system. In the motion controller identifications, the simulation model contains a dynamic model of the human body and a motion controller. The motion controller is optimized such that the simulated closed loop system generates the motion that most closely resembles that of human subjects. The optimized motion controller is assumed to be the controller that the human subjects used in their movements.

The closed loop identification approach has been used in both frequency and time do-

mains. In frequency domain, non-parametric motion controllers are usually identified, which are described as frequency response functions (FRF) [17, 23, 24]. The process of frequency domain identification is finding the FRF of the simulation model, including plant dynamics and motion controller, that best fit the FRF of experimental data. Because the length of data does not matter when transferring to the FRF through the Fourier transform [25], this approach can be easily applied on long duration movement data. In general, longer duration movement data can provide more information which helps identify generalized motion controllers. In addition, random external perturbations can be applied as stimuli to trigger motion controllers in a more varied environment, which helps extract even more generalized controllers. However, the frequency identification method treats identifying systems as linear systems and therefore fails to identify nonlinear properties. Human locomotion includes many nonlinear components, e.g. the multi-segments body dynamics and the nonlinear property of muscles. Even for standing balance, a very simple human movement, studies have shown that we use nonlinear postural feedback controllers to maintain balance [15, 26]. Therefore, a method that can identify the nonlinear properties of human movements is needed.

Parametric controller identification is usually done in the time domain. The goal is to find appropriate control parameters in a predefined control structure that can best explain the movement data through the closed loop simulation model [15, 27, 28]. In this case, the controller identification problems can be solved through trajectory optimizations. Since it is in time domain, both the plant dynamics and the motion controller can be nonlinear since linearization is not required. However, motion controllers have only been identified from short duration movement data [15, 28]. This is a consequence of the shooting method that was used in previous studies, which isn't efficient in long duration forward simulations, especially for human movements [29]. Direct collocation has recently become popular in human movement studies, such as optimal control and predictive simulation problems, due to its efficiency in trajectory optimization [30, 31]. However, to our knowledge, it has not

been used in human motion controller identification.

In summary, current methods for human motion controller identification can only extract linear controllers from long duration movement data or complex controllers from short duration movement data. In this dissertation work, we propose that trajectory optimization combined with direct collocation [22, 32] can identify complex (nonlinear) controllers from long duration motion data. With this method, motion controllers, including postural controllers, step strategy controllers, and impedance controllers, for human standing balance and walking can be identified.

1.1 Research Goals

The following research goals are proposed:

Aim 1: Identify postural feedback controllers for human standing balance.
This work shows that trajectory optimization with direct collocation can identify complex (nonlinear) motion controllers from long duration movement data. Linear postural controllers have been identified from human standing balance data with small or short duration of external perturbations [15–17, 27]. However, they are not suitable for using in powered exoskeletons and P/O devices, since large and long duration external perturbations are common in everyday life, e.g. standing in a moving bus or facing strong wind on a stormy day. Identifying complex postural controllers from standing balance data that includes large and long duration random perturbations better informs the controller design for exoskeletons and P/O devices. In this aim, standing balance experiments were first conducted to collect healthy young adults' standing balance movement data under random square pulse perturbations. Different types of postural feedback controllers, from simple linear to complex nonlinear, were then identified from the measured data. In addition, stochastic trajectory optimization was developed to help identify practically stable motion controllers.

Aim 2: Identify foot placement controllers for human walking.

In this aim, foot placement controllers were identified from perturbed walking data. Walking is a highly nonlinear activity, including dynamic changes (foot contact with ground or swing in the air), high system disturbance (impact at heel strike), and low constraints (can walk in different ways). Studies have focused on linear models to interpret the foot placement control of the human walking [18–20, 33]. However, linear models can only explain part information of the walking control. In this aim, a 7-link nonlinear gait model was used to identify the highly nonlinear foot placement control loop of randomly perturbed walking. The identified controllers can be applied or provide good references for the control systems of humanoid robots, powered exoskeletons, and P/O devices. To verify these application potentials, the foot placement control was applied on a powered leg exoskeleton. Leg muscle activations were measured of two participants wearing the controlled exoskeleton performing walking on a treadmill.

Aim 3: Identify impedance properties of leg joints in human walking.

This aim examines to what extent the trajectory optimization can identify the leg joints' impedance parameters in perturbed walking. Quasi-stiffness is usually calculated as joint stiffness in walking, however, studies have shown that it may not be the real joint stiffness [34]. The real stiffness of the ankle joint has been identified in several studies that rely heavily on specific perturbation devices [35, 36], which prevented the same method been applied on other leg joints, such as the knee and the hip. The advantage of identifying impedance properties through trajectory optimization is that only joint motion data is needed which can be collected easily through motion capture systems or inertial measurement units. However, it is still unknown how accurately trajectory optimization can identify the impedance parameters when the simulation model cannot perfectly represent the human systems, which normally is the case. To answer this question, identification was done on synthetic data where the impedance parameters were known. In the identification,

changes of identifying impedance parameters with respect to the model variation, such as small changes of mass properties or the foot size, were evaluated. After the synthetic study, a preliminary study was done identified the ankle joints impedance properties from two participants' perturbed walking data.

1.2 Outline

This dissertation study is divided into three main parts:

Chapter I discusses the background and main aims of this dissertation study.
Chapter II introduces the general methods for motion controller identifications.

Part I addresses **Aim 1** of this dissertation study:

- *Chapter III:* We designed and conducted a human standing balance experiment to obtain the motion data on how healthy young adults control their ankle, knee, and hip joints under random mechanical perturbations.
- *Chapter IV:* We developed a stochastic trajectory optimization method to help identify practically stable motion controllers from the measured data in chapter III.
- *Chapter V:* We identified several types of postural controllers, from simple linear to complex nonlinear, from the long duration standing balance data collected in chapter III.

Part II addresses **Aim 2** of this dissertation study:

- *Chapter VI:* We identified foot placement controllers from a published perturbed walking data-set. Nine young adults' walking data at three walking speeds were included in this study.

- *Chapter VII:* We evaluated the foot placement control by applying it on an Indego exoskeleton. Walking test was conducted with two healthy adults while wearing the controlled exoskeleton.

Part III addresses **Aim 3** of this dissertation:

- *Chapter VIII:* We identified leg joints' impedance parameters from simulated walking data through the same simulation model but with small changes in mass properties and the foot size. Then, preliminary studies were done identified the ankle joint impedance properties from two participants' perturbed walking data.

1.3 REFERENCES

[1] N. S. C. I. S. Center *et al.*, "Spinal cord injury: Facts and figures at a glance," *https://www. nscisc. uab. edu/Public*, 2019.

[2] D. Mozaffarian, E. J. Benjamin, A. S. Go, D. K. Arnett, M. J. Blaha, M. Cushman, S. R. Das, S. De Ferranti, J.-P. Després, H. J. Fullerton, *et al.*, "Executive summary: heart disease and stroke statistics—2016 update: a report from the american heart association," *Circulation*, vol. 133, no. 4, pp. 447–454, 2016.

[3] M. Owings, *Ambulatory and inpatient procedures in the United States, 1996*. No. 139, US Department of Health and Human Services, Centers for Disease Control and Prevention, 1998.

[4] A. Chu, *Design of the Berkeley lower extremity exoskeleton (BLEEX)*. PhD thesis, University of California, Berkeley, 2005.

[5] H. A. Quintero, R. J. Farris, and M. Goldfarb, "A method for the autonomous control of lower limb exoskeletons for persons with paraplegia," *Journal of Medical Devices*, vol. 6, no. 4, p. 041003, 2012.

[6] A. Esquenazi, M. Talaty, A. Packel, and M. Saulino, "The rewalk powered exoskeleton to restore ambulatory function to individuals with thoracic-level motor-complete spinal cord injury," *American Journal of Physical Medicine & Rehabilitation*, vol. 91, no. 11, pp. 911–921, 2012.

[7] R. Griffin, T. Cobb, T. Craig, M. Daniel, N. van Dijk, J. Gines, K. Kramer, S. Shah, O. Siebinga, J. Smith, *et al.*, "Stepping forward with exoskeletons: Team ihmc's design and approach in the 2016 cybathlon," *IEEE Robotics & Automation Magazine*, vol. 24, no. 4, pp. 66–74, 2017.

[8] A. H. Shultz, B. E. Lawson, and M. Goldfarb, "Running with a powered knee and ankle prosthesis," *IEEE Transactions on Neural Systems and Rehabilitation Engineering*, vol. 23, no. 3, pp. 403–412, 2015.

[9] M. R. Tucker, J. Olivier, A. Pagel, H. Bleuler, M. Bouri, O. Lambercy, J. del R Millán, R. Riener, H. Vallery, and R. Gassert, "Control strategies for active lower extremity prosthetics and orthotics: a review," *Journal of Neuroengineering and Rehabilitation*, vol. 12, no. 1, p. 1, 2015.

[10] F. Sup, A. Bohara, and M. Goldfarb, "Design and control of a powered transfemoral prosthesis," *The International Journal of Robotics Research*, vol. 27, no. 2, pp. 263–273, 2008.

[11] M. S. Orendurff, A. D. Segal, G. K. Klute, M. L. McDowell, *et al.*, "Gait efficiency using the C-Leg," *Journal of Rehabilitation Research and Development*, vol. 43, no. 2, p. 239, 2006.

[12] P. Khalaf, H. Warner, E. Hardin, H. Richter, and D. Simon, "Development and experimental validation of an energy regenerative prosthetic knee controller and prototype," in *ASME 2018 Dynamic Systems and Control Conference*, American Society of Mechanical Engineers Digital Collection, 2018.

[13] S. K. Au, J. Weber, and H. Herr, "Powered ankle–foot prosthesis improves walking metabolic economy," *IEEE Transactions on Robotics*, vol. 25, no. 1, pp. 51–66, 2009.

[14] F. Sup, A. Bohara, and M. Goldfarb, "Design and control of a powered knee and ankle prosthesis," in *Proceedings 2007 IEEE International Conference on Robotics and Automation*, pp. 4134–4139, IEEE, 2007.

[15] S. Park, F. B. Horak, and A. D. Kuo, "Postural feedback responses scale with biomechanical constraints in human standing," *Experimental Brain Research*, vol. 154, no. 4, pp. 417–427, 2004.

[16] H. Van Der Kooij and E. De Vlugt, "Postural responses evoked by platform pertubations are dominated by continuous feedback," *Journal of Neurophysiology*, vol. 98, no. 2, pp. 730–743, 2007.

[17] A. D. Goodworth and R. J. Peterka, "Sensorimotor integration for multisegmental frontal plane balance control in humans," *Journal of Neurophysiology*, vol. 107, no. 1, pp. 12–28, 2011.

[18] Y. Wang and M. Srinivasan, "Stepping in the direction of the fall: the next foot placement can be predicted from current upper body state in steady-state walking," *Biology Letters*, vol. 10, no. 9, p. 20140405, 2014.

[19] N. Seethapathi and M. Srinivasan, "Step-to-step variations in human running reveal how humans run without falling," *eLife*, vol. 8, p. e38371, 2019.

[20] V. Joshi and M. Srinivasan, "A controller for walking derived from how humans recover from perturbations," *Journal of the Royal Society Interface*, vol. 16, no. 157, p. 20190027, 2019.

[21] H. van der Kooij, E. van Asseldonk, and F. C. van der Helm, "Comparison of different methods to identify and quantify balance control," *Journal of Neuroscience Methods*, vol. 145, no. 1-2, pp. 175–203, 2005.

[22] J. Moore and A. van den Bogert, "Human standing controller parameter identification with direct collocation," in *15th International Symposium on Computer Simulation in Biomechanics*, ISB, 2015.

[23] T. A. Boonstra, A. C. Schouten, and H. Van der Kooij, "Identification of the contribution of the ankle and hip joints to multi-segmental balance control," *Journal of Neuroengineering and Rehabilitation*, vol. 10, no. 1, p. 23, 2013.

[24] H. Van Der Kooij and R. J. Peterka, "Non-linear stimulus-response behavior of the human stance control system is predicted by optimization of a system with sensory and motor noise," *Journal of Computational Neuroscience*, vol. 30, no. 3, pp. 759–778, 2011.

[25] R. Pintelon and J. Schoukens, *System identification: a frequency domain approach*. John Wiley & Sons, 2012.

[26] G. Torres-Oviedo and L. H. Ting, "Muscle synergies characterizing human postural responses," *Journal of Neurophysiology*, vol. 98, no. 4, pp. 2144–2156, 2007.

[27] T. D. Welch and L. H. Ting, "A feedback model explains the differential scaling of human postural responses to perturbation acceleration and velocity," *Journal of Neurophysiology*, vol. 101, no. 6, pp. 3294–3309, 2009.

[28] G. Torres-Oviedo and L. H. Ting, "Subject-specific muscle synergies in human balance control are consistent across different biomechanical contexts," *Journal of neurophysiology*, vol. 103, no. 6, pp. 3084–3098, 2010.

[29] O. von Stryk and R. Bulirsch, "Direct and indirect methods for trajectory optimization," *Annals of Operations Research*, vol. 37, pp. 357–373, Dec 1992.

[30] A. J. van den Bogert, D. Blana, and D. Heinrich, "Implicit methods for efficient musculoskeletal simulation and optimal control," *Procedia Iutam*, vol. 2, pp. 297–316, 2011.

[31] A. D. Koelewijn and A. J. van den Bogert, "Joint contact forces can be reduced by improving joint moment symmetry in below-knee amputee gait simulations," *Gait & Posture*, vol. 49, pp. 219–225, 2016.

[32] M. Ackermann and A. J. Van den Bogert, "Optimality principles for model-based

prediction of human gait," *Journal of Biomechanics*, vol. 43, no. 6, pp. 1055–1060, 2010.

[33] T. Koolen, T. De Boer, J. Rebula, A. Goswami, and J. Pratt, "Capturability-based analysis and control of legged locomotion, part 1: Theory and application to three simple gait models," *The International Journal of Robotics Research*, vol. 31, no. 9, pp. 1094–1113, 2012.

[34] E. J. Rouse, R. D. Gregg, L. J. Hargrove, and J. W. Sensinger, "The difference between stiffness and quasi-stiffness in the context of biomechanical modeling," *IEEE Transactions on Biomedical Engineering*, vol. 60, no. 2, pp. 562–568, 2013.

[35] E. J. Rouse, L. J. Hargrove, E. J. Perreault, and T. A. Kuiken, "Estimation of human ankle impedance during the stance phase of walking," *IEEE Transactions on Neural Systems and Rehabilitation Engineering*, vol. 22, no. 4, pp. 870–878, 2014.

[36] H. Lee, E. J. Rouse, and H. I. Krebs, "Summary of human ankle mechanical impedance during walking," *IEEE journal of Translational Engineering in Health and Medicine*, vol. 4, pp. 1–7, 2016.

CHAPTER II

METHODS FOR CONTROLLER IDENTIFICATION

The indirect identification approach has been used in human movement studies to extract motion controllers [1–5]. It has been reported that the indirect approach can avoid the bias introduced by the direct approach, and is therefore more appropriate for the closed loop system identification [6, 7]. Indirect controller identification can be done in both frequency and time domains. In the time domain, trajectory optimization is usually used to solve the identification problems [1, 8].

In general, trajectory optimization requires a simulation model to represent the closed loop system. In controller identification studies, the simulation model includes a feedback controller and a dynamic model of the plant. To identify the feedback controller, control parameters are optimized such that the simulation model generates outputs that are closest to the observed trajectories. For example, in the controller identification for human standing balance, the simulation model consists of a state feedback controller and a two-link pendulum model. The identification process is to optimize the control parameters inside the state feedback controller until the simulation model generates the closest balance movements as human subjects' (Figure 3).

Shooting methods are commonly used in trajectory optimizations. However, they are not efficient, especially for long duration simulation with naturally unstable systems. For instance, in forward simulation of the human standing balance model, if the model falls

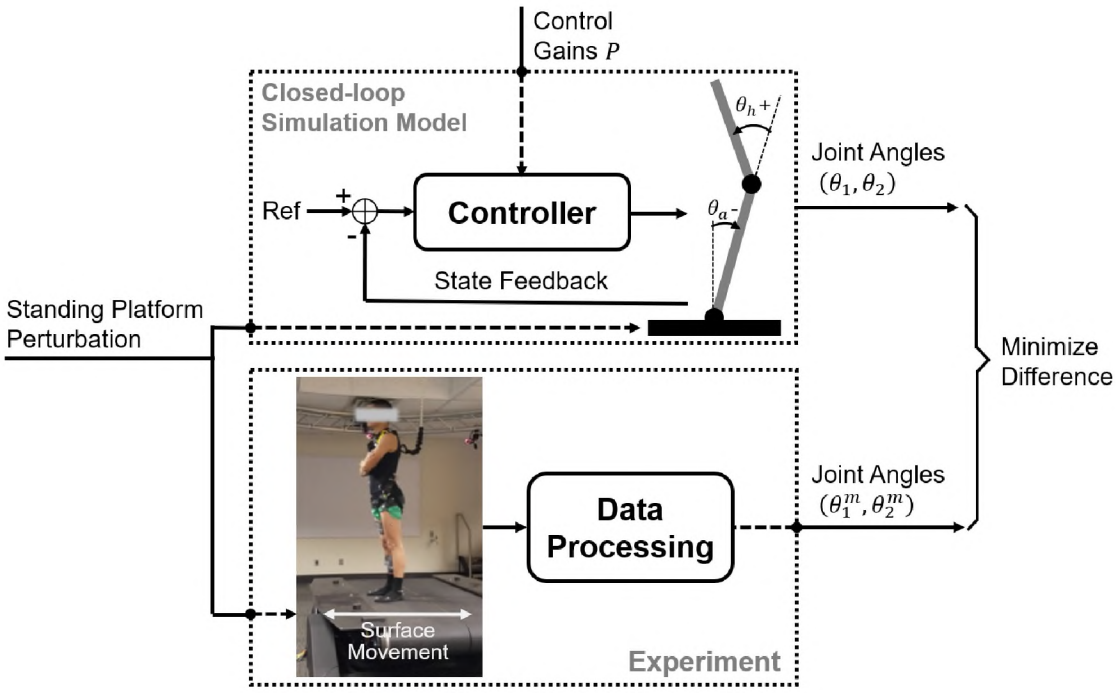

Figure 3: Diagram of the indirect approach in postural controller identification.

down at the beginning of the simulation, the remaining simulation becomes useless and time consuming. In addition, divergence of the forward simulation can cause crash of the optimization process.

One way to avoid forward simulation is to use the direct collocation method. It has recently become popular in human movement studies, such as the optimal control and the predictive simulation problems, because of its efficiency in trajectory optimization [9, 10]. However, to our knowledge, no study has been found that use it for the human motion controller identification. As the motion controller identifications in time domain can be transferred to trajectory optimization problems, We believe that the direct collocation can help identify complex motion controllers from long duration movement data. In this chapter, general formula of the human motion controller identification in the format of trajectory optimization with direct collocation is described.

2.1 Trajectory Optimization

Trajectory optimization is the process of finding the best feasible trajectory for a given system, with a specified movement task and optimization objective.. In the human motion controller identifications, the aim is to let the closed loop simulation model generate the closest fit with the measured human motions. Feasible trajectories mean that these trajectories must satisfy a variety of limits and constraints. For instance, feasible trajectories need to satisfy the dynamics of human body, boundary constraints, and the bounds on system state and control. The definition of trajectory optimization in human motion controller identification is shown in Equation 2.1. Path constraints and boundary constraints were not used in this dissertation study.

$$
\begin{aligned}
&\text{Optimize trajectory } g[x(t)] \text{ and control parameters } P \\
&\text{Minimize the objective function } F = \int_0^T \|g[x(t)]_m - g[x(t)]\|^2 \cdot dt \\
&\text{Subject to: human system dynamics: } f(x(t), \dot{x}(t), P, q(t)) = 0 \\
&\qquad\qquad \text{bounds on state: } x_{low} \leq x(t) \leq x_{upp} \\
&\qquad\qquad \text{bounds on control parameters: } P_{low} \leq P \leq P_{upp}
\end{aligned}
\tag{2.1}
$$

where $x(t)$ is the state trajectory of the simulation model; $g[x(t)]$ represents simulated observations which can be any function of the state trajectory; $g[x(t)]_m$ represents the corresponding measurements; P represents the unknown parameters in the identifying controller; T is the total time duration of the identifying data. $q(t)$ represents external inputs to the closed loop system, such as mechanical perturbations.

Theoretically, the measured data used for human motion controller identification can be any variables as long as they can be generated by the simulation model, for instance, joint motions, joint moments, ground reaction forces (GRF), or even muscle activations. In this dissertation study, joint motions were selected as the tracking variable for the controller

identification for two main reasons. First of all, joint motion data is easy to get in human experiments using either the motion capture system or the inertial measurement units (IMU). GRF rely on force plates or instrumented treadmills which may not available for some active movements, e.g. skiing. Secondly, measured joint motion data can be much cleaner than the GRF or the Electromyography (EMG) data with current available sensors. It is well known that artificial component is included in GRF due to the moving part of the instrumented treadmills [11, 12] and electrical noise can easily affect the EMG data [13].

Take the posture controller identification in standing balance task as an example, the trajectory optimization with joint motion tracking is defined as:

$$\begin{aligned}
&\text{Optimize trajectory } x(t) \text{ and control parameters } P \\
&\text{Minimize the objective function } F = \int_0^T \|\theta_m(t) - \theta(t)\|^2 \cdot dt \\
&\text{Subject to: human system dynamics: } f(x(t), \dot{x}(t), P, a(t)) = 0 \\
&\qquad\qquad \text{bounds on state: } x_{low} \leq x(t) \leq x_{upp} \\
&\qquad\qquad \text{bounds on control parameters: } P_{low} \leq P \leq P_{upp}
\end{aligned} \tag{2.2}$$

where $x(t)$ is the state trajectories of the simulation model for the human system in standing balance task, consisting of joint angles θ and angular velocities $\dot{\theta}$; P represents the unknown parameters of the identifying controller; T is the total time duration of the identifying data. $\theta_m(t)$ is the measured joint motions in experiments; $\theta(t)$ is the optimized joint motions generated from the simulation model. $a(t)$ is the mechanical perturbation, applied as horizontal accelerations of the standing surface.

The human dynamic model for the standing balance task was simplified as a two-link pendulum as shown in Figure 3. Its dynamic equation has the format of $M(\theta(t)) \cdot \ddot{\theta}(t) + C(\theta(t), \dot{\theta}(t)) \cdot \dot{\theta}(t) + G(\theta(t)) + F(\theta(t), a(t)) = \tau(t)$. In which, $F(\theta(t), a(t))$ is the force component that caused by the mechanical perturbation. Combined with the state feedback

control law $\tau(t) = Con(\theta(t), \dot{\theta}(t), P)$, the generalized dynamic equation of the human standing balance system model can be written as: $f(\theta(t), \dot{\theta}(t), \ddot{\theta}(t), P, a(t)) = 0$. By setting the system state $x = [\theta(t), \dot{\theta}(t)]$, the dynamic equation can be finally summarized as: $f(x(t), \dot{x}(t), P, a(t)) = 0$.

2.2 Direct Collocation

Direct collocation has shown better efficiency than the shooting method in trajectory optimization, especially for naturally unstable systems [14]. Direct collocation avoids forward simulation by discretizing the optimizing trajectory into finite collocation nodes. System dynamics is guaranteed by applying constraints on the nearby collocation nodes through Euler or higher order methods. Again, taking the posture controller identification in human standing balance as an example, the formula of trajectory optimization in direct collocation format is shown in Equation 2.3. This trajectory optimization format can be solved by

nonlinear programming (NLP).

Optimize trajectory on collocation nodes $[x(t_1), x(t_2), ..., x(t_N)]$ and control parameters P

Minimize the objective function $F = \sum_{k=1}^{N} \|\theta_m(t_k) - \theta(t_k)\|^2$

$$\text{Subject to: approximate differentiation: } \left\{ \begin{array}{c} \dot{x}(t_2) = (x(t_2) - x(t_1))/h \\ ... \\ \dot{x}(t_k) = (x(t_k) - x(t_{k-1}))/h \\ ... \\ \dot{x}(t_N) = (x(t_N) - x(t_{N-1}))/h \end{array} \right\}$$

$$\text{human system dynamics: } \left\{ \begin{array}{c} f(x(t_1), \dot{x}(t_1), P, a(t_1)) = 0 \\ ... \\ f(x(t_k), \dot{x}(t_k), P, a(t_k)) = 0 \\ ... \\ f(x(t_N), \dot{x}(t_N), P, a(t_N)) = 0 \end{array} \right\}$$

bounds on state: $x_{low} \leq x_{1,...,N} \leq x_{upp}$

bounds on control parameters: $P_{low} \leq P \leq P_{upp}$

(2.3)

where, t_i is the time point of i^{th} direct collocation node; N is the total number of direct collocation nodes; h is the time interval between direct collocation nodes;

2.3 Nonlinear Programming

Nonlinear programming problem is defined as optimization problem which contains nonlinear constraints. In human motion controller identification, the nonlinear constraints are the nonlinear dynamic equations of the simulation model which represents the closed-loop human system. The human motion controller identification in the nonlinear programming

format can be written as:

$$\begin{aligned} &\text{For } Y = (x_1, x_2, ..., x_N, P) \\ &\text{Minimize } F(Y, X_m) \\ &\text{Subject to: } h(Y) = 0 \\ &\qquad Y_{low} \leq Y \leq Y_{upp} \end{aligned} \tag{2.4}$$

where, Y represents the optimizing variables, including state trajectories $x_1, ..., x_N$ and controller parameters P; X_m represents the measured data; $F(Y, X_m)$ is the objective function; $h(Y)$ represents the nonlinear equality constrains.

Nonlinear programming problems can be solved by various numerical methods [15, 16]. In this dissertation, the interior point optimizer (IPOPT) [17], an open source software package for large-scale nonlinear optimization, was chosen. It is a gradient based optimization method, which requires gradient of the objective function and Jacobian matrix of the constrain functions. In my controller identification studies, the objective function is usually defined as a quadratic function. Therefore, its gradient is a vector that contains linear functions, which is easy to obtain. The Jacobian of the nonlinear dynamic constraints is much harder to get, since the dynamic equations can be very complicated, especially for high dimensional systems. In this dissertation, Jacobian, the derivative of nonlinear constraints with respect to system states, was obtained using symbolic dynamic software/toolboxes, such as, Autolev (MotionGenesis), Sympy, and PyDy [18–20].

2.4 Reduce Local Optimum Solutions

Gradient based optimization cannot guarantee finding the global optimum. This is the consequence of a poor initial guess and the non-convex property of the optimizing problem. One way to increase the chance of finding global optimum is to run multiple optimizations with different random initial guesses and choose the best result among these optimizations.

Particularly, if a best solution (lowest objective value) can be found multiple times with different initial guesses, there is a high confidence that this best result is a global optimum. This method for increasing the chance of finding global optimum was used in all identification studies in this dissertation.

2.5 REFERENCES

[1] S. Park, F. B. Horak, and A. D. Kuo, "Postural feedback responses scale with biomechanical constraints in human standing," *Experimental Brain Research*, vol. 154, no. 4, pp. 417–427, 2004.

[2] H. Van Der Kooij and E. De Vlugt, "Postural responses evoked by platform pertubations are dominated by continuous feedback," *Journal of Neurophysiology*, vol. 98, no. 2, pp. 730–743, 2007.

[3] A. D. Goodworth and R. J. Peterka, "Identifying mechanisms of stance control: a single stimulus multiple output model-fit approach," *Journal of Neuroscience Methods*, vol. 296, pp. 44–56, 2018.

[4] T. D. Welch and L. H. Ting, "A feedback model explains the differential scaling of human postural responses to perturbation acceleration and velocity," *Journal of Neurophysiology*, vol. 101, no. 6, pp. 3294–3309, 2009.

[5] V. Joshi and M. Srinivasan, "A controller for walking derived from how humans recover from perturbations," *Journal of the Royal Society Interface*, vol. 16, no. 157, p. 20190027, 2019.

[6] H. van der Kooij, E. van Asseldonk, and F. C. van der Helm, "Comparison of different methods to identify and quantify balance control," *Journal of Neuroscience Methods*, vol. 145, no. 1-2, pp. 175–203, 2005.

[7] J. Moore and A. van den Bogert, "Human standing controller parameter identification with direct collocation," in *15th International Symposium on Computer Simulation in Biomechanics*, ISB, 2015.

[8] T. D. Welch and L. H. Ting, "A feedback model predicts muscle activity during human postural responses to support surface translations," *Journal of Neurophysiology*, 2008.

[9] A. J. van den Bogert, D. Blana, and D. Heinrich, "Implicit methods for efficient musculoskeletal simulation and optimal control," *Procedia Iutam*, vol. 2, pp. 297–316, 2011.

[10] A. D. Koelewijn and A. J. van den Bogert, "Joint contact forces can be reduced by improving joint moment symmetry in below-knee amputee gait simulations," *Gait & Posture*, vol. 49, pp. 219–225, 2016.

[11] S. K. Hnat and A. J. van den Bogert, "Inertial compensation for belt acceleration in an instrumented treadmill," *Journal of Biomechanics*, vol. 47, no. 15, pp. 3758–3761, 2014.

[12] S. K. Hnat, B. J. van Basten, and A. J. van den Bogert, "Compensation for inertial and gravity effects in a moving force platform," *Journal of Biomechanics*, vol. 75, pp. 96–101, 2018.

[13] P. Konrad, "The abc of emg," *A practical Introduction to Kinesiological Electromyography*, vol. 1, no. 2005, pp. 30–35, 2005.

[14] M. Kelly, "An introduction to trajectory optimization: how to do your own direct collocation," *SIAM Review*, vol. 59, no. 4, pp. 849–904, 2017.

[15] D. Solow, "Linear and nonlinear programming," *Wiley Encyclopedia of Computer Science and Engineering*, 2007.

[16] J. T. Betts, *Practical methods for optimal control and estimation using nonlinear programming*, vol. 19. Siam, 2010.

[17] L. T. B. A. Wachter, "On the implementation of a primal-dual interior point filter line search algorithm for large-scale nonlinear programming," *Mathematical Programming*, vol. 106, no. 1, pp. 25–57, 2006.

[18] "Motiongenesis." `http://www.motiongenesis.com/index.html`. Accessed: 2019-04-22.

[19] "Pydy: Multibody dynamics with python." `http://www.pydy.org/`. Accessed: 2019-04-22.

[20] A. Meurer, C. P. Smith, M. Paprocki, O. Čertík, S. B. Kirpichev, M. Rocklin, A. Kumar, S. Ivanov, J. K. Moore, S. Singh, T. Rathnayake, S. Vig, B. E. Granger, R. P. Muller, F. Bonazzi, H. Gupta, S. Vats, F. Johansson, F. Pedregosa, M. J. Curry, A. R. Terrel, v. Roučka, A. Saboo, I. Fernando, S. Kulal, R. Cimrman, and A. Scopatz, "Sympy: symbolic computing in python," *PeerJ Computer Science*, vol. 3, p. e103, Jan. 2017.

PART I.

CONTROL OF STANDING

CHAPTER III

STANDING BALANCE EXPERIMENT WITH LONG DURATION RANDOM SQUARE PERTURBATION

Non-peer Reviewed Publication:

1. Wang, Huawei, van den Bogert, Antonie. (2020). Standing Balance Experiment with Long Duration Random Pulses Perturbation (Version 1.0) [Data set]. Zenodo. http://doi.org/10.5281/zenodo.3631958

ABSTRACT

Standing balance experiment and its measurements are fundamental for identifying postural feedback controllers. As the complex feedback controllers can only be identified from long duration balance data (under random external perturbations), a standing balance experiment was conducted and the long duration motion data was recorded. The recorded data-set consists of the standing balance data of 8 participants. Each participant performed 4 experiment trials, including 2 quiet standing and 2 perturbed standing trials. Each trial lasted 5 minutes long. A total of 80 minutes quiet standing and 80 minutes perturbed standing data are included in the data-set. Recorded data includes three dimensional (3d) motion of 32 markers (27 on participants' trunks and legs and 5 on treadmill frame), six dimensional ground reaction forces (GRF), and nine Electromyography signals (EMGs, of participants' right legs' muscles). In addition, the marker data was post-processed that filled the missing frames. The GRF was compensated to remove the inertia artifacts of the moving treadmill. The joint angles and torques were calculated using a 2d human body model.

3.1 Introduction

Standing balance experiment with external stimuli has become a common way to study the postural feedback control in humans' central nervous system (CNS)[1–5]. External stimuli evoke participants' body sway motion at variety situations, so that generalized motion controllers that cover these situations can be extracted. Two types of stimuli signals were mainly used in previous studies: short duration ramp perturbation[2, 4] and long duration random perturbation [1, 3, 5–8]. Postural feedback controllers and the mathematical models of CNS have been identified from the experimental data with these two types of stimuli. However, these identified controllers are far from engineering applicable (on humanoid robots and P/O devices). The postural controllers identified from ramp pertur-

bations showed that the control gains vary based on the amplitude of ramp perturbations, whereas it is impossible, in practise, to predict perturbation amplitudes before choosing the feedback control gains. This also suggested that the postural control in human standing balance is nonlinear in overall. Mathematical models of CNS identified from the experimental data with random perturbations have an assumption that the human standing balance system is linear. To make this assumption valid, the power spectrum of random perturbation was usually small. In this dissertation work, we proposed that a new controller identification method (trajectory optimization with direct collocation) can identify nonlinear controllers from long duration experimental data. As a result, human standing balance data with perturbation that is long duration and large amplitude is required. Whereas, no suitable data sets were shared by previous studies. Therefore, the human standing balance experiment was conducted to provide motion data for the postural controller identification in chapter IV and V. We also shared this data set on Zenodo for public usage `https://doi.org/10.5281/zenodo.3631958`.

3.2 Methods

In this section, the experiment design, participants, and the experiment setup are described first. Then, the design of mechanical perturbation is described.

3.2.1 Participants

Eight able bodied participates, including one female and seven males, with an average age of 27 $\pm$ 5.3 years, an average height of 1.71 $\pm$ 0.08 m, an average mass of 65.3 $\pm$ 9.2 kg joined in this study. This study was approved by the Institutional Review Board of Cleveland State University(# IRB-FY2018-40). Also, written informed consent was obtained from each participant. Participation exclusion criteria is showing below. All five conditions need to be satisfied.

- No any past extremity injuries on legs or feet and still affect movement and balance functions now.
- Not diagnosed with any neuron-muscle disease.
- Body Mass Index (BMI: body wight/body height) below 30 lbs/ft^2.
- No neurological or other impairments that affects movements and balance.
- No pain or discomfort that could affect your movements.

Recorded data were anonymized with respect to the participants' identities. A unique identification number was assigned to each subject. A selection of the meta data collected for each participant is shown in Table V. Participants were divided into those that were used for the protocol pilot trials, i.e., the first two (grey background), and those used for the final protocol (last six). The final four columns provide the trial numbers associated with each experiment trials, Q means the quiet standing trial; P means the perturbed trial. The mass information was computed from the mean of vertical ground reaction forces at quiet standing trials, if possible. Additional trial in the data set with the trial number 0 is the unloaded trial that was used for the inertial artifact compensation.

Table I: Information of the eight participants in the order of collection date.

Id	Gender	Age (yr)	Height (m)	Mass (kg)	Q1	P1	P2	Q2
1	male	22	1.60	74.29 ± 0.26	1	2	3	4
2	female	–	–	48.37 ± 0.21	5	6	7	8
3	male	18	1.80	79.12 ± 0.20	9	10	11	12
4	male	27	1.78	63.10 ± 0.16	13	14	15	16
5	male	32	1.79	70.56 ± 0.19	17	18	19	20
6	male	35	1.65	58.24 ± 0.27	21	22	23	24
7	male	28	1.75	68.75 ± 0.17	25	26	27	28
8	male	27	1.63	60.33 ± 0.19	29	30	31	32

3.2.2 Equipment

Experiments were conducted in the Human Motion and Control lab at the Cleveland State University. In the experiment, ten Osprey motion capture cameras (Motion Analysis) were used to track participants' motions during experiment. A computer software *Cortex* (version 5.0.1.1497) was used to control the recording process of these cameras. Motion data was recorded at a frame rate of 100 Hz. A four degree of freedom (DOF) V-Gait (Motek Medical) treadmill was used as standing platform to execute perturbation. Force sensors in the V-Gait were used to detect the six DOF ground reaction forces and moments under both feet. Nine EMG sensors (Delsys Inc.) were used to record participants' muscle activation. EMG data was recorded at 1000Hz rate. The experiment setting is shown in Figure 4. In the experiment, *D-Flow* (version 3.26.0) software was used as an integral control tool that controlled all equipment as well as saved the measured data. The *D-Flow* application designed for the standing balance experiment is shown in Figure 5. The MoCap module controlled the motion capture system and recorded the EMG, ground reaction forces, and 32 markers' data. The V-Gait module controlled the motion of V-Gait treadmill with a perturbation signal written in a text file. The XSens module connected with two accelerometers on the V-Gait. The record data module recorded the V-Gait motion and XSens accelerometers' data.

In the experiment, 27 markers were used to track the participants' movement (trunk and legs). Five extra markers were placed on the standing platform to record its movement during the experiment. Table II describes the landmarks of these 32 markers. Nine Electromyography (EMG) sensors were used in the experiment to record nine muscle activations in the right leg. The EMG sensors were placed according to ABC of EMG (SENIAM) [9]. The EMG sensor number, corresponding analog channel number, and the measuring muscles are shown in Table III.

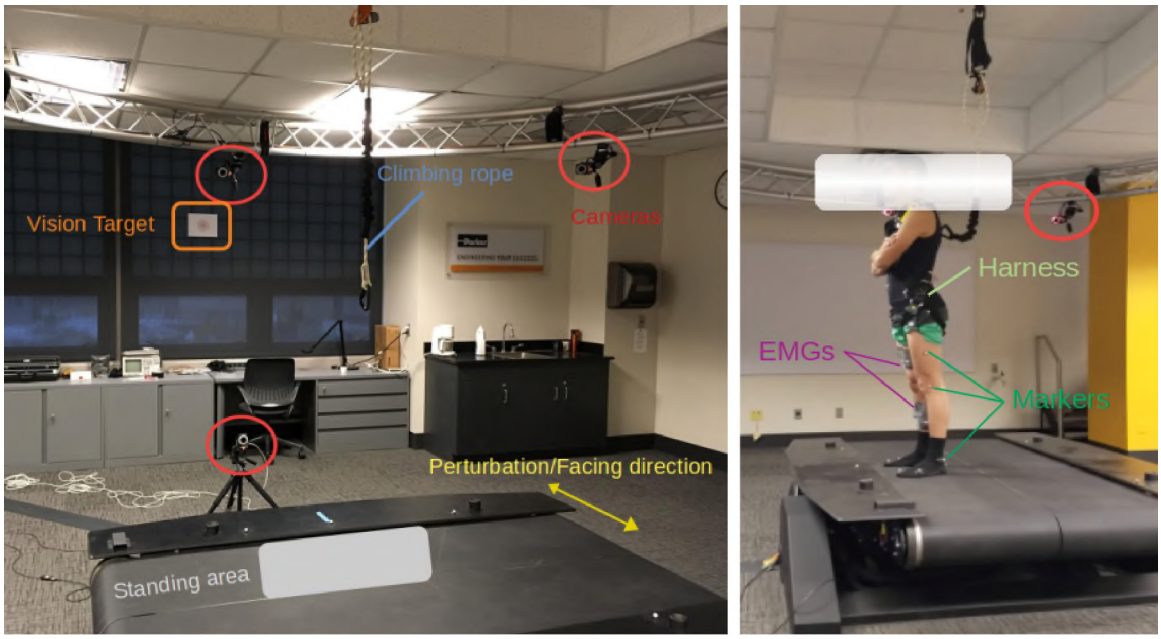

Figure 4: Standing balance experiment setting. Perturbation was applied in anterior and posterior direction using the sway motion of V-Gait. EMG sensors were placed on the right leg. Twenty-seven markers were put on participant's body to tracking motion.

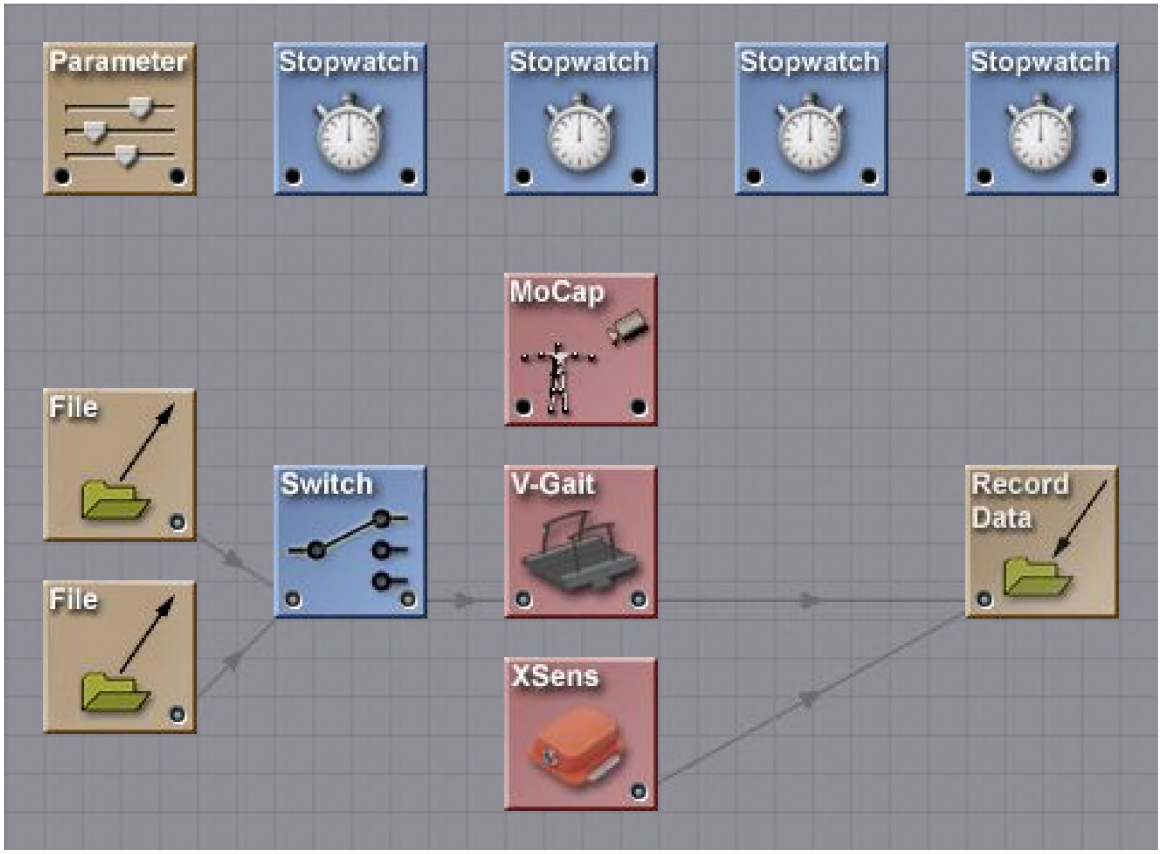

Figure 5: D-Flow application in standing balance experiment.

Table II: Reflex markers used in the experiment, including 27 subject markers and 5 treadmill markers. The label column matches the column headers in the mocap-xxx.txt files. Location of these markers on human body are in the last column.

Label	Name	Description
T10	T10	On the 10th thoracic vertebrae
SACR	Sacurm bone	On the sacral bone
NAVE	Navel	On the navel
XYPH	Xiphoid process	Xiphoid process of the sternum
STRN	Sternum	On the jugular notch of the sternum
LASIS	Pelvis bone left front	Left anterior superior iliac spine
RASIS	Pelvic bone right front	Right anterior superior iliac spine
LPSIS	Pelvic bone left back	Left posterior superior iliac spine
RPSIS	Pelvic bone right back	Right posterior superior iliac spine
LGTRO	Left greater trochanter of the femur	On the center of the left greater trochanter
FLTHI	Left thigh	At 1/3 of the line between the LGTRO and LLEK
LLEK	Left lateral epicondyle of the knee	On the lateral side of the joint axis
LATI	Left anterior of the tibia	On 2/3 on the line between the LLEK and LLM
LLM	Left lateral malleoulus of the ankle	The center of the heel at the same height as the toe
LHEE	Left heel	Center of the heel at the same height as the toe
LTOE	Left toe	Tip of the big toe
LMT5	Left 5th metatarsal	Caput of the 5th metatarsal bone, on joint line midfoot/toes
RGTRO	Right greater trochanter of the femur	On the center of the right greater trochanter
FRTHI	Right thigh	At 1/3 of the line between the RGTRO and RLEK
RLEK	Right lateral epicondyle of the knee	On the lateral side of the joint axis
RATI	Right anterior of the tibia	At 2/3 of the line between the RLEK and RLM
RLM	Right lateral malleoulus of the ankle	The center of the heel at the same height as the toe
RHEE	Right heel	Center of the heel at the same height as the toe
RTOE	Right toe	Tip of the big toe
RMT5	Right 5th metatarsal	Caput of the 5th metatarsal bone, on joint line midfoot/toes
RACR	Right shoulder	Right acromion
LACR	Left shoulder	Left acromion
T1	Treadmill marker 1	On the left rear corner of the treadmill
T2	Treadmill marker 2	At 1/2 of the line between T1 and T2
T3	Treadmill marker 3	On the left front corner of the treadmill
T4	Treadmill marker 4	On the right front corner of the treadmill
T5	Treadmill mraker 5	On the right rear corner of the treadmill

Table III: Nine EMG sensors used in this study. # means the EMG numbers in Delsys system. EMG 6 was not used due to a wireless connection issue. Analog channel column listed the corresponding analog column number in the recorded analog files.

#	Analog Channel	Muscle Names	Muscle Locations
EMG 1	17	Tibialis anterior	In the upper two-thirds of the lateral (outside) surface of the tibia
EMG 2	21	Soleus	In the back part of the lower leg (the calf)
EMG 3	25	Medial gastrocnemius	On the medial back portion of the lower leg
EMG 4	29	Lateral gastrocnemius	On the lateral back portion of the lower leg
EMG 5	37	Vastus medialis	In the anterior and medial compartment of thigh
EMG 7	41	Vastus lateralis	In the anterior and lateral compartment of thigh
EMG 8	45	Rectus femoris	Situated in the middle of the front of the thigh
EMG 9	49	Biceps femoris	Begins in the thigh area and extends to the head of the fibula near the knee
EMG 10	53	Gluteus maximus	Located in the buttocks

3.2.3 Perturbation Signal

In the standing balance experiment, perturbation was designed as random square signals, instead of the Gaussian random signals used in previous studies [1, 3, 5]. The main reason is to avoid damaging the V-Gait treadmill. The total mass of the V-Gait is a about 800 lbs. In the experiment, the whole V-Gait will move laterally according to the perturbation signal (Figure 4). Large impact forces can be generated on the treadmill motors due to the frequent direction changes in the Gaussian random perturbation.

Parameters that determined the random square signal are the stage amplitude and the stage duration. The principle of designing the signal is to let participants feel a large perturbation but no so large that they respond by taking a step. After several tests, a suitable perturbation signal was designed using square pulses with five amplitudes [-5, -2.5, 0, 2.5, 5] cm, and six stage duration [0.25, 0.5, 0.75, 1.0, 1.25, 1.5] seconds. Amplitudes and duration series were randomly generated to obtain a 300 second perturbation signal. All

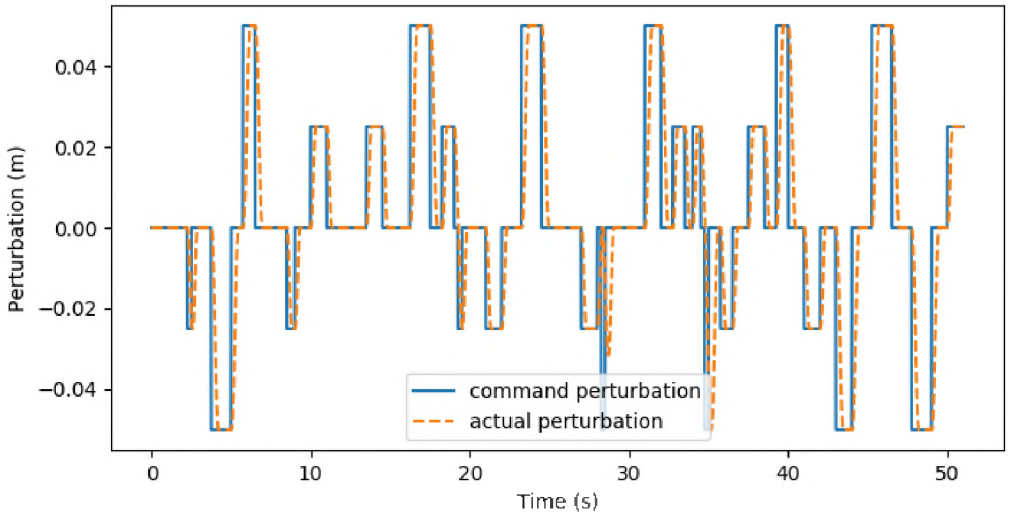

Figure 6: Comparison between the designed and actual standing balance perturbation. Designed perturbation has no dynamics and actual perturbation has a slow transient because of dynamics. Only the first 50 seconds is shown here.

participants experienced the same random square perturbations to check whether they have similar responses.

The actual sway motion of the V-Gait was calculated by averaging the motion of five reflect markers that were placed on the treadmill frame. The comparison between designed perturbation command and recorded V-Gait movement is shown in Figure 6. The difference between them was mainly caused by the dynamics of the V-Gait treadmill. In general, the actual perturbation closely tracked the designed signal.

3.2.4 Protocol

The experimental protocol consisted of both static measurements and experimental recordings. Experimental recordings include standing on the treadmill for five minutes with and without perturbation. On the day of experiment, the motion capture system was calibrated first using the manufacturer's recommended procedure. Prior testing, participants were asked to change into barefoot, shorts, and tight t-shirts (sports bra for female). All twenty-seven markers were applied directly to the skin except for the heel, toe, and hip markers,

which were placed on the respective article of clothing. Then age, gender, height, and mass were documented. Their knee and ankle widths were measured by the experimentalist. After obtaining the informed consent and a briefing by the experimentalist on the trial protocol, the experimental protocol for a participant was as follows:

1. The participant stepped onto the treadmill and markers were identified with Cortex.

2. A safety rope was attached loosely to the rock climbing harness such that no forces were acting on the subject during experiment. But the harness would prevent a full fall.

3. The participant started by stepping on sides of treadmill so that feet did not touch the force plates and the force plate signals were zeroed. Then participants were asked to step back to the treadmill.

4. A verbal countdown to the first quiet standing trial (Trial 1) was given by the experimentalist. Participants were asked to look at a target at roughly same height as their eyes. The quiet standing trial was five minutes long.

5. After the quiet standing trial, participant was asked to continue the first perturbation trial (Trial 2), in which 5 minutes anterior and posterior perturbation was applied on the treadmill . In the perturbation trial, participants were asked to keep balance without taking a step. However, he/she is free to adjust his/her pose by actively control his/her joints.

6. The participant was instructed to step off the force plate after the second trial to have a rest for five minutes.

7. The participant was asked to repeat the perturbation trial after rest (Trial 3).

8. The participant was asked to have another five minutes quiet standing trial (Trial 4) after the repeated perturbation trial.

Participants 3-8 were instructed to keep their vision on the horizontal target, having the feet width similar to the width of shoulder, and feel free to bend their trunk to keep balance. The first two participants were in the process of testing experiment protocol. The first participant had a wider stance, and the second participant used a strange (freezing) strategy to keep balance, instead of the normal strategy. The identification work in chapter IV and V used the last six participants' data.

3.3 Raw Experimental Data and Post Processing

3.3.1 Raw Data

Each participant performed four trials. Each trial produced three raw data files.

1. Mocapxxxx.txt: contains motion capture marker data, ground reaction force, and 76 analog channels. Data was recorded at 100 Hz sampling rate.

2. Mocapxxxx_Motion Analysis_analog.txt: contains 76 high sampling rate (1000Hz) analog channels' data (Figure III)

3. Recordxxxx.txt: contains the sway motion data of treadmill and the three-axis acceleration data of two Xsens MTi-10 series sensors. Data was recorded at roughly 300 Hz.

The mocap data (marker motion) might missed some frames when markers were obscured or not recognized by the Cortex software. The quality of the marker data of all eight participants was assessed by determining the percentage of data missing and the maximum missing gaps. Most of the 32 markers had very small missing percentages, which were less than 0.5%, except the marker of NAVE, XYPH, STRN, LASIS. The data quality of these four markers over all participants and experiment trials is shown in Table IV. These markers had relatively bad quality in the experiment trials of participant 2. In other participants' data, their missing percentages were either lower than 1% or the maximum gaps of them were less than 200 frames (2 seconds).

Table IV: Maximum numbers of continual missing frames and overall percentage of missing frames of all participants.

Marker names		NAVE	XYPH	STRN	LASIS
Participant No.	Trial	Maximum gap (frames) {Missing data (%)}			
Participant 1	1	0 {0.0}	144 {2.4}	0 {0.0}	0 {0.0}
	2	6 {0.03}	9 {0.32}	5 {0.07}	0 {0.0}
	3	0 {0.0}	8 {0.5}	6 {0.14}	0 {0.0}
	4	4 {0.2}	20 {0.46}	0 {0.0}	0 {0.0}
Participant 2	1	0 {0.0}	28 {0.46}	0 {0.0}	0 {0.0}
	2	0 {0.0}	49 {20.36}	1581 {5.12}	256 {37.06}
	3	76 {2.22}	45 {7.44}	1434 {7.55}	2021 {90.93}
	4	0 {0.0}	0 {0.0}	0 {0.0}	402 {4.34}
Participant 3	1	0 {0.0}	0 {0.0}	0 {0.0}	0 {0.0}
	2	6 {0.08}	15 {2.84}	1 {0.0}	0 {0.0}
	3	2 {0.11}	22 {1.03}	10 {0.55}	0 {0.0}
	4	99 {17.29}	0 {0.0}	16 {0.24}	0 {0.0}
Participant 4	1	0 {0.0}	0 {0.0}	0 {0.0}	0 {0.0}
	2	0 {0.0}	5 {0.15}	3 {0.03}	0 {0.0}
	3	0 {0.0}	1 {0.0}	0 {0.0}	0 {0.0}
	4	0 {0.0}	0 {0.0}	0 {0.0}	0 {0.0}
Participant 5	1	0 {0.0}	0 {0.0}	0 {0.0}	0 {0.0}
	2	65 {1.29}	6 {0.13}	0 {0.0}	0 {0.0}
	3	0 {0.0}	0 {0.0}	0 {0.0}	0 {0.0}
	4	0 {0.0}	0 {0.0}	0 {0.0}	0 {0.0}
Participant 6	1	0 {0.0}	159 {32.72}	0 {0.0}	0 {0.0}
	2	14 {0.08}	95 {4.33}	4 {0.11}	2 {0.01}
	3	15 {0.17}	82 {3.8}	1 {0.0}	0 {0.0}
	4	0 {0.0}	0 {0.0}	0 {0.0}	0 {0.0}
Participant 7	1	0 {0.0}	0 {0.0}	0 {0.0}	0 {0.0}
	2	8 {0.14}	2 {0.02}	13 {0.59}	3 {0.02}
	3	0 {0.0}	0 {0.0}	64 {1.75}	0 {0.0}
	4	0 {0.0}	0 {0.0}	0 {0.0}	0 {0.0}
Participant 8	1	0 {0.0}	0 {0.0}	0 {0.0}	0 {0.0}
	2	0 {0.0}	2 {9.68}	3 {9.68}	0 {0.0}
	3	0 {0.0}	0 {0.0}	1 {3.23}	0 {0.0}
	4	0 {0.0}	0 {0.0}	0 {0.0}	0 {0.0}

3.3.2 Missing Data Filling

Gaps (missing) of the marker data were filled using the interpolation function in *MATLAB*.

The filling process contained the following three steps:

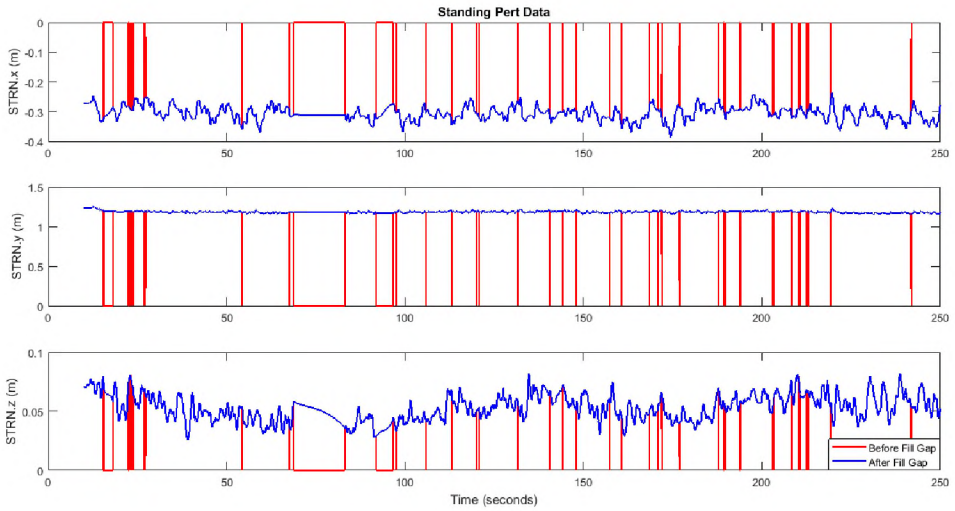

Figure 7: Gap filling result in experiment trial three of participant two. Red lines are original recorded data, which several frames' data were zero due to marker missing. Blue lines are filled marker data, which all the gaps were filled with reasonable data.

1. Find out the index of marker data with value zero. (D-Flow writes zero value in the file when a marker is not recognized. We assume that the position of marker will never be exactly zero if the marker was not missing.)

2. Generate recorded marker data and corresponding time vector after removing the missing marker data and corresponding time stamps.

3. Generate the estimated value of missing marker data using interp1 function in *MATLAB* with generated marker data in the above step.

Piece-wise Cubic Hermite Interpolating Polynomial (PCHIP) option was used in the 'interp1' function in *MATLAB*. Good filling results were achieved even with large data gap period. One example of the gap filling is shown in Figure 7.

3.3.3 Calculation of Joint Angles and Torques

Joint angles and torques were calculated using a 2d gait model (`https://github.com/csu-hmc/GaitAnalysisToolKit`). In the calculation, joint angles were averaged between the left and right legs based on the assumption that participants' movement

were symmetric. Sign definition of the ankle, knee, and hip joints are shown in Figure 8. Ground reaction forces(GRF) in the perturbed trials were compensated [10] to remove the inertia artifact of the moving treadmill. A comparison of raw GRF and the compensated GRF is shown in Figure 9. Compensated GRF has much lower amplitude than the raw GRF, showing that the measured GRF was largely affected by the inertia of the heavy treadmill. Since almost all reactions to perturbation were in the sagittal plane, a two dimensional seven-link human body model was used [11] to calculate joint torques through inverse dynamics. Joint torques were also averaged between left and right legs. The sign convention for joint torques are the same as joint angles. An example (participant 7 trial 3) of the calculated joint angles and torques is shown in Figure 10. Both joint angles and torques were zeroed by subtracting the mean value of the quiet standing period (first 10 second) in each trial. The assumption here is that human trends to save energy in quiet standing, so that the joint angles should be close to zero which requires the minimum joint torques. In addition, because the postural feedback controllers that will be identified from the motion data is for controlling the humanoid robots or P/O devices, it is better to have zero joint angles at quiet standing, so that less joint torques will be required.

3.3.4 Repository of Processed Data

Processed data in each experiment trial were saved into four files:

1. Mocapxxxx.txt: contains the gap filled motion capture data and the inertia compensated ground reaction force data.

2. Motionxxxx.txt: contains the calculated trajectories of three joints' (hip, knee, and ankle) angles, angular velocities, moments, and joint contact forces.

3. Data_infoxxxx.txt: contains the quality of recorded raw marker data (percentage and biggest duration of missing marker data), and the percentage of removed the inertia artifacts in ground reaction forces.

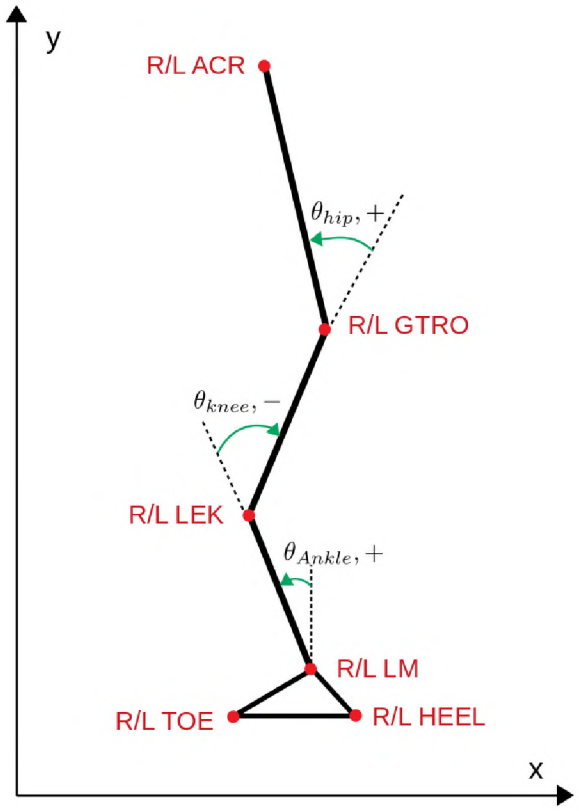

Figure 8: Human body diagram in standing balance task. The markers used for joint angles calculation is named in red color. The definition of joint angles is shown in the plot. Positive joint angles are defined with counterclockwise rotation. Joint torques have the same sign as joint angles.

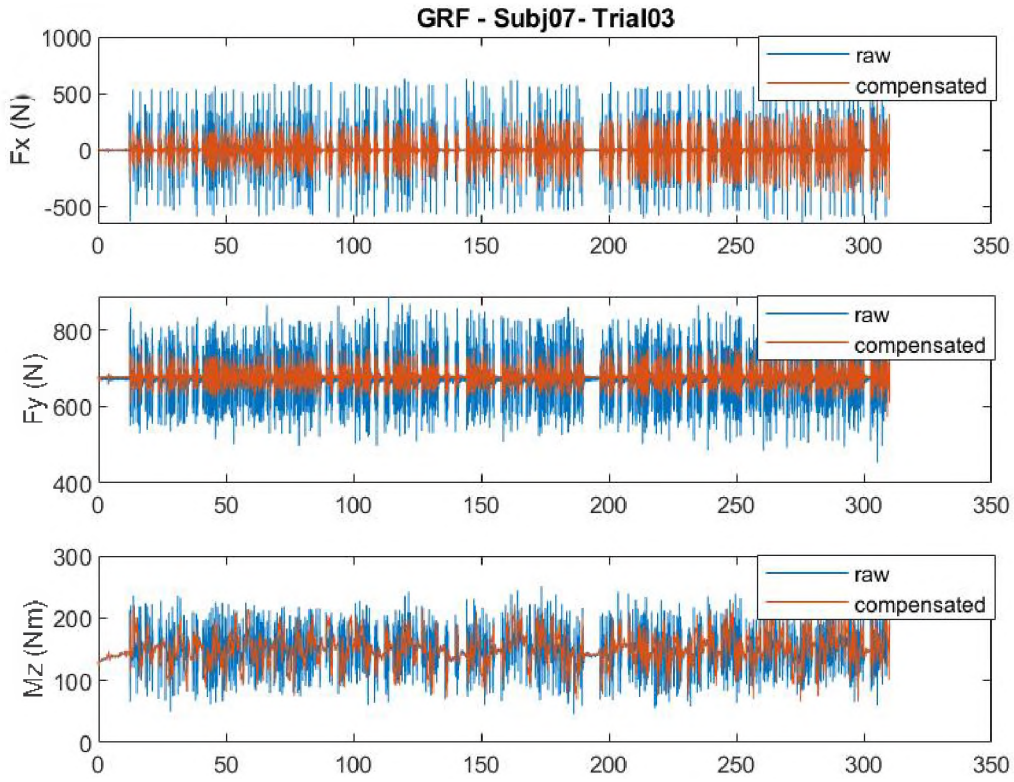

Figure 9: A comparison of raw ground reaction force and compensated ground reaction force.

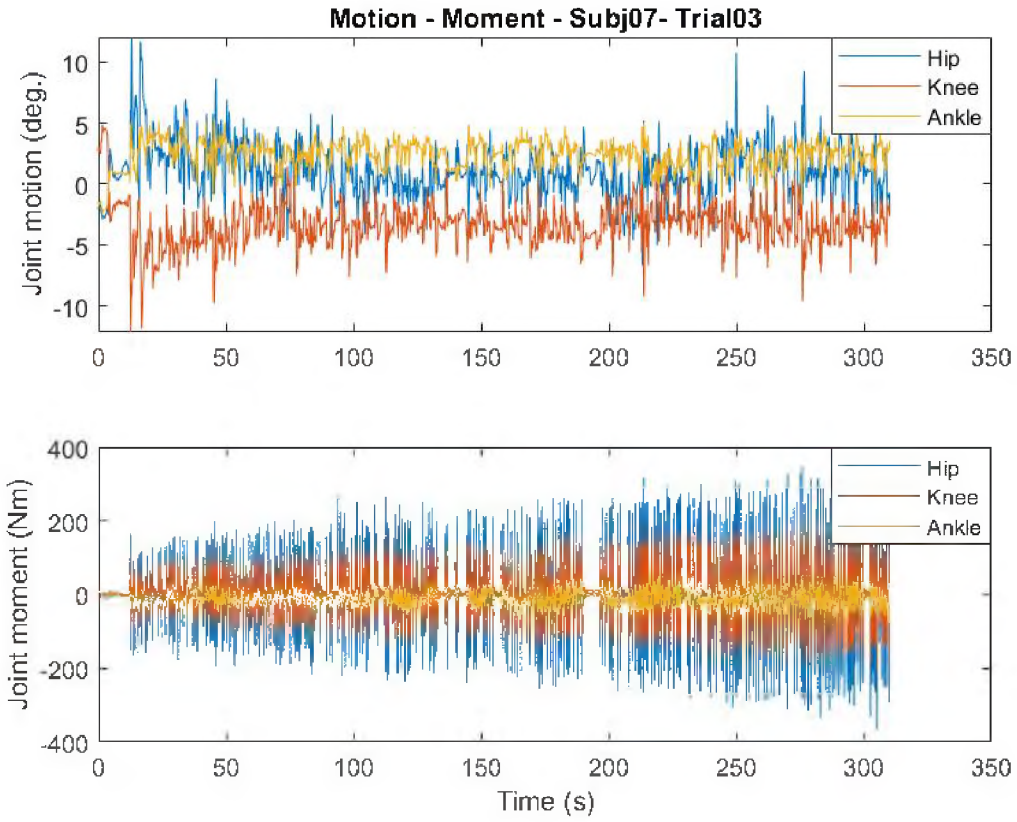

Figure 10: Joint angles and torques of participant 7 and experiment trial 3.

4. MotionAnalysis.fig: shows the mean and standard deviation of three joints' trajectories in four experimental trials.

3.3.5 Analysis of Joint Motions

Here we calculated the means and standard deviations of the joint angles for the last six participants. These statistical information are shown in Figure 11 - 16. The first and fourth experimental trials were quiet standing trials. The second and third trials were perturbed trials. Motion variations in perturbed trials were much larger than quiet standing trials, showing that perturbation had evoked the human standing system in a larger variety situations. The two quiet standing trials had similar variation of joint motion. However, there was a difference in the variation of joint motion between two perturbed trials. The second perturbation trials (repeated perturbation trial) had a relative smaller variation than the first perturbation trial for almost all participants.

3.4 Discussion

Based on our analysis, the measured data from the standing balance experiment has good quality for postural controller identification. Most marker data had less than 1% missing data or less than 20 frames (0.2 second) of the maximum missing gap, except for the third trial of the second participant. With 0.2 second data missing period, interpolation can help fill them up very well. Considering the first two participants were pilot studies (their data were not used in the identification study), the quality of the standing experiment data is good.

As expected, the perturbation trials had larger motions than the quiet standing trials. This means that perturbation did cause participants to control their body motions while maintaining standing balance. The averaged knee angles are positive and averaged hip angles are negative for most participants. This means that they bent their knee and leaned their trunk forward in the standing balance experiment. This is typical reaction for most

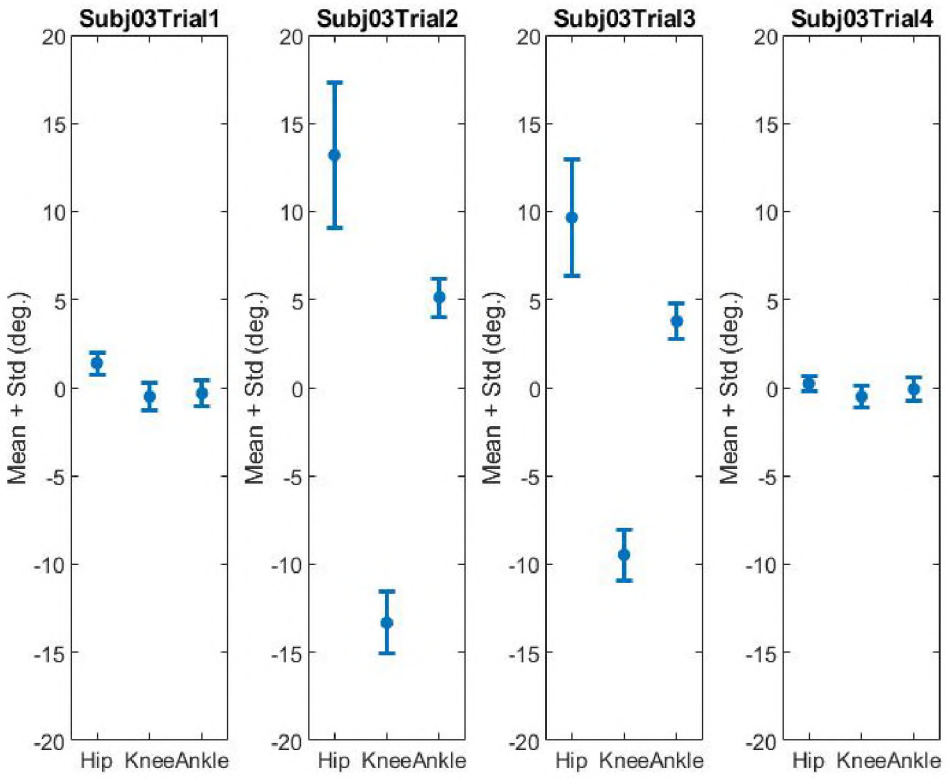

Figure 11: Joint angle analysis of subject 3. Analysis includes the mean and standard deviation of the ankle, knee, and hip joint motions.

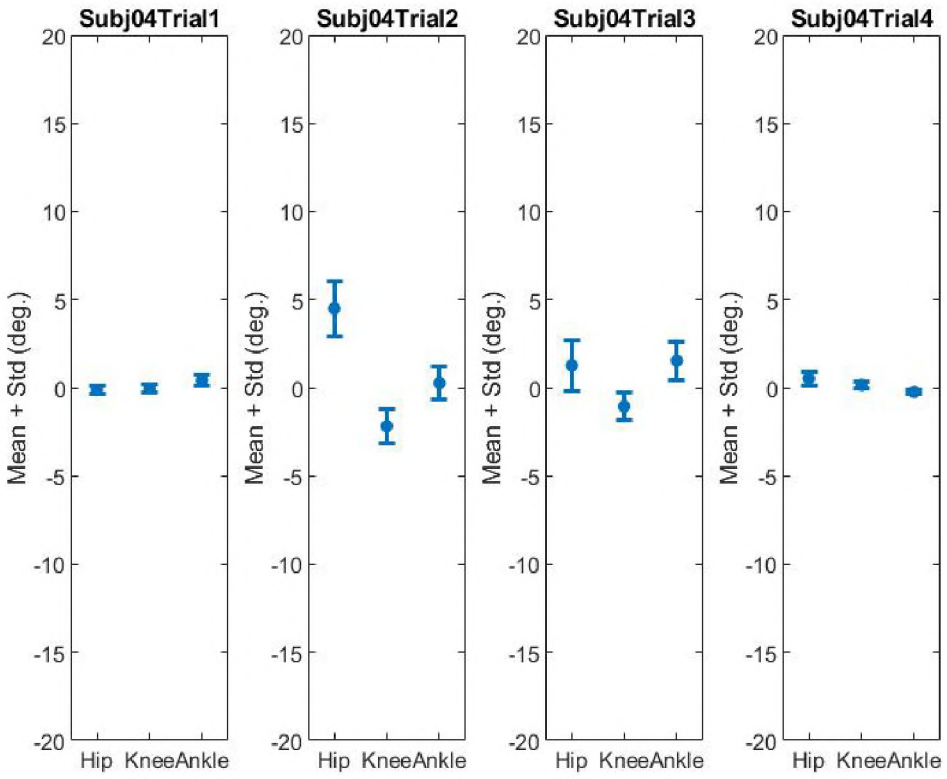

Figure 12: Joint angle analysis of subject 4. Analysis includes the mean and standard deviation of the ankle, knee, and hip joint motions.

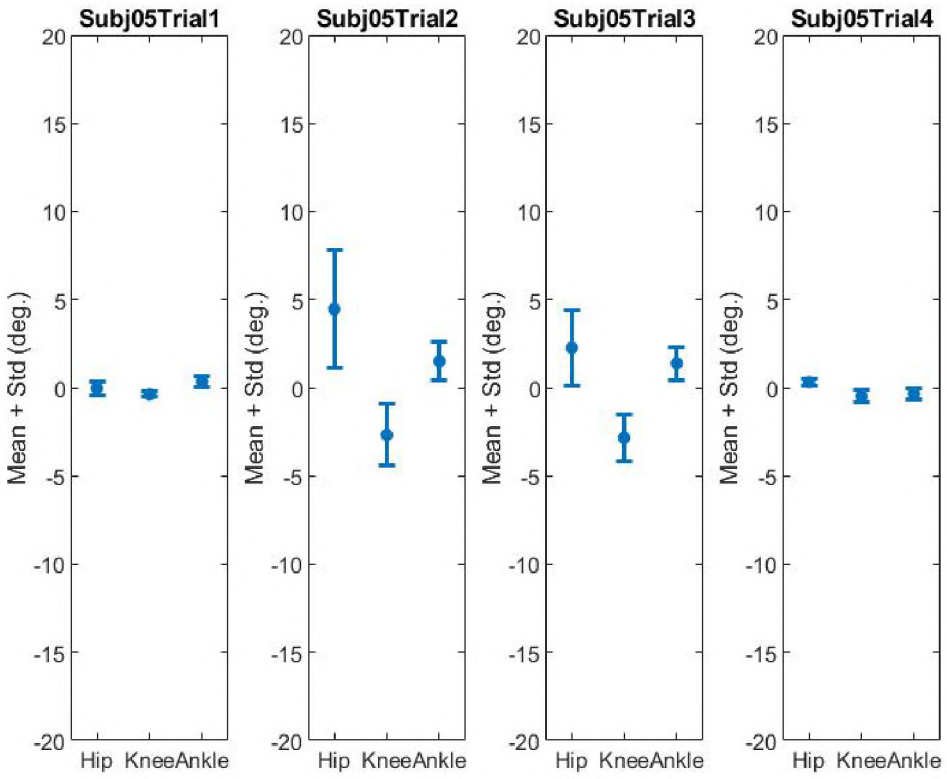

Figure 13: Joint angle analysis of subject 5. Analysis includes the mean and standard deviation of the ankle, knee, and hip joint motions.

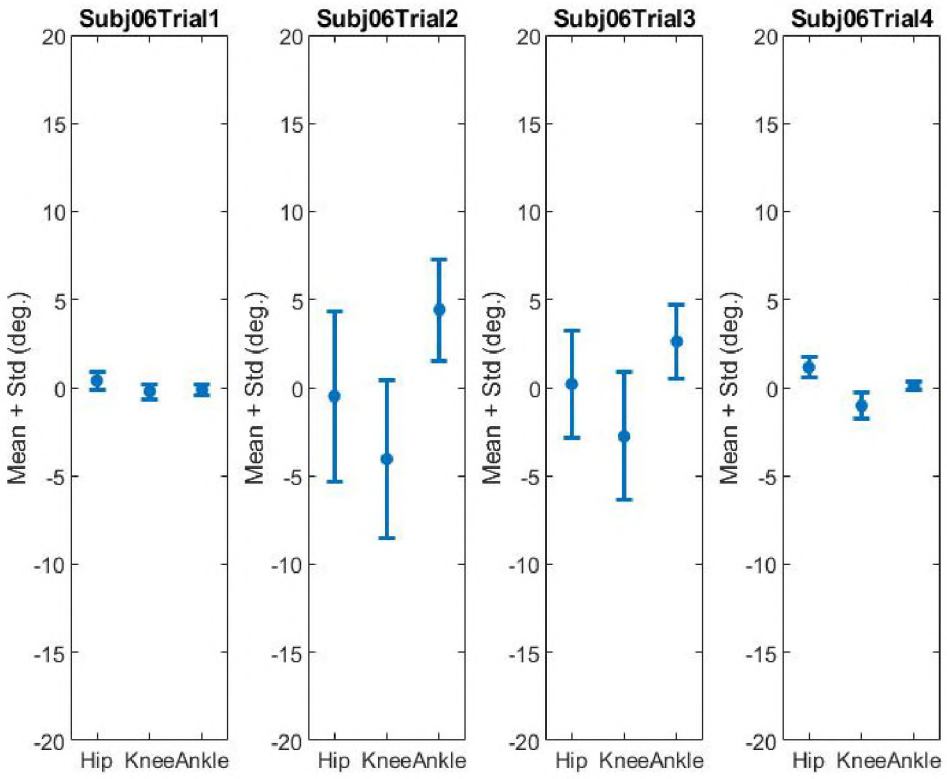

Figure 14: Joint angle analysis of subject 6. Analysis includes the mean and standard deviation of the ankle, knee, and hip joint motions.

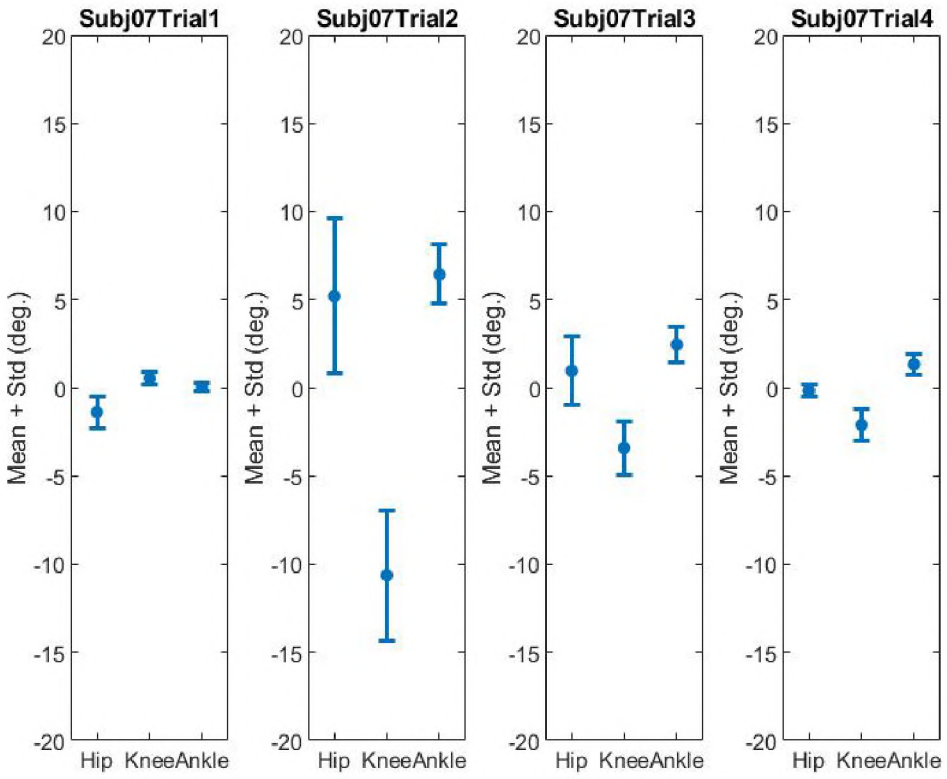

Figure 15: Joint angle analysis of subject 7. Analysis includes the mean and standard deviation of the ankle, knee, and hip joint motions.

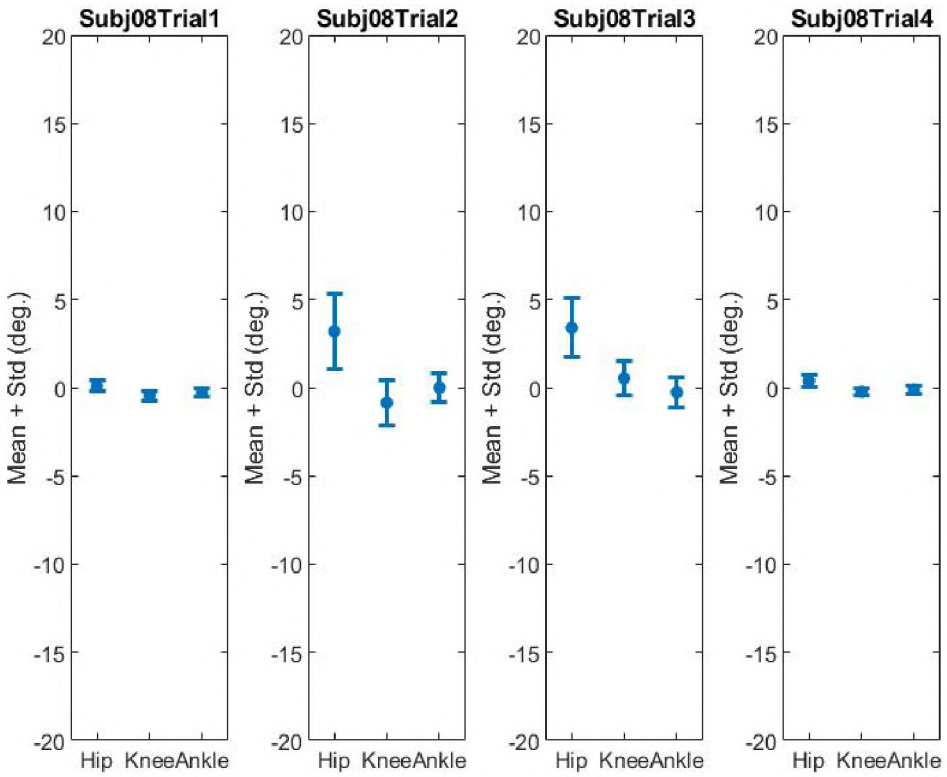

Figure 16: Joint angle analysis of subject 8. Analysis includes the mean and standard deviation of the ankle, knee, and hip joint motions.

people in daily experience during standing balance.

Perturbation trials did not have a significant effect on the quiet standing balance. The first and fourth trials of each participant are two quiet standing trials which were before and after perturbation trials. The range of joint motion in these two trials does not have a significant difference. This suggests that perturbation experience does not affect quiet standing balance. However, this have not been confirmed by qualitative study. We encourage some qualitative studies be done with the experiment data in future.

Participants had smaller joint motion range after the first perturbation experience. The repeated perturbation trial always has smaller motion range than the first perturbation trial when comparing the motion range for each participant. Since the same perturbation signal was used in both trials, this means participants adapted to the perturbation and could keep balance using smaller body swing motions. The first perturbation trial was more appropriate for extracting postural balance information in daily activity situation, since participants haven't got used to the perturbation yet.

3.5 Conclusion

In the standing balance experiment, over 160 minutes standing balance data of 8 participants were recorded. From the analysis, the collected standing balance data are in good quality. Joint motions are reasonable and confirm with our daily standing balance experience. The collected experiment data is suitable for identifying generalized postural feedback controllers in the standing balance task.

3.6 REFERENCES

[1] R. Peterka, "Sensorimotor integration in human postural control," *Journal of Neurophysiology*, vol. 88, no. 3, pp. 1097–1118, 2002.

[2] S. Park, F. B. Horak, and A. D. Kuo, "Postural feedback responses scale with biome-

chanical constraints in human standing," *Experimental Brain Research*, vol. 154, no. 4, pp. 417–427, 2004.

[3] H. Van Der Kooij and E. De Vlugt, "Postural responses evoked by platform pertubations are dominated by continuous feedback," *Journal of Neurophysiology*, vol. 98, no. 2, pp. 730–743, 2007.

[4] T. D. Welch and L. H. Ting, "A feedback model explains the differential scaling of human postural responses to perturbation acceleration and velocity," *Journal of Neurophysiology*, vol. 101, no. 6, pp. 3294–3309, 2009.

[5] A. D. Goodworth and R. J. Peterka, "Sensorimotor integration for multisegmental frontal plane balance control in humans," *Journal of Neurophysiology*, vol. 107, no. 1, pp. 12–28, 2011.

[6] D. Engelhart, A. C. Schouten, R. G. Aarts, and H. van der Kooij, "Assessment of multi-joint coordination and adaptation in standing balance: a novel device and system identification technique," *IEEE transactions on Neural Systems and Rehabilitation Engineering*, vol. 23, no. 6, pp. 973–982, 2014.

[7] T. A. Boonstra, A. C. Schouten, and H. Van der Kooij, "Identification of the contribution of the ankle and hip joints to multi-segmental balance control," *Journal of Neuroengineering and Rehabilitation*, vol. 10, no. 1, p. 23, 2013.

[8] C. Maurer, T. Mergner, and R. Peterka, "Multisensory control of human upright stance," *Experimental Brain Research*, vol. 171, no. 2, p. 231, 2006.

[9] P. Konrad, "The abc of emg," *A practical Introduction to Kinesiological Electromyography*, vol. 1, no. 2005, pp. 30–35, 2005.

[10] S. K. Hnat, B. J. van Basten, and A. J. van den Bogert, "Compensation for inertial

and gravity effects in a moving force platform," *Journal of Biomechanics*, vol. 75, pp. 96–101, 2018.

[11] D. A. Winter, *Biomechanics and motor control of human movement*. John Wiley & Sons, 2009.

CHAPTER IV

IDENTIFICATION OF THE HUMAN POSTURAL CONTROLLERS THROUGH STOCHASTIC TRAJECTORY OPTIMIZATION

Journal Publication:

1. H. Wang and A. J. van den Bogert, 2020. Identification of the Human Postural Control System through Stochastic Trajectory Optimization. Journal of Neuroscience Methods, 334(15) p.108580.

Conference Abstract:

1. H. Wang and A. J. van den Bogert, Controller Identification in Human Standing Balance. Dynamic Walking 2018.

ABSTRACT

System identification can be used to obtain a model of the human postural control system from experimental data in which subjects are mechanically perturbed while standing. However, unstable controllers were sometimes found, which obviously do not explain human balance and cannot be applied in control of humanoid robots. Eigenvalue constraints can be used to avoid unstable controllers. However, this method is hard to apply to highly nonlinear systems and large identification datasets. To address these issues, we perform the system identification with a stochastic system model where process noise is modeled. The parameter identification is performed by simultaneous trajectory optimizations on multiple episodes that have different instances of the process noise. The stochastic and deterministic identification methods were tested on three types of controllers, including both linear and nonlinear controller architectures. Stochastic identification tracked the experimental data nearly as well as the deterministic identification, while avoiding the unstable controllers that were found with a deterministic system model. Comparing to eigenvalue constraints, stochastic identification has wider application potentials. Since linearization is not needed in the stochastic identification, it is applicable to highly nonlinear systems, and it can be applied on large data-sets. Stochastic identification can be used to avoid unstable controllers in human postural control identification.

4.1 Introduction

Feedback control is a well accepted paradigm for human postural balance [1]. Identification of a feedback control system from human experiments has several important applications. In neuroscience, control system models are used to understand how humans maintain balance. In clinical applications, a quantitative description of the control system, e.g. as feedback gains and time delays, may have clinical applications. Finally, in humanoid robotics, a control system identified from human subjects can produce behavior that is more human-

like than a control system designed from conventional control engineering principles.

System identification methods have been used, in both frequency and time domains, to identify feedback controllers from human experiments [2–4]. In the frequency domain, information of human neuromuscular control were identified on experimental data with multiple random perturbations [2, 4–8]. In the time domain, parametric controllers were usually identified and it has been shown that a single stimulus is sufficient for multiple-input multiple-output (MIMO) system identification [9]. For instance, full-state proportional-derivative (FPD) controllers were identified on short experimental data where ramp perturbations were applied to the standing surface. Results showed that controller gains were proportional to the amplitudes of ramp perturbations [3, 10], which suggests a nonlinear control system.

However, one common issue of the time domain identification work is that the best fit to the experiment was sometimes achieved with a controller that causes the closed loop system to be unstable. [3, 9]. While the best fit controller is always treated as the best identified controller, it is not useful since it can neither be applied to humanoid robots nor explain how humans control themselves. One possible reason of finding unstable controllers is that the process noise in both human system and experiment is not modeled. The identified controllers may take advantage of instability and sensitivity to initial conditions to achieve the best fit without falling.

To avoid instability, eigenvalue constraints have been used in the controller identification. It enforces eigenvalues of the modeled closed loop system to be negative at a specific pose while identifying the controller parameters. This method was successful in avoiding unstable linear controllers in standing balance identification under ramp perturbations [3]. However, the application of this method is limited. For instance, it cannot work with highly nonlinear systems, since only a limited set of linearization points can be checked. For complex tasks such as walking, this could become impractical. In addition, it is hard to incorporate eigenvalue constraints into identifications with long experimental recordings,

in which gradient-based optimization and collocation methods are needed. Long recordings, under continuous random perturbation, are needed to collect sufficient information to identifying more complex posture controllers. Direct collocation has been reported to be more efficient in such parameter identification problems [11, 12].

In this study, we hypothesize that a stochastic optimization, in which process noise is modeled, can help avoid finding unstable controllers in the standing balance identification problem. The stochastic optimization was applied on the identification of three types of controllers. Eigenvalue and forward simulations tests were done to examine the practical stability of the identified systems.

4.2 Methods

An indirect identification approach was used in this study [2–4, 9]. In the indirect approach, a model is built, which mathematically represents the closed loop system and an optimization method is used to fit experiment data by optimizing the model parameters. It has been reported that, in identifying the feedback controllers, the indirect approach can avoid the bias introduced by the direct approach which only uses the information of controller input and output [13]. In this study, the mathematical model of the human standing balance system was treated as a closed-loop system which includes a body dynamics model and a feedback controller. The body dynamics model was simplified as a double-link pendulum, since ankle and hip strategies are mostly used for standing balance [14, 15]. Three feedback controllers, as described below, were identified. The goal of the identification is to find the feedback controller parameters P which enable the closed-loop system generate the response that is closest to the human experimental data (Fig. 17).

4.2.1 Experiments

Experiments were performed on six participants (five male, one female, age 18-34 years) with approval from the Institutional Review Board of Cleveland State University with the

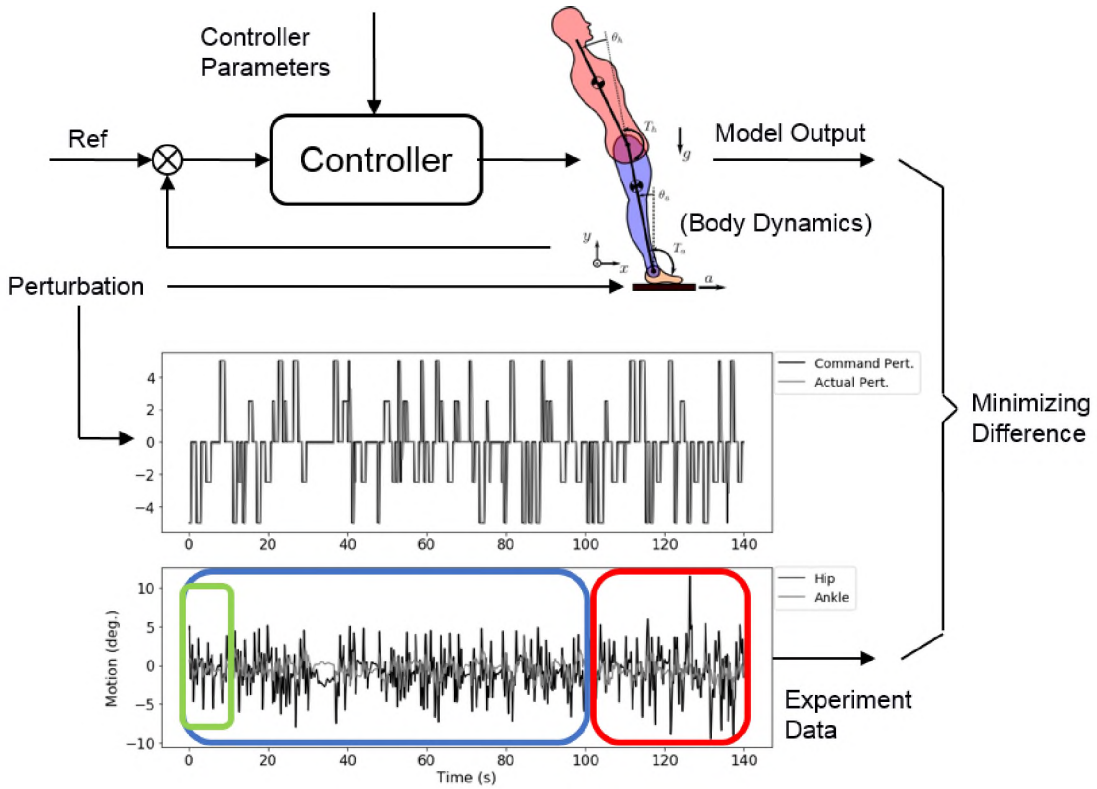

Figure 17: For identification of controller parameters, the same perturbation which was applied in the experiment was applied to the closed-loop system model. Controller parameters are optimized to fit the experimental data. The experimental data (140 seconds) was divided into 3 sections. The first 100 seconds (blue) were used to identify the linear controllers. The first 10 seconds (green) were used to identify the nonlinear controller. The last 40 seconds (red) were used to verify all identified controllers.

study number IRB-FY2018-40. A R-Mill instrumented treadmill (Forcelink, Netherlands) was used to induce anterior-posterior (AP) perturbations of the standing platform through its ”sway” mechanism. Participants were asked to stand with their arms crossed in front of their chest and instructed to keep balance without taking a step. The perturbation signal was designed using random square pulses with five amplitudes ([-5, -2.5, 0, 2.5, 5] cm), and six pulse durations ([0.25, 0.5, 0.75, 1.0, 1.25, 1.5] seconds). Amplitudes and durations were randomly selected to generate a 140 second perturbation signal. Twenty-seven reflective markers were placed on each participant to record their reactions using a 10-camera motion capture system (Osprey 00882967, Motion Analysis Corp. Santa Rosa, CA). Hip and ankle joint motions were calculated from the recorded marker data, and the platform

motion was recorded from encoders. The commanded perturbation signal, actual perturbation signal (standing platform motion) and balance reaction data (ankle and hip motion) of one participant can be found in figure 17. Data from this participant was used to show how the modeling of a stochastic environment affects the practical stability of identified controllers.

4.2.2 Controller Structures

Three feedback controllers were identified on the data described in Section A. Two of them are linear: a proportional-derivative (PD) controller and a full-state proportional-derivative (FPD) controller. The other one is nonlinear: neural network (NN) controller. Formulas of these three controllers are shown below:

PD controller:

$$\begin{bmatrix} T_a \\ T_h \end{bmatrix} = \begin{bmatrix} K_{p_a} & 0 & K_{d_a} & 0 \\ 0 & K_{p_h} & 0 & K_{d_h} \end{bmatrix} \begin{bmatrix} \theta_a - \theta_a^r \\ \theta_h - \theta_h^r \\ \dot{\theta}_a \\ \dot{\theta}_h \end{bmatrix} \tag{4.1}$$

FPD controller:

$$\begin{bmatrix} T_a \\ T_h \end{bmatrix} = \begin{bmatrix} K_{p_{aa}} & K_{p_{ah}} & K_{d_{aa}} & K_{d_{ah}} \\ K_{p_{ha}} & K_{p_{hh}} & K_{d_{ha}} & K_{d_{hh}} \end{bmatrix} \begin{bmatrix} \theta_a - \theta_a^r \\ \theta_h - \theta_h^r \\ \dot{\theta}_a \\ \dot{\theta}_h \end{bmatrix} \tag{4.2}$$

where T_a and T_h are ankle and hip joint torques; θ_a and θ_h are ankle and hip joint angles; θ_a^r and θ_h^r are the reference joint angles for ankle and hip at quiet standing; $\dot{\theta}_a$ and $\dot{\theta}_h$ are ankle and hip joints angular velocities; K_p and K_d are proportional and derivative gains of feedback controllers.

For the nonlinear controller, a standard neural network architecture [16] with 1 hidden layer and 4 hidden nodes was used. The inputs are the system state and a constant value node, and the outputs are joint torques (figure 18).

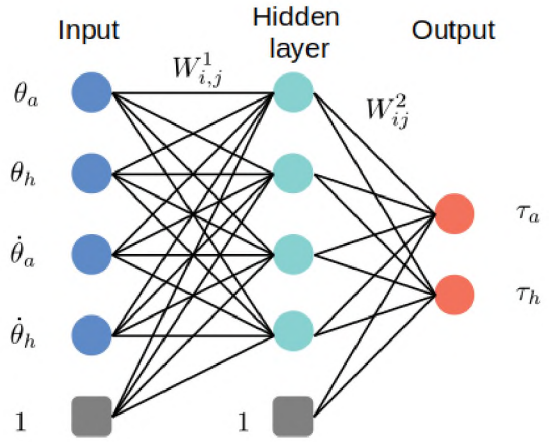

Figure 18: Structure of neural network controller that with 1 hidden layer and 4 hidden nodes.

The smoothed leaky-ReLU function was used as activation function and is showing in equation 4.3. The reason to smooth the activation function is make it continuously differentiable, which is essential to gradient-based optimization.

$$f(x) = x + 0.7(\frac{x - \sqrt{x^2 + 0.0001}}{2}) \tag{4.3}$$

The control parameters in these two types of linear controllers are the proportional-derivative gains K and reference joint angles θ^r. The control parameters in the neural network are the weights W_{ij} applied in between the input layer, the hidden layer, and the output layer. The total number of controller parameters in the PD, FPD, and NN controllers are 6, 10 and 30, respectively.

4.2.3 Controller Identification in Deterministic Environment

Models with a deterministic environment, without modeling of process noise, have been used in many controller identification studies [3, 4, 9]. The deterministic standing balance

controller identification problem can be defined as a combined trajectory and parameter optimization problem:

$$\begin{aligned} &\text{Optimize trajectory } x(t) \text{ and control parameters } P \\ &\text{Minimize objective function } F = \int_0^T \|\theta_m(t) - \theta(t)\|^2 dt \\ &\text{Subject to: body dynamics: } f(x(t), \dot{x}(t), P, a) = 0 \end{aligned} \tag{4.4}$$

where $x(t)$ is the state trajectory of the identified system, including ankle/hip joint angles θ and angular velocities $\dot{\theta}$; P represents the control parameters inside the feedback controller; T is the total time period of the measured experimental data; θ_m is the measured joint angles; θ is the optimized joint angles; a represents the acceleration of external perturbation;

4.2.4 Controller Identification in Stochastic Environment

In a stochastic environment, process noise is considered in the controller identification process. In controller identification with stochastic environment, the optimization is carried out over multiple episodes. Each episode simulates the motions with the same controller, and the same perturbation signal, but with a different process noise signal. The identifica-

tion problem for the stochastic environment is defined below:

$$\begin{aligned}
&\text{Optimize trajectory } \{x^1(t), ..., x^M(t)\} \text{ and Controller Parameters } P \\
&\text{Minimize objective function: } F = \sum_{s=1}^{M} \left(\int_0^T \|\theta_m(t) - \theta^s(t)\|^2 * dt \right) \\
&\text{Subject to: body dynamics: } \left\{ \begin{array}{c} f_1(x(t), \dot{x}(t), P, a) + n_1(0, \sigma) = 0 \\ ..... \\ f_s(x(t), \dot{x}(t), P, a) + n_s(0, \sigma) = 0 \\ ..... \\ f_M(x(t), \dot{x}(t), P, a) + n_M(0, \sigma) = 0 \end{array} \right\}
\end{aligned} \tag{4.5}$$

where M is the total number of episodes; s is the s^{th} episode; $x^s(t)$ is the state trajectory of human system model in s^{th} episode; $n_s(0, \sigma)$ is random noise added to s^{th} episode.

The direct collocation method [17] was used in this study. This transforms the trajectory optimization problem into a nonlinear program (NLP) with a finite number of unknowns: the states x at N collocation nodes, and the controller parameters [12, 15]. The Midpoint Euler approximation was used to convert the body dynamics constraint into algebraic constraints:

$$f(\frac{x_{i+1} + x_i}{2}, \frac{x_{i+1} - x_i}{h}, P, a) = 0, \quad for\ i = 1, 2, ..., N - 1. \tag{4.6}$$

The number of collocation nodes was 50 per second, and IPOPT was used to solve the NLP [18].

Four identification problems were solved for each controller structure. For each controller, a deterministic identification was performed first. For the linear controllers (PD, FPD), stochastic identifications with 2, 3, and 4 episodes were performed. For the nonlinear neural network controller, stochastic identification were performed with 6, 8, and 10

episodes. The process noise was modeled as Gaussian random noise with amplitude of $\pm$ 0.25 Nm, added to the controller outputs (joint torques) at each time step. The process noise in each episode was randomly generated, and kept the same during the optimization process. For each identification problem, 10 optimizations with random initial guesses were performed. By selecting the best fit with experiment data among 10 optimizations, local optimum results can be largely prevented.

4.2.5 Practical stability evaluation

Eigenvalues and forward simulations were used to evaluate the finite time practical stability of the closed loop standing balance system with the identified controllers. In practice, it is very hard to quantify the stability of a nonlinear system, especially under external perturbations. The practical stability [19] is a more appropriate concept to examine the stability of the identified systems here. In the eigenvalue test, the closed loop system dynamics were linearized to obtain eigenvalues at different operating points. These points covered the range of motion observed in the experiment. In the forward simulation tests, the identified controllers were used to perform 40 seconds simulations with all possible initial conditions inside the experiment data range. The perturbation (in red block) used in the forward simulation was different from the perturbation used in identifications. No process noise was used in these tests.

The distribution of four state variables (ankle angle, hip angle, ankle angular velocity, hip angular velocity) in the experimental data is shown in figure 2A. Ranges of these four state variables in degree and degree/s are between [-3.87, -9.49, -16.53, -50.74] and [2.41, 11.50, 18.38, 65.00]. To check the stability of identified controllers in a standard way, eleven equidistant values were chosen within the range of each state variable, resulting in $11 \cdot 11 \cdot 11 \cdot 11 = 14641$ operating points where eigenvalues were calculated. The percentage of stable operating points (all eigenvalues negative) was calculated. Forward simulation tests used each of these operating points as an initial condition. A simulation

was considered practically stable if the root mean square (RMS) between the forward simulations and the experiment data was within 3 times the standard deviation of experiment data. The percentage of practically stable simulations was calculated for each identified controller. The eigenvalue and forward simulation tests were performed using the Ohio Super Computer System [20].

4.3 Results

Results of the identifications are summarized in Fig. 19. The percentage of stable eigenvalues and practically stable forward simulations (Fig. 2b) is always below 100%. One reason is that many of the checking points were outside of the range of actual state trajectories. Nevertheless, the effect of identification method on practical stability was clearly seen.

In the PD and NN controllers, results suggest that mostly controllers found through the stochastic identification can achieve practically stable for the simulation system, while unstable controllers were found in the deterministic identifications. When the stochastic environment was introduced and the episode number increased to a specific number (3 episodes for PD controller type, 8 episodes for NN controller type), the identified controllers suggests practically stable, which has high percentages of stable eigenvalues and practically stable forward simulations.

In the FPD control architecture, the deterministic identification already suggested practical stability in about half of the tests. With the stochastic environment (2, 3, and 4 episodes), the percentage of stable eigenvalues and forward simulation remained high.

4.4 Discussion

Our results confirmed previous findings of unstable controllers when a deterministic model is used for identification of the human postural control system [3, 9]. The optimization is likely taking advantage of instability to improve the fit. In a deterministic unstable system, the final state can be made equal to the corresponding measurement, by extremely

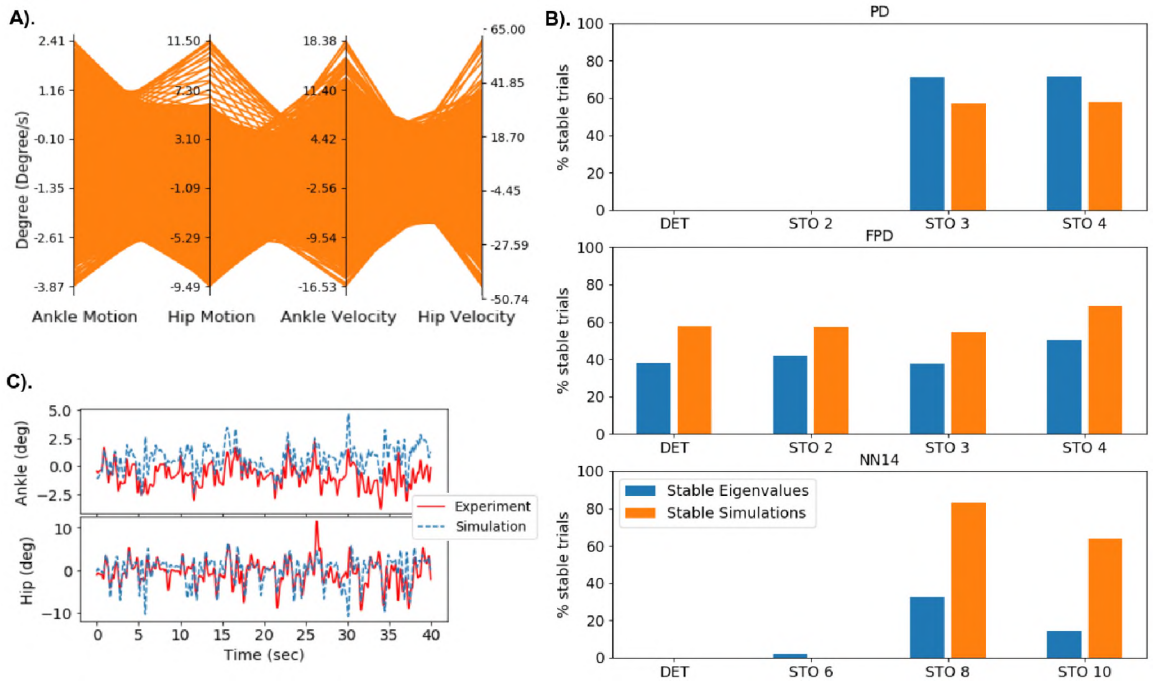

Figure 19: Eigenvalue and forward simulation test of identified best controllers on the operating points. Subplot A shows the range of each state variable from the human standing experiment data. subplot B is the percentages of stable eigenvalue and practically stable forward simulations of all 12 identified best controllers on selected operating points. "DET" means deterministic optimization. "STO i" means stochastic optimization with i episodes. Subplot C is one comparison between forward simulation and experiment data. RMS of this this forward simulation is about 1.3 STD of experiment data.

small changes in initial condition or controller parameters. We hypothesized that with a stochastic model, the optimization can no longer take advantage of instability to improve the fit with the experiment. The practical stability tests using eigenvalue analysis and forward simulation tests supported our hypothesis. We also found that stochastic approach did not affect the practical stability very much when the deterministic approach already found a practically stable controller. Identified control gains and eigenvalue distributions of PD and FPD controllers are shown in Appendix. In general, practically stable controllers identified from stochastic model are close to these unstable controllers identified through deterministic approach.

It needs to be noted that the forward simulation test was not a fully sufficient proof of the practical stability, since not 'any' $x(t_0)$ were tested. However, since a high density

mesh was used to generate the initial conditions $x(t_0)$, the high percentage of forward simulations that were within the 3 times STD of the experimental motion did suggest the finite time practical stability of the identified system.

The eigenvalue analysis and forward simulation tests were mostly in agreement about the practical stability of the system, except in the NN controller. This is not surprising because linearization may not give a reliable evaluation of stability in a system with strong nonlinearities. This finding also suggests that the use of eigenvalues as constraints in the identification problem [3] is not likely to give useful results for nonlinear controllers. In contract, the stochastic trajectory optimization presented here is directly applicable to nonlinear systems without linearization.

Generally, more episodes were needed to find practically stable controllers for more complex controller types with more free parameters. In the case of our study, identification of a practically stable PD controller requires three episodes, while identification of a practically stable NN controller required eight episodes. Because controller parameters (which are the same in each episode) and free initial conditions (which are different in each episode) can both be used to take advantage of instability, we suspect that the required number of episodes equals the number of control parameters divided by the number of system state variables.

The amplitude of Gaussian noise used in this study was 0.25 Nm, applied to the joint torques of human balance system. This is approximately one percentage of the standard deviation of the joint torques in the standing balance experiment. An amplitude of 0.5 Nm was also tried, which had the same practical stability effect of 0.25 Nm but resulted in slightly larger control parameter differences between the identified practically stable controllers.

Recently, similar ideas of using a stochastic environment were also used in other studies to get realistic and practically stable results in robotic control. Mordatch increased the success rate of path planning in a biped robot by adding model uncertainty [21]. Policies

for robot arm control were obtained by reinforcement learning in a simulated stochastic environment, making them robust enough for transfer to hardware [22]. Although these control optimization studies were not system identifications from experimental data, they share with our work the use of a simplified model of the real system. In order to avoid overly specialized controllers, stochastic dynamics can be used to produce better and more realistic solutions.

4.5 Conclusion

In this work, we showed that identification of human standing balance controllers by stochastic trajectory optimizations will produce controllers that are more robust than those obtained with a deterministic system model. When applied in robotic systems, these identified controllers will result in human-like behavior that is practically stable against small perturbations.

4.6 REFERENCES

[1] A. D. Kuo, "An optimal control model for analyzing human postural balance," *IEEE transactions on Biomedical Engineering*, vol. 42, no. 1, pp. 87–101, 1995.

[2] R. Peterka, "Sensorimotor integration in human postural control," *Journal of Neurophysiology*, vol. 88, no. 3, pp. 1097–1118, 2002.

[3] S. Park, F. B. Horak, and A. D. Kuo, "Postural feedback responses scale with biomechanical constraints in human standing," *Experimental Brain Research*, vol. 154, no. 4, pp. 417–427, 2004.

[4] H. Van Der Kooij and E. De Vlugt, "Postural responses evoked by platform pertubations are dominated by continuous feedback," *Journal of Neurophysiology*, vol. 98, no. 2, pp. 730–743, 2007.

[5] T. A. Boonstra, A. C. Schouten, and H. Van der Kooij, "Identification of the contribution of the ankle and hip joints to multi-segmental balance control," *Journal of Neuroengineering and Rehabilitation*, vol. 10, no. 1, p. 23, 2013.

[6] T. Kiemel, Y. Zhang, and J. J. Jeka, "Identification of neural feedback for upright stance in humans: stabilization rather than sway minimization," *Journal of Neuroscience*, vol. 31, no. 42, pp. 15144–15153, 2011.

[7] D. Engelhart, T. A. Boonstra, R. G. Aarts, A. C. Schouten, and H. van der Kooij, "Comparison of closed-loop system identification techniques to quantify multi-joint human balance control," *Annual Reviews in Rontrol*, vol. 41, pp. 58–70, 2016.

[8] M. Afschrift, I. Jonkers, J. De Schutter, and F. De Groote, "Mechanical effort predicts the selection of ankle over hip strategies in nonstepping postural responses," *Journal of Neurophysiology*, vol. 116, no. 4, pp. 1937–1945, 2016.

[9] A. D. Goodworth and R. J. Peterka, "Identifying mechanisms of stance control: a single stimulus multiple output model-fit approach," *Journal of Neuroscience Methods*, vol. 296, pp. 44–56, 2018.

[10] T. D. Welch and L. H. Ting, "A feedback model explains the differential scaling of human postural responses to perturbation acceleration and velocity," *Journal of Neurophysiology*, vol. 101, no. 6, pp. 3294–3309, 2009.

[11] M. Kelly, "An introduction to trajectory optimization: how to do your own direct collocation," *SIAM Review*, vol. 59, no. 4, pp. 849–904, 2017.

[12] J. K. Moore and A. J. van den Bogert, "opty: Software for trajectory optimization and parameter identification using direct collocation.," *J. Open Source Software*, vol. 3, no. 21, p. 300, 2018.

[13] H. van der Kooij, E. van Asseldonk, and F. C. van der Helm, "Comparison of different methods to identify and quantify balance control," *Journal of Neuroscience Methods*, vol. 145, no. 1-2, pp. 175–203, 2005.

[14] F. B. Horak and L. M. Nashner, "Central programming of postural movements: adaptation to altered support-surface configurations," *Journal of Neurophysiology*, vol. 55, no. 6, pp. 1369–1381, 1986.

[15] J. Moore and A. van den Bogert, "Human standing controller parameter identification with direct collocation," in *15th International Symposium on Computer Simulation in Biomechanics*, ISB, 2015.

[16] A. K. Jain, J. Mao, and K. Mohiuddin, "Artificial neural networks: A tutorial," *Computer*, no. 3, pp. 31–44, 1996.

[17] C. R. Hargraves and S. W. Paris, "Direct trajectory optimization using nonlinear programming and collocation," *Journal of Guidance, Control, and Dynamics*, vol. 10, no. 4, pp. 338–342, 1987.

[18] A. Wächter and L. T. Biegler, "On the implementation of an interior-point filter line-search algorithm for large-scale nonlinear programming," *Mathematical Programming*, vol. 106, pp. 25–57, Mar 2006.

[19] L. Vangipuram *et al.*, *Practical stability of nonlinear systems*. World Scientific, 1990.

[20] O. S. Center, "Ohio supercomputer center." `http://osc.edu/ark:/19495/f5s1ph73`, 1987.

[21] I. Mordatch, K. Lowrey, and E. Todorov, "Ensemble-cio: Full-body dynamic motion planning that transfers to physical humanoids," in *Intelligent Robots and Systems (IROS), 2015 IEEE/RSJ International Conference on*, pp. 5307–5314, IEEE, 2015.

[22] X. B. Peng, M. Andrychowicz, W. Zaremba, and P. Abbeel, "Sim-to-real transfer of robotic control with dynamics randomization," in *2018 IEEE International Conference on Robotics and Automation (ICRA)*, pp. 1–8, IEEE, 2018.

CHAPTER V

IDENTIFICATION OF POSTURAL CONTROLLERS IN HUMAN STANDING BALANCE

Conference Abstract:

1. H. Wang and A. J. van den Bogert. Standing balance Controller Identification with Direction Collocation. Dynamic Walking 2016.

ABSTRACT

Standing balance is a simple task for healthy humans but it is not known which control laws are used by the central nervous system (CNS). Identification methods have been used by numerous studies and many mathematical models of the CNS have been extracted, however, limitations exist in these commonly used identification methods. In this chapter, we propose that the trajectory optimization with direct collocation method can identify parametric CNS models from long duration motion data without assuming the identifying system to be linear. We first examined this identification method using synthetic motion data which showed that it can extract correct control parameters. Then, six types of controllers, from simple linear to complex nonlinear, were identified from 100 seconds experimental data. Results from the identifications showed that time-delay and nonlinear property are both needed in order to explain the standing balance motions under randomly external perturbations.

5.1 Introduction

Standing balance is a simple motion task which allows researchers to investigate the function of humans' central nervous system (CNS). Numerous studies have treated the CNS in human standing balance as a postural feedback controller and identification methods have been used to find it's mathematical model [1–13]. In most of these studies, an external stimulus or multiple stimuli, such as push/pull forces and standing platform motions, was used to evoke participants' body sway motion at larger variety situations. Indirect identification approaches were usually used in these studies, in which a closed-loop mathematical model of the human standing balance system is required. It has been reported that the indirect approach (closed-loop identification) can avoid the bias caused by the open-loop identification that only use the information of CNS inputs (joint motions) and outputs (joint torques) [14, 15]. Even though both non-parametric and parametric mathematical models

have been identified which have no doubt helped understand the function of the CNS in human standing balance activity, limitations exist in both study directions which prevented finding better mathematical models of the CNS.

In non-parametric postural controller identifications, the CNS was described as a frequency response function (FRF) [11, 12, 16]. The frequency domain identification method was usually used to find the FRF of the closed-loop model including the CNS that can best explain the experimental data. Because the length of data does not matter when transferring to frequency domain through Fourier transform [17], this approach can be easily applied on long duration standing balance data that recorded from experiment where the random or multi-sine external perturbations were applied. In general, longer duration of an experiment with random perturbation can provide more information of the CNS which helps identify a generalized CNS model. However, this frequency domain approach requires multiple stimulating sources to identify a multi-input and multi-output (MIMO) system which is typical for human standing balance task since at least the ankle and hip strategies were used. Developing a hardware device that could provide multiple stimuli across body segments may be very difficult for many research groups and clinic applications. In addition, this approach treat the identifying systems as linear systems which missed the ability to identify the nonlinear property of the CNS. The human system itself includes many nonlinear components, e.g., the multibody dynamics and the nonlinear mechanical properties of muscles. It is reasonable to believe that the human standing balance task involves nonlinear properties, especially when external stimuli are large. For instance, studies have shown that humans use different feedback control gains to control postural on different amplitudes of perturbations [4, 7].

Parametric identification is to find appropriate control gains in a predefined control structure that can best explain the experimental data. Trajectory optimization can be used to solve this identification problem[18–20]. In this approach, both plant dynamics and the CNS control structure can be nonlinear since the identification is in time-domain and lin-

earization is not needed. However, only linear controllers have been identified on short duration motion data that perturbed by short ramp perturbations [4, 7, 21]. One of the reasons is that the shooting method used in these studies cannot handle long duration trajectory optimization, as the standing balance is naturally an unstable system. It is hard for the shooting method to find a long duration stable motion. Identifying postural controller on a long duration of motion data is essential to get a generalized controller than can explain humans' reactions at different situations, such as with ramp perturbations that have different amplitudes. Only recently, parametric identification has been done on long duration randomly perturbed standing motion data [22]. Whereas, the objective function in this study is to compare the FRF of the closed-loop model and the motion data in the frequency domain, which did avoid the forward simulation of the unstable system but has an assumption that identifying system is a linear system.

The goal of this study is to identify complex CNS models (control parameters) through trajectory optimization with the direct collocation method. This method has the advantage that it can identify complex nonlinear controllers from long duration experimental data. We first validate this method by doing identification on simulated data where the feedback control parameters are known. Then, we identified six types of feedback controller, from simple linear to complex nonlinear, on 100 seconds experimental data from a standing balance experiment. In the simulation study, we also investigated the effect of data length on the accuracy of identified control gains. In the controller identification of experimental data, identified control gains and suggesting properties of the CNS in standing balance were provided. The identification method proposed in this dissertation study is not limited on the postural controller identification, but can be extended to other studies, for example identifying step controllers from walking data.

5.2 Methods

An indirect identification approach was used in this study [3, 4, 22, 23]. In the indirect approach, a mathematical model is built, which represents the identifying system and an optimization method is used to fit experimental data by optimizing the model parameters. In this chapter, the mathematical model of the human standing balance system was treated as a closed-loop system which includes a standing dynamics model and a feedback controller. The standing dynamics model was simplified as a double-link pendulum without a knee, since ankle and hip strategies are mostly used for standing balance [19, 24]. Detail of the dynamic model can be found in Appendix A. The goal of the identification is to find the feedback controller parameters P which enable the closed-loop system model generate the response that is closest to the human experimental data (figure 20).

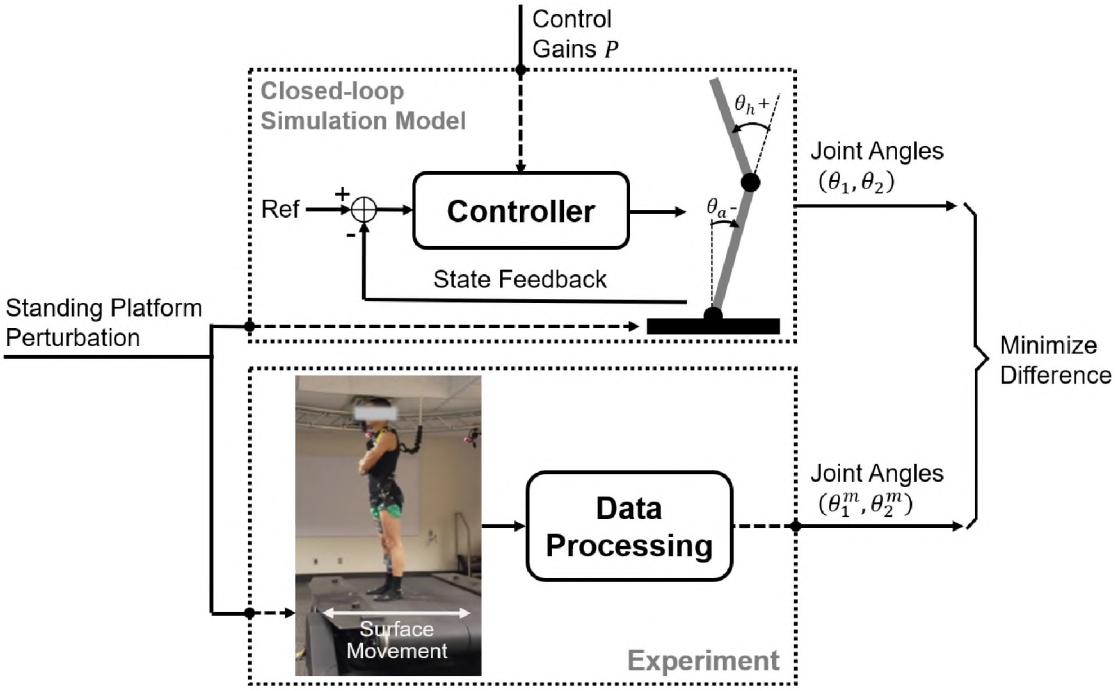

Figure 20: The indirect approach of standing balance controller identification. Identification can be treated as a trajectory optimization problem, in which the control parameters are optimized to minimize the difference between the model output and the experimental data.

5.2.1 Standing Balance Experiments

Experiments were performed on eight able-bodied participants (seven male, one female, age 18-35 years) with approval from the Institutional Review Board of Cleveland State University with the study number IRB-FY2018-40. A R-Mill instrumented treadmill (Forcelink, Amsterdam, Netherlands) was used to induce anterior-posterior (AP) perturbations of the standing platform through its "sway" mechanism. Participants were asked to stand with their arms crossed in front of their chest and instructed to keep balance without taking a step. The perturbation signal was designed using random square pulses with five amplitudes ([-5, -2.5, 0, 2.5, 5] cm), and six pulse durations ([0.25, 0.5, 0.75, 1.0, 1.25, 1.5] seconds). Amplitudes and durations were randomly selected to generate a 300 seconds perturbation signal. Twenty-seven reflective markers were placed on each participant to record their reactions using a 10-camera motion capture system (Osprey 00882967, Motion Analysis Corp. Santa Rosa, CA). Hip and ankle joint motions were calculated from the recorded marker data, and the platform motion was recorded from encoders.

The experimental procedure started with a 300 seconds quiet standing trial and then followed by a 300 seconds perturbation trial. Then participants were asked to sit down and rest for 300 seconds. After the rest, another 300 seconds perturbation trial which used the same perturbation as the previous trial was recorded. Finally, participants were asked to do another trial of 300 seconds quiet standing. General information of the participants are shown in Table V Experimental data and some preliminary analysis were shared on Zenodo: `https://doi.org/10.5281/zenodo.3631958`.

Simulated Motion Data

The identification method used in this chapter was first validated through simulated motion data. The closed-loop mathematical model in the indirect identification work was used to generate the simulation data. Parameters of the standing dynamics model, such as the segment mass, length, inertia, and the center of mass, were calculated based on the height and

Table V: Information of the eight participants in the order of collection date.

Id	Gender	Age (yr)	Height (m)	Mass (kg)
1	male	22	1.60	74.29 ± 0.26
2	female	–	–	48.37 ± 0.21
3	male	18	1.80	79.12 ± 0.20
4	male	27	1.78	63.10 ± 0.16
5	male	32	1.79	70.56 ± 0.19
6	male	35	1.65	58.24 ± 0.27
7	male	28	1.75	68.75 ± 0.17
8	male	27	1.63	60.33 ± 0.19

weight of participant No. 4 using the anthropometry table in Winter's book[25]. External perturbation used here is the randomized square pulses that used in the standing balance experiment. The postural feedback controller, a full state feedback PD controller with time delay, was the same as in the simulation study did by Goodworth and Peterka [22] Mathematical equation of the controller is shown in Eqn. 5.3. Pink noise (similar to Goodworth's study) was added at the motion feedback loop of each joint as sensor noise. One hundred seconds simulation data was generated using the Midpoint Euler method [26] and sampled in 100 Hz. Ten different realizations of sensor noise were generated and ten trials of simulated data under each sensor noise were generated. External perturbation, sensor noise, and simulated motion of one trial were shown in figure 21.

5.2.2 Controller Identification on Simulated Data

Controller identification on the simulated motion data was done through the described indirect approach by replacing the experimental data with simulated data. Five lengths (10, 30, 50, 70, and 90 seconds) of the simulation data (figure 21) were selected to be used for the controller identification. Lower and upper boundaries of the identifying controller parameters are 0 and 2 times the real control parameters. Ten optimizations were performed on each controller identification problem (controller identification on one period of data) with randomized initial guesses within the boundaries to eliminate local minimum. The identification result with the lowest objective function among ten optimizations was selected as

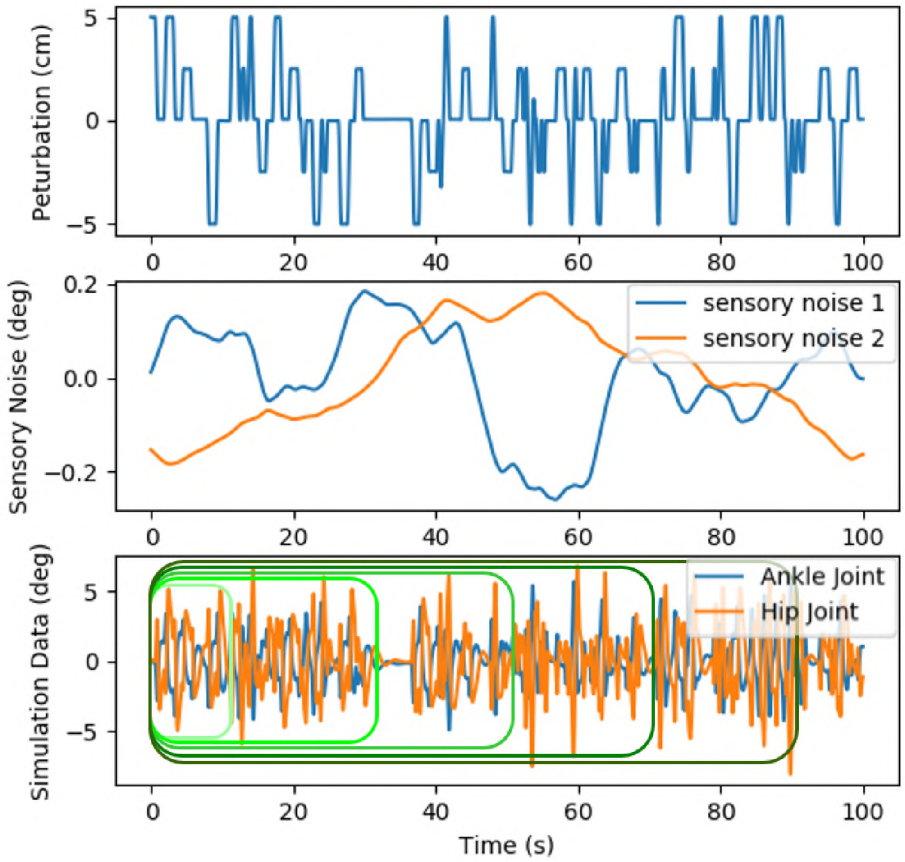

Figure 21: Simulated motion data with one realization of sensor noise. Sensor noise 1 is for ankle joint and 2 is for hip joint. Five data periods (10, 30, 50, 70, 90 seconds) were selected to identify the feedback control gains.

the best result and shown in the results section.

5.2.3 Controller Identification on Experimental Data

Controller identification on experimental data using the same indirect approach as the simulated data identification. One hundred seconds of the experimental data was selected in the middle of each perturbation trial of each participant to avoid the transit period of balance motion. Last six participants in the Table V were identified in this chapter, since the first two participants were in the preliminary testing of the experiment protocol. In total, there are 12 periods of experimental data (6 participants and 2 perturbation trials for each participant) that been selected to identify the standing balance controller.

Six types of controllers, from simple linear to complex nonlinear, were identified on

each selected data period. Three of them are linear: the proportional-derivative (PD) controller, the full-state proportional-derivative (FPD) controller, and the full-state proportional-derivative feedback with time delay controller (FPDTD) (a controller type that Goodworth used in his simulation study [22]). The other three are nonlinear: the linear state combination with time delay (LSCTD) controller, the neural network (NN) controller, and the neural network with time delay (NNTD) controller. The formulas of these six controllers are:

PD controller:

$$\begin{bmatrix} T_1(t) \\ T_2(t) \end{bmatrix} = \begin{bmatrix} K_{11} & B_{11} & 0 & 0 \\ 0 & 0 & K_{22} & B_{22} \end{bmatrix} \begin{bmatrix} r_1 - \theta_1(t) \\ 0 - \dot{\theta}_1(t) \\ r_2 - \theta_2(t) \\ 0 - \dot{\theta}_2(t) \end{bmatrix} \tag{5.1}$$

FPD controller:

$$\begin{bmatrix} T_1(t) \\ T_2(t) \end{bmatrix} = \begin{bmatrix} K_{11} & B_{11} & K_{21} & B_{21} \\ K_{12} & B_{12} & K_{22} & B_{22} \end{bmatrix} \begin{bmatrix} r_1 - \theta_1(t) \\ 0 - \dot{\theta}_1(t) \\ r_2 - \theta_2(t) \\ 0 - \dot{\theta}_2(t) \end{bmatrix} \tag{5.2}$$

FPDTD controller:

$$\begin{bmatrix} T_1(t+t_{d1}) \\ T_2(t+t_{d2}) \end{bmatrix} = \begin{bmatrix} K_{pas1} & 0 \\ 0 & K_{pas2} \end{bmatrix} \begin{bmatrix} r_1 - \theta_1(t+t_{d1}) \\ r_2 - \theta_2(t+t_{d2}) \end{bmatrix} + \begin{bmatrix} K_{11} & B_{11} & K_{21} & B_{21} \\ K_{12} & B_{12} & K_{22} & B_{22} \end{bmatrix} \begin{bmatrix} r_1 - \theta_1(t) \\ 0 - \dot{\theta}_a(t) \\ r_2 - \theta_h(t) \\ 0 - \dot{\theta}_h(t) \end{bmatrix} \tag{5.3}$$

LSCTD Controller:

$$\begin{bmatrix} T_1(t) \\ T_2(t) \end{bmatrix} = \sum_{i=0}^{D} \left(\begin{bmatrix} K_{11}^i & B_{11}^i & K_{21}^i & B_{21}^i \\ K_{12}^i & B_{12}^i & K_{22}^i & B_{22}^i \end{bmatrix} \begin{bmatrix} r_1 - \theta_1(t - i \cdot \Delta t) \\ 0 - \dot{\theta}_1(t - i \cdot \Delta t) \\ r_2 - \theta_2(t - i \cdot \Delta t) \\ 0 - \dot{\theta}_2(t - i \cdot \Delta t) \end{bmatrix} \right) \tag{5.4}$$

where $T_1(t)$ and $T_2(t)$ are the ankle and hip joint torques at time t; $\theta_1(t)$ and $\theta_2(t)$ are the ankle and hip joint angles at time t; r_1 and r_2 are the reference angles of the ankle and hip joints; K_{11} and B_{11} are the proportional and derivative gains for the ankle joint; K_{22} and B_{22} are the proportional and derivative gains for the hip joint; K_{21} and B_{21} are the proportional and derivative gains for the ankle joint from the hip joint angle and angular velocity feedback; K_{12} and B_{12} are the proportional and derivative gains for the hip joint from the ankle joint angle and angular velocity feedback; K_{pas1} and K_{pas2} are the passive proportional gains for ankle and hip joints; t_{d1} and t_{d2} are the delay time for the ankle and hip joints in the FPDTD controller; $\theta_1(t - i \cdot \Delta t)$ and $\theta_2(t - i \cdot \Delta t)$ are ankle and hip joint angles at $i \cdot \Delta t$ time prior to the current time t; K^i and B^i are the proportional and derivative gains that multiply with the state at $i \cdot \Delta t$ time prior to the current time t; D is the total number of delayed state feedback.

NN Controller:

The NN controller in this chapter was defined as standard neural network with one hidden layer and four hidden nodes (figure 22). It is a nonlinear controller, since its activation function is defined as a smoothed leaky-ReLU function: $f(x) = x + 0.7(\frac{x-\sqrt{x^2+0.0001}}{2})$. Inputs of the NN controller are the state of the closed-loop model (two joint angles and two angular velocities) and a constant node (unit input). The hidden layer included a constant node (unit input) also. Outputs of the NN controller are two joint torques.

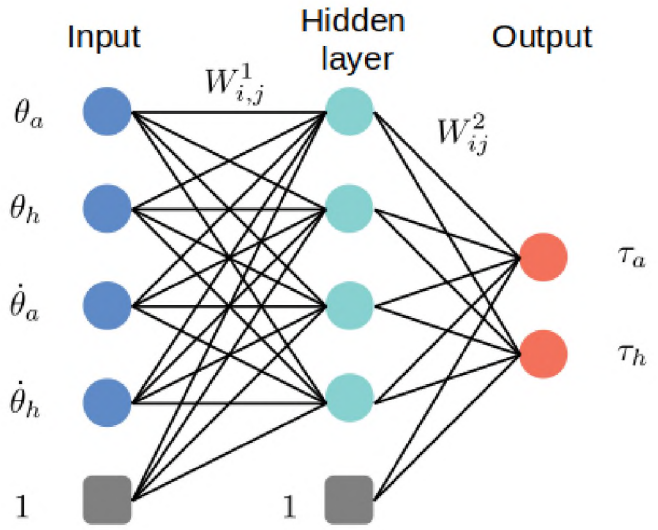

Figure 22: Structure of neural network controller with 1 hidden layer and 4 hidden nodes.

NNTD Controller:

The NNTD controller in this chapter also used the standard neural network but with one hidden layer and eight hidden nodes. Inputs of the NNTD controller are the current state information and several prior state information (delayed feedback). Outputs of the NNTD controller are two joint torques. Same activation function used in NN controller was used here.

In these six types of controllers, optimizing parameters are the control gains, reference angles, and the time delay parameters. In LSCTD and NNTD controllers, three prior state information (60ms, 120ms, and 180ms delayed feedback) were used to form the feedback

control loop. The total number of optimizing parameters in the PD, FPD, FPDTD, LSCTD, NN, and NNTD controllers are 6, 10, 14, 34, 30, and 154, respectively.

5.2.4 Trajectory Optimization with Direct Collocation

The indirect identification approach mentioned above can be treated as trajectory optimization problems where the state trajectories and control parameters are optimized at the same time. In this chapter, the direct collocation method [27, 28], instead of shooting method [29], is used in the trajectory optimization, which transferred the continuous state trajectories into finite discrete points and the dynamics of forward simulation was transferred into constraints of the optimization problem. As a result, we only need to solve a nonlinear program problem, instead of run the forward simulation for the trajectory optimization. Formula of the trajectory optimization with direct collocation in standing balance controller

identification task is:

$$
\begin{aligned}
&\text{Find state trajectories: } X = \{x_1, x_2, ..., x_N\} \\
&\qquad \text{and control parameters: } P \\
&\text{To minimize the objective function:} \\
&\qquad F = \sum_{n=1}^{N} \frac{(\theta_1^{n,m} - \theta_1^n)^2 + (\theta_2^{n,m} - \theta_2^n)^2}{2 \cdot N} \\
&\text{Subject to: system dynamics: } \begin{bmatrix} f_1(x_1, \dot{x}_1, P, v_{belt,1}) = 0 \\ f_2(x_2, \dot{x}_2, P, v_{belt,2}) = 0 \\ ... \\ f_N(x_N, \dot{x}_N, P, v_{belt,N}) = 0 \end{bmatrix} \\
&\qquad \text{bounds on state trajectories: } \begin{bmatrix} x_{low,1} < x_1 < x_{upp,1} \\ x_{low,2} < x_2 < x_{upp,2} \\ ... \\ x_{low,N} < x_N < x_{upp,N} \end{bmatrix} \\
&\qquad \text{bounds on control parameters: } P_{low} < P < P_{upp}
\end{aligned}
\tag{5.5}
$$

where, x_n is the state of the closed-loop model at the n^{th} collocation node, including joint angles and joint angular velocities $[\theta_1, \dot{\theta}_1, \theta_2, \dot{\theta}_2]$; θ_1, θ_2 are the ankle and hip joint angles; $\dot{\theta}_1, \dot{\theta}_2$ are the joint angular velocities of the ankle and hip joints; $\theta_1^{n,m}, \theta_2^{n,m}$ are the ankle and hip joint angles of the measured data at time point n; $f_n = 0$ is the dynamic constraint of the closed-loop model at the n^{th} collocation node. Equations of the dynamic model can be found in the appendix A.

The Interior Point Optimizer (Ipopt) [30] was used to solve the large scaling nonlinear program in this chapter. The Ohio supercomputer [31] was used to speed up the optimization process.

Ten optimizations were performed with random initial guesses of the optimizing con-

trol parameters in each identification problem to eliminate local optimum. An identification problem is defined as the identification of one type of controller on one period of experimental data. The optimizing result which has the lowest objective function among these ten optimizations was select as the best solution for the identification problem. For the NNTD controller type, only one optimization was run in each identification problem due to the very long computational time. In total, we solved 72 identification problems (12 periods of data and 6 types of controllers) which include 612 large scaling optimizations in this chapter.

For the PD and FPD controllers, we also applied stochastic identification [20] to help identify practically stable controllers by enforcing the closed-loop model generates practically stable motions among multiple episodes of process noises. Two and three episodes were used in the stochastic identifications for the PD and FPD controllers, respectively.

5.3 Results

5.3.1 Identification Results on Simulated Data

Figure 23 shows the mean and standard deviation (STD) of identified control gains among ten realizations of sensor noise (identified gains in each realization of sensor noise was selected as the best fit result from the ten random initial guess optimizations). The leftmost bar in each subplot indicates the "true" value of the control gain that was used to generate the simulated motion data. The other five bars from left to right in each subplot shows the identified control gains from five lengths of simulated data periods (10, 30, 50, 70, and 90 seconds). In general, the identified control gains are close to the 'true' value, except for the two passive proportional gains. However, the differences between the 'true' value and identified results are small when adding the passive and active proportional control gains together (bottom two subplots). Another significant result is that with the increase of the data length, the standard deviation of identified gains among different realizations of sensor noise is decreasing.

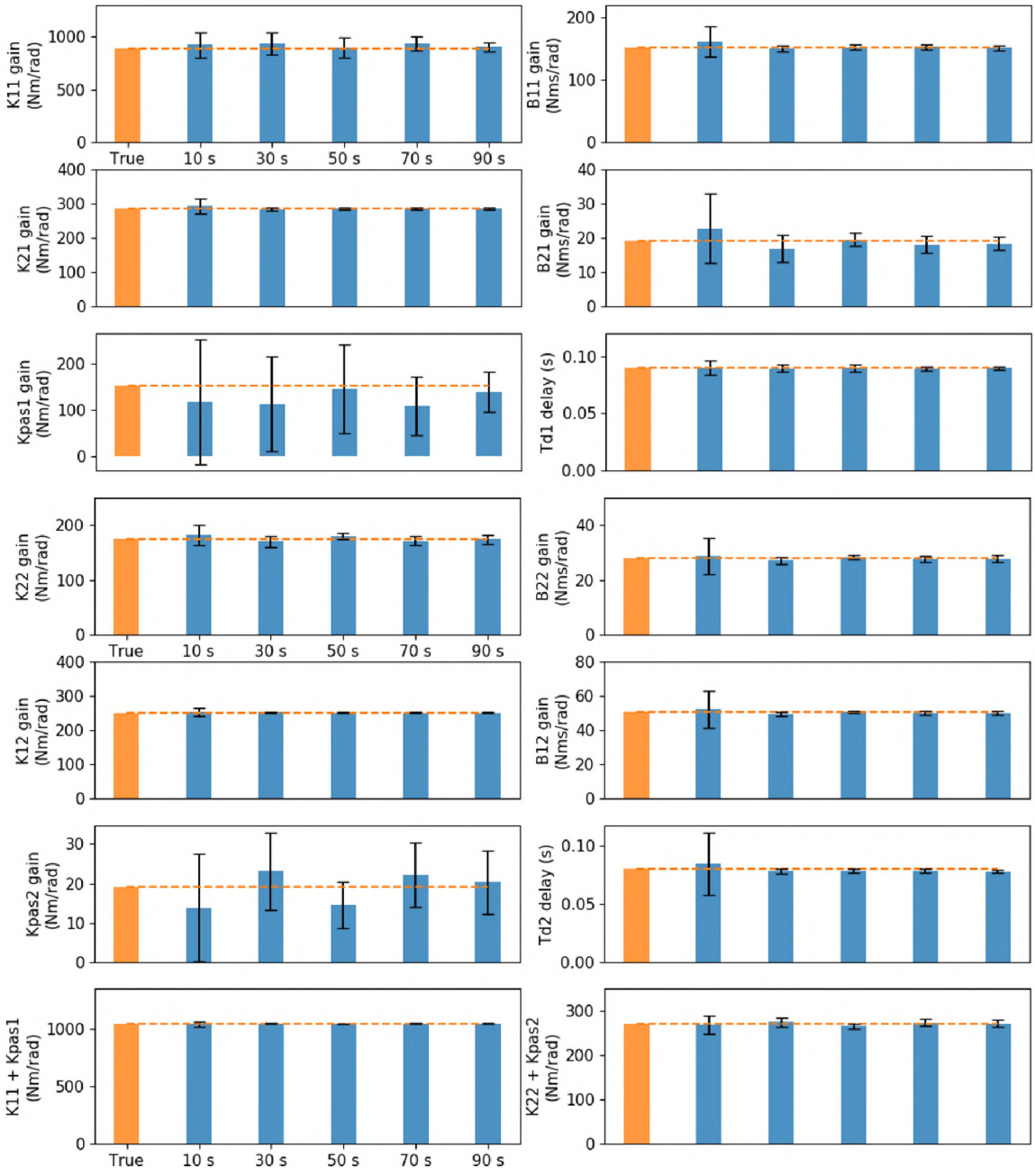

Figure 23: Identified control gains from simulated data.

Percentage of bias error and variability across 10 noise seeds of all identifying control parameters are shown in Figure 24. This result is from the identification of fifty seconds of simulated data. The bias error of all identified parameters are less than 2.5% of the 'true' value, except the two passive proportional gains. The variation of identified control gains among ten realizations of noise are below 10% of the averaged gain values, except the two

passive proportional gains.

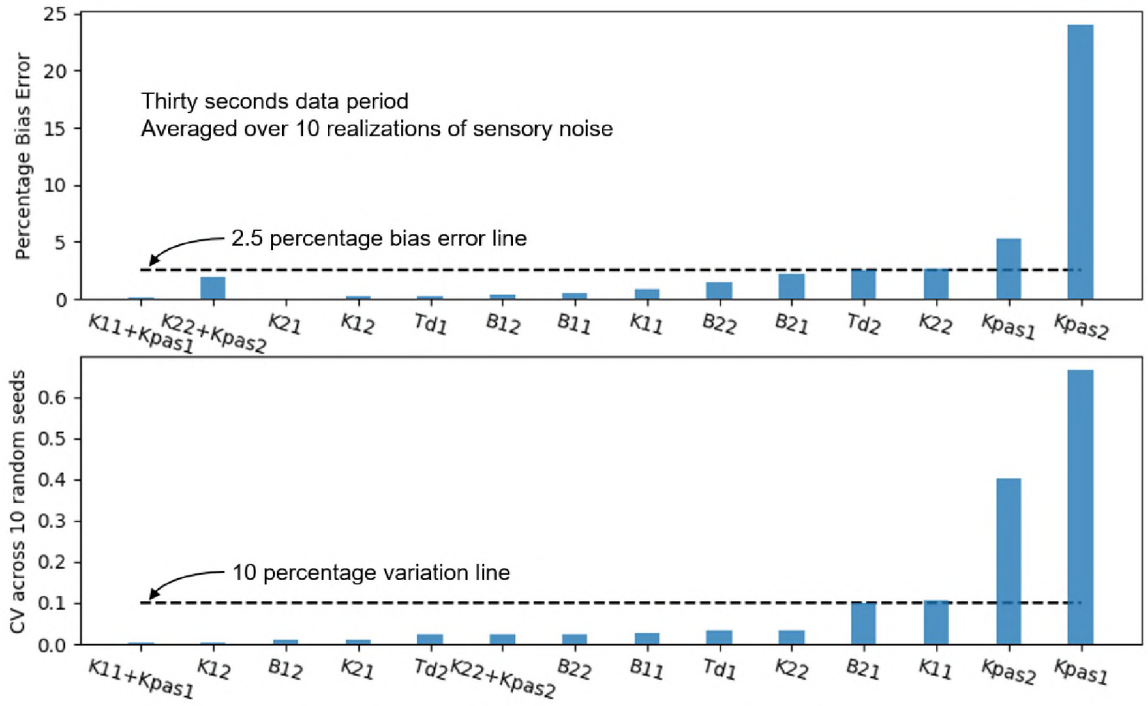

Figure 24: Bias error and variation of the identified control gains from simulated data.

5.3.2 Identification Results on Experimental Data

Figure 25 shows the root mean square (RMS) of the experimental data (first two box plots) and the fits (difference) between experimental data and the motion output of the closed-loop model with the six controller types (rest box plots). With the increase of the controller complexity, RMS is gradually decreasing which suggests better fit. Specifically, the FPD controller has lower RMS than the PD controller indicating that the cross joints feedback can better explain the CNS of human standing balance. However, the FPDTD controller does not has a significant lower RMS than the FPD controller, which suggests that the time delay component added to the FPDTD controller may not be sufficient to explain the CNS system. LSCTD controller has a more generalized delay structure, which generated better fit with experimental data than the FPD controller type. Controller NN also has lower RMS

than the FPD controller type given the only difference is that NN is a nonlinear controller. Lastly, the NNTD controller has both generalized time delay and non-linearity, which resulted the lowest RMS among all six types of controllers. This shows that human CNS has both non-linearity and time delay to control standing balance at randomly perturbed simulation. Fit of ankle and hip joints' motion of one participant can be found in Appendix C.

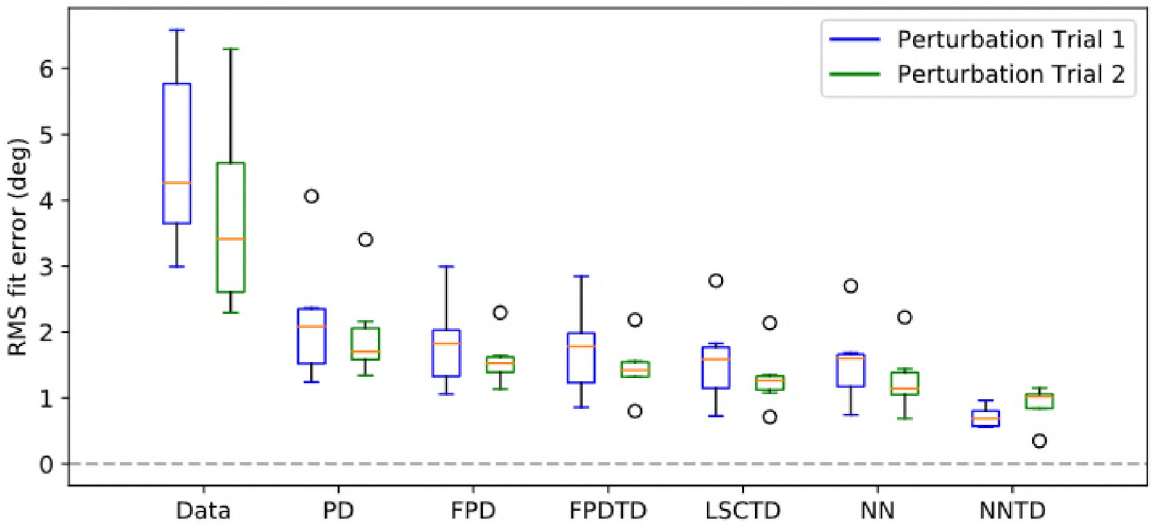

Figure 25: Root mean square (RMS) of the experimental data (first two box plots) and the fits between experimental data and the motion output of the closed-loop mathematical model with the six controller types (rest box plots).

RMS value of the PD controller is about half of the RMS value of the experimental data showing that the PD controller can only explain about 50% amplitude of the standing balance motion. RMS value of the NNTD controller is about one fourth of the RMS value of the experimental data showing that the NNTD controller can explain about 75% amplitude of the standing balance motion. Considering there is one optimization in the NNTD controller identification, whereas PD controller result is the best result among ten optimizations. The actual RMS of NNTD controller could be even lowers than what is showing in the plot.

Even though the variation of experimental motion among different subjects is large, the RMS of the controller fit are much smaller of all controller types. This means that the

amplitude difference of balance motion can be explained by the feedback controllers that have the same structure. Considering that human have the same biological structure and function, it is reasonable to believe that human used the same structure of CNS to control standing balance. Another interesting fact is that the perturbation trial 2 has a relative smaller RMS than the perturbation trial 1 at most controller types. This is because that participants have a relatively smaller body sway motion in trial 2 comparing to the trial 1 showing that participants got adapted to this type of perturbation at the second perturbation trial.

Identified control gains of PD, FPD, and FPDTD type of controllers are shown in the figure 26, 27, and 28. These gains were normalized to a standard human with weight of 70 kg and height of 1.75 m. In the normalization process, joint torques were normalized by the product of body mass and height; joint angular velocities were normalized by the square root of the gravity divided by the body height. In general, the identified feedback control gains were consistent among subjects and two perturbation trials. In all three types of controllers, proportional control gain K_{11} ($K_{11} + K_{pas1}$) of the ankle joint has a larger value than the hip joint's K_{22} ($K_{22} + K_{pas2}$). This makes sense since the ankle joint responds to the balance of full body segments and the hip joint only responds to the trunk balance. The $K_{21}, B_{21}, K_{12}, B_{12}$ in the FPD controller type are significantly different from zero confirmed with previous analysis that human use cross-joint feedback to control standing balance. In FPDTD controller type, time delay parameter of ankle joint is smaller than the hip joint, which are not as expected, as the distance for the nervous signal translation is longer for ankle joint so that larger delay time should exist. The proportional feedback gain K_{22} ($K_{22} + K_{pas2}$) of the hip joint has a higher value in the second perturbation trial than the first perturbation trial, which explained the smaller balance motion in the second perturbation trial.

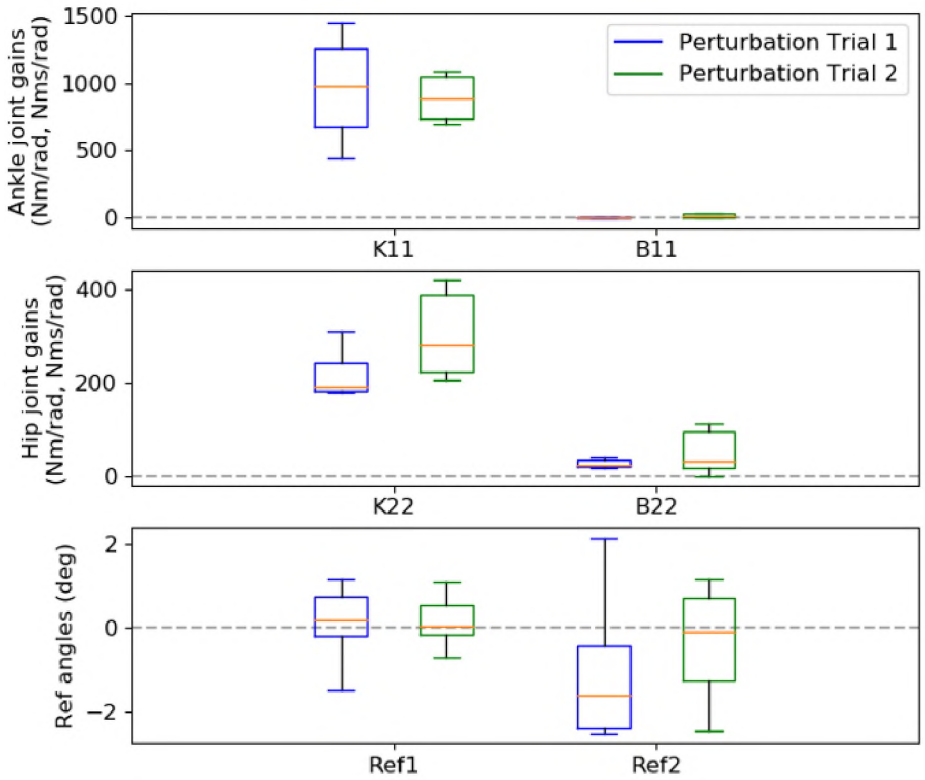

Figure 26: Identified PD control gains from experimental data.

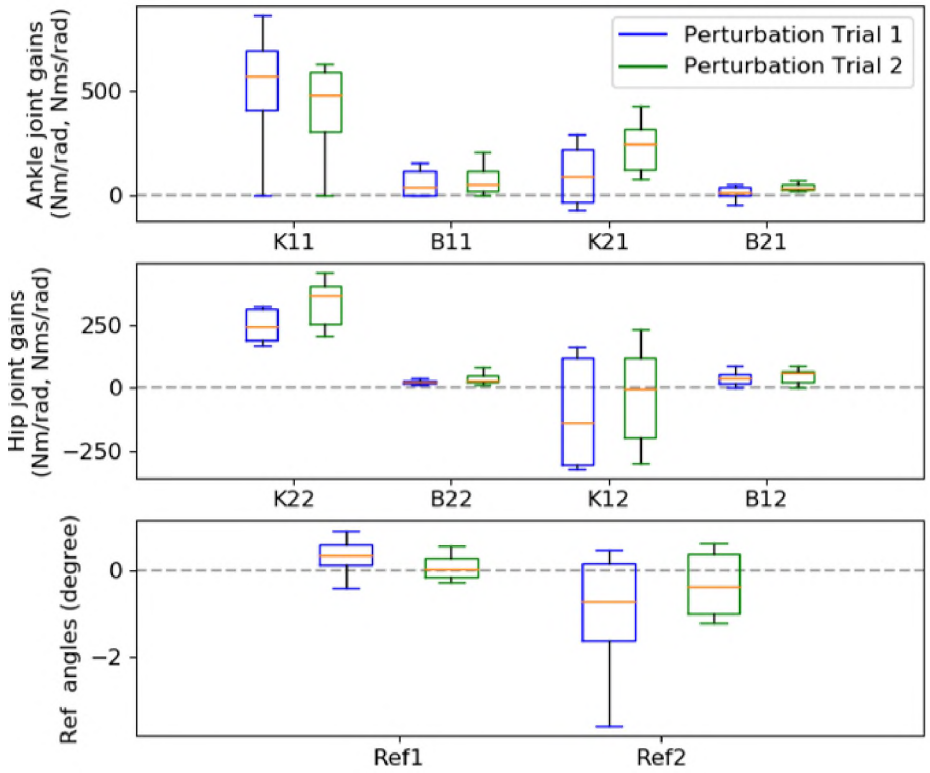

Figure 27: Identified FPD control gains from experimental data.

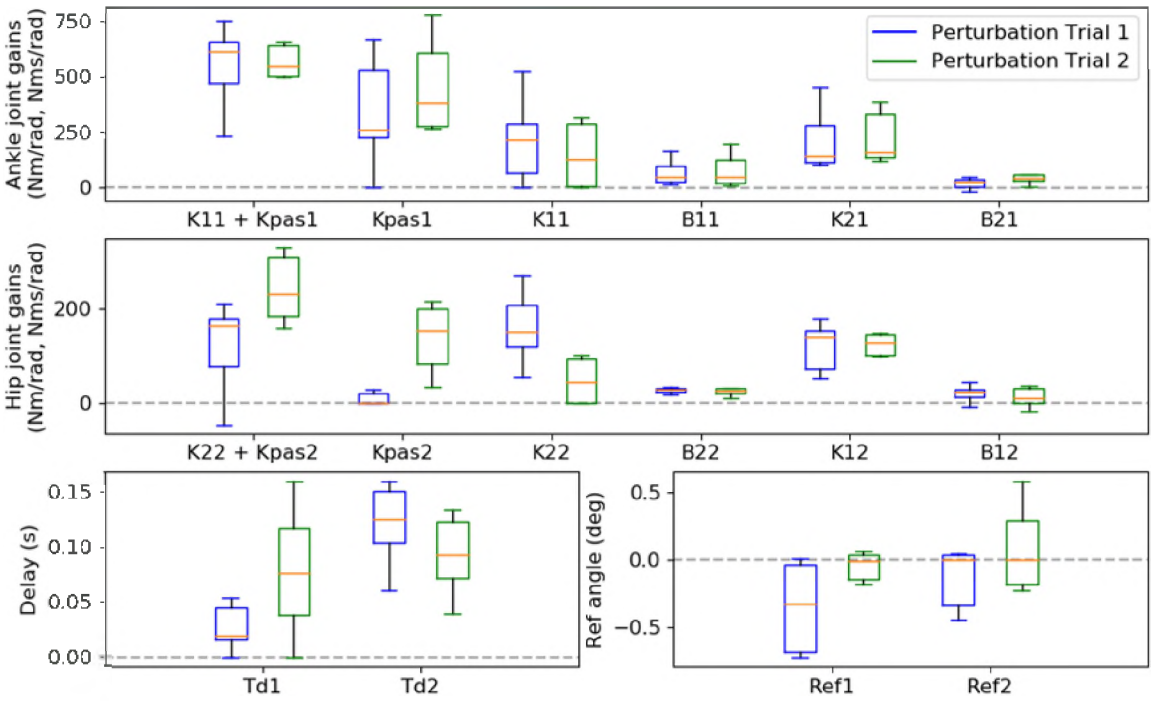

Figure 28: Identified FPDTD control gains from experimental data.

5.4 Discussion

5.4.1 Identification on Simulated Data

Identification results on simulated data showed that the identification method (trajectory optimization with direct collocation) used in this study was able to find the correct control parameters. More importantly, the identified control gains in our study had less bias error and variation comparing to Goodworth and Peterka's simulation study [22]. One possible reason is that the external stimulus in this study is much larger than what Goodworth used in his study. The peak value of the stimulus in their study is only 5 Nm. We used an stimulus which the peak value of equivalent torque perturbation reached around 30 Nm for the hip joint and 50 Nm for the ankle joint. In general, large perturbation generates low noise-to-signal ratio (NSR) which helps find true control parameters. This indicates that the external stimulus used in this study was large enough to collect useful human reaction data from experiment. This also confirmed with the recently published results of Schut et al. (2019) [32]. They showed that the 10 cm peak to peak perturbation amplitude is sufficient

to collect low NSR data in the standing balance experiment.

Another possible reason that Goodworth and Peterka's results have large variation is that the trajectory optimization method used in their papers makes it harder to find a good solution than the optimization method used in this study. In their study, optimizations were performed with the objective function to minimize the FRF between the experimental data and the closed-loop mathematical model. It is hard to calculate the derivatives of the FRF with respect to the optimizing parameters, which limited the optimization performance. In our optimization, the gradient of objective function and Jacobian matrix of the dynamic constraints can be easily provided in the analytical format which helped the optimizer quickly find good solutions. As a result, we are able to get small standard deviation among different sensor noise seeds by selecting the best solution from only 10 optimizations with random initial guesses comparing to 50 optimizations that was done in their study.

5.4.2 Identification on Experimental Data

RMS results of the six types of controllers suggests that both time delay and nonlinear control laws are needed to explain human's standing balance control under random external perturbations. This confirmed with the results of previous studies [4, 33] that the control gains vary with respect to the amplitude of the ramp perturbations, which suggested nonlinear property in humans' postural control. In addition, the identified feedback control gains in this study have similar amplitudes with the study that Park et al. (2004) did. One difference is that we allow the control gains on the cross-joint feedback to be negative. As a result, the proportional gain for the hip joint from the feedback of ankle angle have slightly negative values for most participants.

The identification approach used in this study does not require a linear model and can extract human postural controllers from a long duration of experimental data. As far as we aware, it is the first time that highly nonlinear controllers were identified from 100 seconds

of standing balance data under random perturbations. This method can be applied to more complex controller identification tasks, for instance the step strategy controller in human walking. In addition, this approach is not limited to human-related studies, but can be applied to other areas.

Due to the long computational time, only one optimization was applied on the NNTD controller identification. Considering the possibility of only finding local minimum results, the RMS in Figure 25 can be even lower. Neural network controller has the generalized nonlinear property which is good for testing the ability of nonlinear controllers. However, it may not be a good controller because the control performance is not predictable beyond the trained sections. Normally, its performance can be tested through the so called validation process, which is to perform forward simulation with the other perturbations that were not used for the identifications and check how close they are comparing to the human subjects' motions. This was not included in this study because the NNTD controllers were just used to demonstrate the ability of nonlinear and time delay. For engineering applicable nonlinear controllers, we suggest to try deterministic nonlinear structures, such as polynomials functions, in which the identified controller parameters have a physical meaning and their performance is predictable.

5.5 Conclusion

In this work, we showed that trajectory optimization with direct collocation method can identify the correct control parameters from simulated motion data. Six types of postural controllers, from simple linear to complex nonlinear, were identified from 100 seconds experimental data indicating that the identification method used in this dissertation study have the ability to identify complex nonlinear controllers from long duration motion data. Identification results suggest that humans' CNS includes both time delay and strong nonlinear properties.

5.6 REFERENCES

[1] A. D. Kuo, "An optimal control model for analyzing human postural balance," *IEEE transactions on Biomedical Engineering*, vol. 42, no. 1, pp. 87–101, 1995.

[2] K. S. Oie, T. Kiemel, and J. J. Jeka, "Multisensory fusion: simultaneous re-weighting of vision and touch for the control of human posture," *Cognitive Brain Research*, vol. 14, no. 1, pp. 164–176, 2002.

[3] R. Peterka, "Sensorimotor integration in human postural control," *Journal of Neurophysiology*, vol. 88, no. 3, pp. 1097–1118, 2002.

[4] S. Park, F. B. Horak, and A. D. Kuo, "Postural feedback responses scale with biomechanical constraints in human standing," *Experimental Brain Research*, vol. 154, no. 4, pp. 417–427, 2004.

[5] A. V. Alexandrov, A. A. Frolov, F. Horak, P. Carlson-Kuhta, and S. Park, "Feedback equilibrium control during human standing," *Biological Cybernetics*, vol. 93, no. 5, pp. 309–322, 2005.

[6] C. Maurer, T. Mergner, and R. Peterka, "Multisensory control of human upright stance," *Experimental Brain Research*, vol. 171, no. 2, p. 231, 2006.

[7] G. Torres-Oviedo and L. H. Ting, "Muscle synergies characterizing human postural responses," *Journal of Neurophysiology*, vol. 98, no. 4, pp. 2144–2156, 2007.

[8] T. Kiemel, A. J. Elahi, and J. J. Jeka, "Identification of the plant for upright stance in humans: multiple movement patterns from a single neural strategy," *Journal of Neurophysiology*, vol. 100, no. 6, pp. 3394–3406, 2008.

[9] T. Mergner, "A neurological view on reactive human stance control," *Annual Reviews in Control*, vol. 34, no. 2, pp. 177–198, 2010.

[10] J. T. Bingham, J. T. Choi, and L. H. Ting, "Stability in a frontal plane model of balance requires coupled changes to postural configuration and neural feedback control," *Journal of Neurophysiology*, vol. 106, no. 1, pp. 437–448, 2011.

[11] A. D. Goodworth and R. J. Peterka, "Sensorimotor integration for multisegmental frontal plane balance control in humans," *Journal of Neurophysiology*, vol. 107, no. 1, pp. 12–28, 2011.

[12] T. A. Boonstra, A. C. Schouten, and H. Van der Kooij, "Identification of the contribution of the ankle and hip joints to multi-segmental balance control," *Journal of Neuroengineering and Rehabilitation*, vol. 10, no. 1, p. 23, 2013.

[13] D. Engelhart, A. C. Schouten, R. G. Aarts, and H. van der Kooij, "Assessment of multi-joint coordination and adaptation in standing balance: a novel device and system identification technique," *IEEE transactions on Neural Systems and Rehabilitation Engineering*, vol. 23, no. 6, pp. 973–982, 2014.

[14] H. van der Kooij, E. van Asseldonk, and F. C. van der Helm, "Comparison of different methods to identify and quantify balance control," *Journal of Neuroscience Methods*, vol. 145, no. 1-2, pp. 175–203, 2005.

[15] D. Engelhart, T. A. Boonstra, R. G. Aarts, A. C. Schouten, and H. van der Kooij, "Comparison of closed-loop system identification techniques to quantify multi-joint human balance control," *Annual Reviews in Rontrol*, vol. 41, pp. 58–70, 2016.

[16] H. Van Der Kooij and R. J. Peterka, "Non-linear stimulus-response behavior of the human stance control system is predicted by optimization of a system with sensory and motor noise," *Journal of Computational Neuroscience*, vol. 30, no. 3, pp. 759–778, 2011.

[17] R. Pintelon and J. Schoukens, *System identification: a frequency domain approach*. John Wiley & Sons, 2012.

[18] M. Ackermann and A. J. Van den Bogert, "Optimality principles for model-based prediction of human gait," *Journal of Biomechanics*, vol. 43, no. 6, pp. 1055–1060, 2010.

[19] J. Moore and A. van den Bogert, "Human standing controller parameter identification with direct collocation," in *15th International Symposium on Computer Simulation in Biomechanics*, ISB, 2015.

[20] H. Wang and A. J. van den Bogert, "Identification of the human postural control system through stochastic trajectory optimization," *Journal of Neuroscience Methods*, p. 108580, 2020.

[21] G. Torres-Oviedo and L. H. Ting, "Subject-specific muscle synergies in human balance control are consistent across different biomechanical contexts," *Journal of neurophysiology*, vol. 103, no. 6, pp. 3084–3098, 2010.

[22] A. D. Goodworth and R. J. Peterka, "Identifying mechanisms of stance control: a single stimulus multiple output model-fit approach," *Journal of Neuroscience Methods*, vol. 296, pp. 44–56, 2018.

[23] H. Van Der Kooij and E. De Vlugt, "Postural responses evoked by platform pertubations are dominated by continuous feedback," *Journal of Neurophysiology*, vol. 98, no. 2, pp. 730–743, 2007.

[24] F. B. Horak, "Clinical measurement of postural control in adults," *Physical Therapy*, vol. 67, no. 12, pp. 1881–1885, 1987.

[25] D. A. Winter, *Biomechanics and motor control of human movement*. John Wiley & Sons, 2009.

[26] J. Crank and P. Nicolson, "A practical method for numerical evaluation of solutions of partial differential equations of the heat-conduction type," in *Mathematical Pro-*

ceedings of the Cambridge Philosophical Society, vol. 43, pp. 50–67, Cambridge University Press, 1947.

[27] C. R. Hargraves and S. W. Paris, "Direct trajectory optimization using nonlinear programming and collocation," *Journal of Guidance, Control, and Dynamics*, vol. 10, no. 4, pp. 338–342, 1987.

[28] M. Kelly, "An introduction to trajectory optimization: how to do your own direct collocation," *SIAM Review*, vol. 59, no. 4, pp. 849–904, 2017.

[29] J. T. Betts, "Survey of numerical methods for trajectory optimization," *Journal of Guidance, Control, and Dynamics*, vol. 21, no. 2, pp. 193–207, 1998.

[30] A. Wächter and L. T. Biegler, "On the implementation of an interior-point filter line-search algorithm for large-scale nonlinear programming," *Mathematical programming*, vol. 106, no. 1, pp. 25–57, 2006.

[31] O. S. Center, "Ohio supercomputer center." `http://osc.edu/ark:/19495/f5s1ph73`, 1987.

[32] I. Schut, J. Pasma, J. D. V. Mestdagh, H. Van Der Kooij, and A. Schouten, "Effect of amplitude and number of repetitions of the perturbation on system identification of human balance control during stance," *IEEE Transactions on Neural Systems and Rehabilitation Engineering*, vol. 27, no. 12, pp. 2336–2343, 2019.

[33] T. D. Welch and L. H. Ting, "A feedback model explains the differential scaling of human postural responses to perturbation acceleration and velocity," *Journal of Neurophysiology*, vol. 101, no. 6, pp. 3294–3309, 2009.

PART II.

CONTROL OF WALKING

CHAPTER VI

IDENTIFICATION OF THE FOOT PLACEMENT CONTROL IN HUMAN WALKING

Conference Presentation:

1. H. Wang and A. J. van den Bogert. Identification of Swing Leg Feedback Control in Human Walking. Midwest ASB Conference, 2019.

ABSTRACT

Humans and humanoid robots use foot placement to control balance during walking. Humanoid robots have been successfully controlled by placing the foot at the capture point of a simple inverted pendulum, resulting in a control law with linear feedback from center of mass position and velocity. It is not known, however, whether humans use the same control algorithm, or whether they use the same feedback gains. In this study, step controllers with a control structure from capture theory were identified on 27 trials of perturbed walking data (nine participants, three speeds) through a closed-loop identification approach using a 9-dof planar model of gait dynamics. The identified step controllers generated perturbation responses in the model that were nearly the same as in the human participants. The controller gains were similar among participants and close to the capture theory, but with generally smaller position gains and larger velocity gains. The identified step control gains were dependent on walking speed, which suggests that the step controller might be nonlinear in humans.

6.1 Introduction

Bipedal locomotion in humans and humanoid robots is unstable. Joint angle control is not sufficient, because the system is under-actuated, requiring control of foot placement to prevent falling [1–3]. In general, falls of humanoid robots and humans can always be prevented if the swing leg can step to the appropriate location with correct timing. However, finding an effective control algorithm for the step strategy could be difficult, especially in the case of an unpredictable environment. One successful paradigm is capture theory [4], which predicts the desired foot placement based on a linear inverted pendulum (LIP) model [5]. Both simulation and hardware tests have proven its usefulness in humanoid robots to maintain stable walking under external perturbations [6]. Nonetheless, the algorithm for estimating the desired foot placement inside the capture theory requires some assumptions.

The desired foot placement is based on the capture point, in which the LIP will fully stop ("captured") at the subsequent mid-stance [4, 7]. However, the center of mass (CoM) in human gait has a relatively constant speed during the gait cycle. In addition, the swing leg dynamics and the landing energy lost (heel strike) were not considered [8, 9]. Studies have pointed out that humans do not step on the capture point or the extrapolated center of mass (XCoM), but behind and outward of them [10, 11].

In order to determine how humans control their foot placement, system identification methods can be used. Control identification can be performed using open loop methods, i.e. observing the input and output of the controller, and fitting a control law to the data. It has been shown, however, that this approach biases the control law towards the inverse plant dynamics [12]. To avoid this, it is important to employ proper closed loop identification methods, such as the indirect method where the input and output of the closed loop system are observed and a controller and/or plant model is fit to the data. For example, one can use mechanical perturbations as the input, assume a known plant dynamics model, and determine which controller explains the output of the closed loop system. Open-loop and indirect controller identification methods have been used to extract phase-dependent step controllers from both unperturbed and randomly perturbed walking data through linear models [13–15]. These studies have shown correlations between foot placement and changes of pelvis position and velocity. However, these phase-dependent step controllers may not be able to explain the correct foot placement when walking in the presence of random perturbations. Variation of pelvis position and velocity at a certain phase in walking cycle cannot determine the foot placement by itself since the foot placement could be largely affected by perturbation after that phase. Furthermore, a poor fit has been found when using a simple plant model [14], suggesting a more complicated plant model may be necessary for predicting human foot placement.

In this study, we hypothesis that phase-independent foot placement controllers can be identified from human walking data. To prove it, this type of controllers were identified

from randomly perturbed walking data with a 9-dof gait dynamics model (plant) through an indirect system identification approach. The results of this work have potential applications in robotics and in human gait assessment. Robots can behave more human-like with the foot placement controllers obtained from humans. In humans, the ability to quantify the feedback gains of an individual's step strategy could be useful as a clinical assessment of walking balance.

6.2 Methods

A flowchart of the indirect approach for the step controller identification is shown in Figure 29. There are two components in the identification: One is the closed loop simulation model which includes the gait dynamics and the gait controller (the hypothesized step strategy control law). Another component is the experimental data obtained from participants exposed to perturbations during walking. The overall goal of the indirect approach is to minimize the difference between the outputs of the closed loop model and the experimental data, by optimizing the controller parameters. Therefore, the foot placement control gains were identified through a trajectory optimization. We assume that the correct step controllers are found if the nonlinear gait dynamics can reproduce the motions of testing participants under the same perturbation.

6.2.1 Experimental Data

All identifications were done using previously published data [16]. In the experiment, participants' motions were recorded while they were walking on a treadmill with a continuously perturbed belt speed. Each participant was tested under three walking speeds: 0.8m/s, 1.2m/s, and 1.6m/s. Optical motion capture with 10 cameras (Motion Analysis Corp., Rohnert Park, CA) and 47 markers was used to obtain full-body motion. An instrumented treadmill (Motekforce Link) was used to perturb belt speed and record ground reaction forces. Joint angles were calculated by inverse kinematics using the Human Body

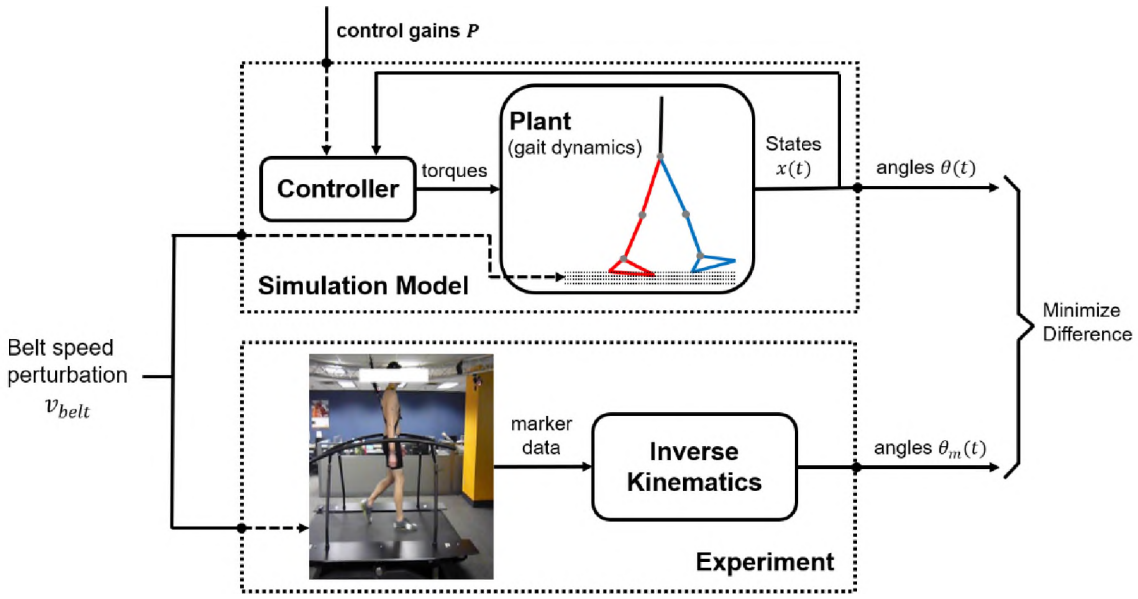

Figure 29: Indirect approach for identification of foot placement in walking. This approach consists of two components: a simulation model and an experiment. The simulation model is a closed loop system, with external perturbation as the input. Experiment recorded participant's reaction under the same external perturbation. The control gains P were optimized by letting the simulation model reproduce the angle trajectories of the experiment. In this gait controller identification, angle trajectories are the motion of trunk, hip, knee, and ankle.

Model (HBM) (van den Bogert et al., 2013). Nine participants (Table VI), which have high quality data recorded, were selected from the data-set. For the controller identification, ten seconds of perturbed walking data was selected for each participant at each walking speed

Table VI: Information about the selected nine participants. There are four females and five males. They are all young adults with the average age of 24. There are two male participants with over-weighted BMI and one male participant in Obesity. All other participants are in normal weight category.

Id	Gender	Age (yr)	Height (m)	Mass (kg)	Original Id
1	female	29	1.72	64.5 ± 0.8	7
2	female	32	1.62	54 ± 2	3
3	female	21	1.70	58 ± 2	13
4	female	28	1.69	56.2 ± 0.6	16
1	male	20	1.57	74.9 ± 0.9	8
2	male	20	1.69	67 ± 2	9
3	male	23	1.73	71.2 ± 0.9	5
4	male	26	1.77	86.8 ± 0.6	6
5	male	19	1.77	92 ± 0.2	10

6.2.2 Gait Dynamics

The gait dynamics (plant) used in the identification is a two-dimensional torque-driven seven-link gait model [17, 18], as shown in Figure 29. The model has 9 degrees of freedoms and 6 controllable joints. Hip flexion, knee extension, and ankle dorsiflexion were defined positive. In identification, the model was scaled based on the weight and segment lengths of each participant [19]. Belt speed perturbation was modeled by varying the ground speed in the foot-ground contact model. Details are provided in Appendix D(1).

6.2.3 Gait Controller

The gait controller used in this study has a similar control architecture as the M2V2 robot [6] and consists of two components: open-loop torque control and feedback control (Figure 30). Feedback control was used to control the motion of the hip and knee joints of the swing leg. The ankle joint of the swing leg and all joints of the stance leg were controlled by open-loop torques. The focus of this study is to identify control parameters inside the swing leg feedback control loop. Joints controlled by the open-loop torques can generate arbitrary motion, which converged towards experimental data in the identification process. The feedback control consists of four items: a foot placement controller, a swing path generator, an inverse kinematics module, and a local tracking controller.

Foot Placement Controller

The function of foot placement controller is to generate a proper foot placement for the swing leg based on the state of the system. Our feedback control structure is largely based on capture theory [7]. Capture theory predicts foot placement using linear feedback from position and velocity of the CoM projected on the ground relative to the standing foot. Our modification replaces the CoM position and velocity with the pelvis position and velocity. Pelvis position and velocity were calculated from the stance leg's trunk, hip, and knee angles and velocities and the leg geometry. In addition, we take a linear combination of these

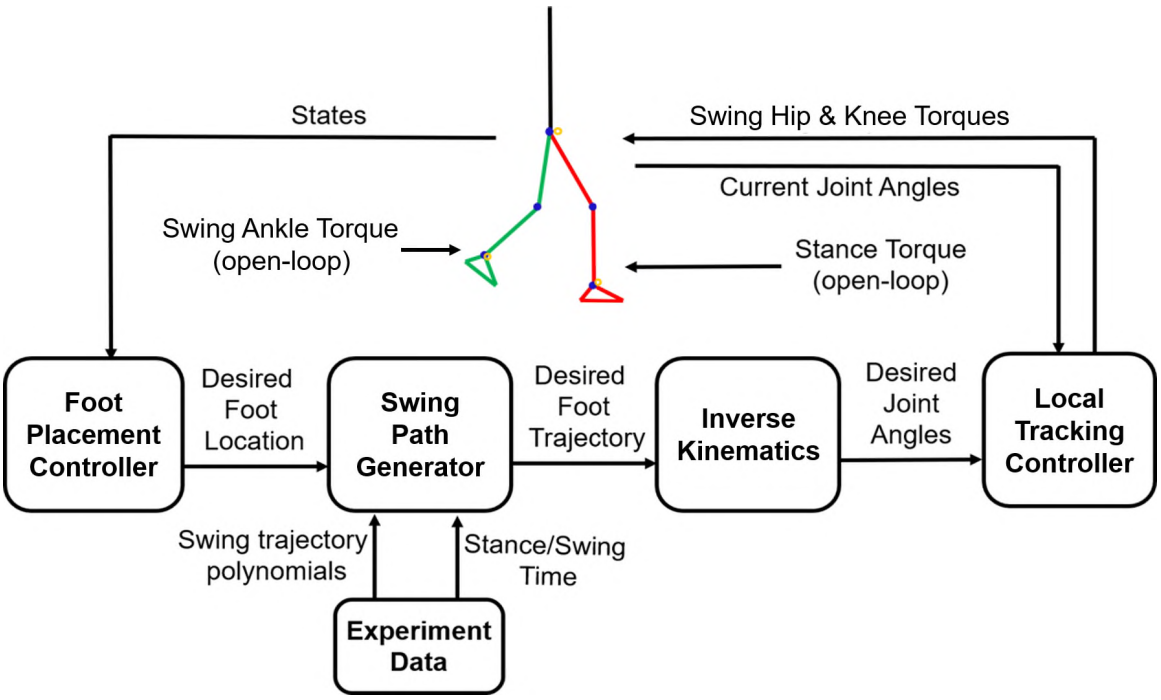

Figure 30: Structure of the locomotion control system for the step strategy identification. The stance leg and the ankle joint in swing leg are controlled by open-loop torques. The hip and knee joints of swing leg are controlled by the state feedback control loop. The purpose of open-loop torque control is just to let these controlled joints following the experimental data. The focus of this study is to identify control parameters inside the swing leg control loop.

two terms with the coefficients as control parameters to be identified from experimental data. The foot placement controller used in this study is:

$$\begin{aligned} x_{ifp}(t) &= P_1 \cdot x_p(t) + P_2 \cdot \frac{\dot{x_p}(t)}{\omega_0} \\ x_{fp}(t + \Delta t) &= x_{ifp}(t) \cdot e^{\omega_0 \cdot \Delta t} \end{aligned} \tag{6.1}$$

where, x_{ifp} is the instantaneous desired foot placement based on the pelvis position and velocity feedback; x_p is the pelvis position that projected on the ground in sagittal plane relative to standing foot; $\dot{x_p}$ is the horizontal velocity of pelvis; P_1 and P_2 are the two gains applied on the two feedback signals, which needs identified; $\omega_0 = \sqrt{g/L_{leg}}$ is the reciprocal of the time constant of the human dynamic model, where g represents the gravity and L_{leg} is the length of leg;; and $x_{fp}(t + \Delta t)$ is the desired foot placement when Δt is the

remaining swing time.

Swing Path Generator

The swing path generator calculates the trajectory of the swing ankle joint in Cartesian space and in the x and y directions separately. Considering that the overall shape of the swing paths is consistent, a normalized polynomial function was used to describe it. The polynomial function in both the x and y directions have the same structure:

$$f(P_{sta}, P_{des}, T, t) = \sum_{n=1}^{N} A_n * (P_{des} - P_{sta}) * (\frac{t}{T})^n \tag{6.2}$$

where, P_{sta} is the starting swing position; P_{des} is the estimated foot placement; T is the total swing time; t is the current swing time; N is the total order of the polynomial function; A_n is the coefficient of the n^{th} order polynomial term.

The polynomial coefficients A_n were optimized over 500 experimental swing paths for each participant at one walking speed. Details are provided in appendix D(2). The output of the foot placement controller is used to scale the horizontal component of the swing path.

Inverse Kinematics

The inverse kinematics module resolves the joint angles of the swing leg to produce the swing ankle position at each time frame. Based on the geometry of the leg, the kinematic function between swing leg joint angles and ankle joint position can be described as:

$$\begin{aligned} P_x &= l_{thigh} * sin(\theta_h) + l_{shank} * sin(\theta_h + \theta_k) \\ P_y &= -l_{thigh} * cos(\theta_h) - l_{shank} * cos(\theta_h + \theta_k) \end{aligned} \tag{6.3}$$

where, P_x is the foot position in x direction; P_y is the foot position in y direction; l_{thigh} is

the length of thigh; l_{shank} is the length of shank; θ_h is the hip joint angle; θ_k is the knee joint angle.

In a controller, one would solve for the two joint angles. In our controller identification, equation 7.3 were added as constraints to the trajectory optimization, which produces the same result when the optimization is completed.

Local Tracking Controller

The local tracking controller controls the hip and knee joints to track the commanded joint angles from the inverse kinematics module. A proportional-derivative (PD) controller was used:

$$\begin{aligned} \tau_h &= Kp_h * (\theta_h^{ref} - \theta_h) + Kd_h * (\dot{\theta}_h^{ref} - \dot{\theta}_h) \\ \tau_k &= Kp_k * (\theta_k^{ref} - \theta_k) + Kd_k * (\dot{\theta}_k^{ref} - \dot{\theta}_k) \end{aligned} \tag{6.4}$$

where θ_h and θ_k are the hip and knee angles; τ_h and τ_k are the hip and knee joint torques; The proportional and derivative gains $Kp_{h/k}$ and $Kd_{h/k}$ were assumed constant for each joint and optimized during the identification process. Reference angles and angular velocities $\theta_{h/k}^{ref}$ and $\theta_{h/k}^{ref}$ were commanded by the inverse kinematics module.

Indirect Identification Approach

The indirect identification approach finds control parameters such that the output of the closed-loop model best fits the participants' motions in the presence of same perturbation (Figure 29). This system identification problem can be treated as a trajectory optimization problem, where the state trajectory $x(t)$ and unknown parameters P are optimized

simultaneously [20]. The problem was formulated as:

$$
\begin{aligned}
&\text{Find state trajectories: } x(t) \text{ and control parameters: } P \\
&\text{To minimize the objective function: } F = \int_0^T \|\theta_m(t) - \theta(t)\|^2 dt \\
&\text{Subject to: system dynamics: } f(x(t), \dot{x}(t), P, V_{belt}(t)) = 0 \\
&\qquad\qquad \text{bounds on state: } x_{low} \leq x(t) \leq x_{upp} \\
&\qquad\qquad \text{bounds on control parameters: } P_{low} \leq P \leq P_{upp}
\end{aligned}
\tag{6.5}
$$

where, $f = 0$ represents the dynamics of the closed-loop system model, consisting of the gait dynamics and gait controller; $x(t)$ is the state of gait model which included generalized coordinates q and velocities $\dot{q}$; $\theta(t)$ represents the angles in trunk, hip, knee, and ankle; $P = [P_1, P_2, Kp_h, Kd_h, Kp_k, Kd_k, \tau_open(t)]$ represents the control parameters inside the locomotion controller. Time-discretized open-loop joint torques τ_open were used to drive the stance leg joints and the swing leg ankle. T is the duration of the experimental data; $v_{belt}(t)$ is the known (measured) velocity of the treadmill belt, including random perturbations in the walking experiment.

This trajectory/parameter optimization problem was solved with the direct collocation method [17, 21] and gradient-based optimizer IPOPT [22]. Trajectories were time-discretized at 20 ms intervals and the dynamics were approximated by the backward Euler formula. In total, there were 27 identification problems (9 participants, 3 walking speeds for each participant). Each optimization problem was solved 10 times, with a random initial guess for P. Experimental data was used as initial guess for $x(t)$.The solution with the lowest objective value F was selected and shown in results. Overall, 270 optimizations were conducted in this study, requiring about 500 computing hours in an Intel i5-8300H CPU.

6.3 Results

Twenty-five out of twenty-seven identification problems were solved successfully. Table VII shows the best coefficients of determination (R^2) between the identified joint trajectories and the experimental data for all twenty-seven trials. Two 'N/A' values in the table indicate cases where IPOPT failed to produce a solution with any of the ten initial guesses. Best solutions of other identification problems all have very high R^2 values (R^2¿0.97), which indicates that the nonlinear gait model was able to reproduce participants' responses with the identified step controllers. A typical example (participant M5 at 1.2m/s) is shown in Figure 31. With the high R^2, the joint motion generated by the identified step controller is almost identical to the participant's responses under the same belt speed perturbation. Specifically, almost every large and small variations among gait cycles was matched, instead of only fitting the average motions.

Table VII: Coefficient of determination (R^2) between identified trajectories and experiment data. 'M' means male subjects; 'F' means female subjects. 'N/A' means the identification problem was not successful.

Speed	M1	M2	M3	M4	M5	F1	F2	F3	F4
0.8 m/s	0.990	0.982	0.991	0.973	0.964	0.991	0.988	0.983	0.992
1.2 m/s	0.989	0.977	0.991	0.981	0.983	0.992	0.993	0.989	N/A
1.6 m/s	0.979	0.974	0.989	0.983	0.982	0.988	0.988	N/A	0.986

Identified step control gains of nine participants at three walking speeds are shown in Figure 32. There are two dimensionless gains in the step strategy as motioned in the section 2.4: position gain and velocity gain. In general, the identified gains are not far from those suggested by capture theory (grey lines). Specifically, identified position gains have an average value of 0.86 and velocity gains have an average value of 1.12. Despite variations among participants, both single participant results and overall results clearly indicate that there are trends in both position and velocity gains versus walking speed. This dependence on walking speed suggests that constant gains in the feedback control structure of capture theory cannot explain the foot placement choice of the testing participants. There was no

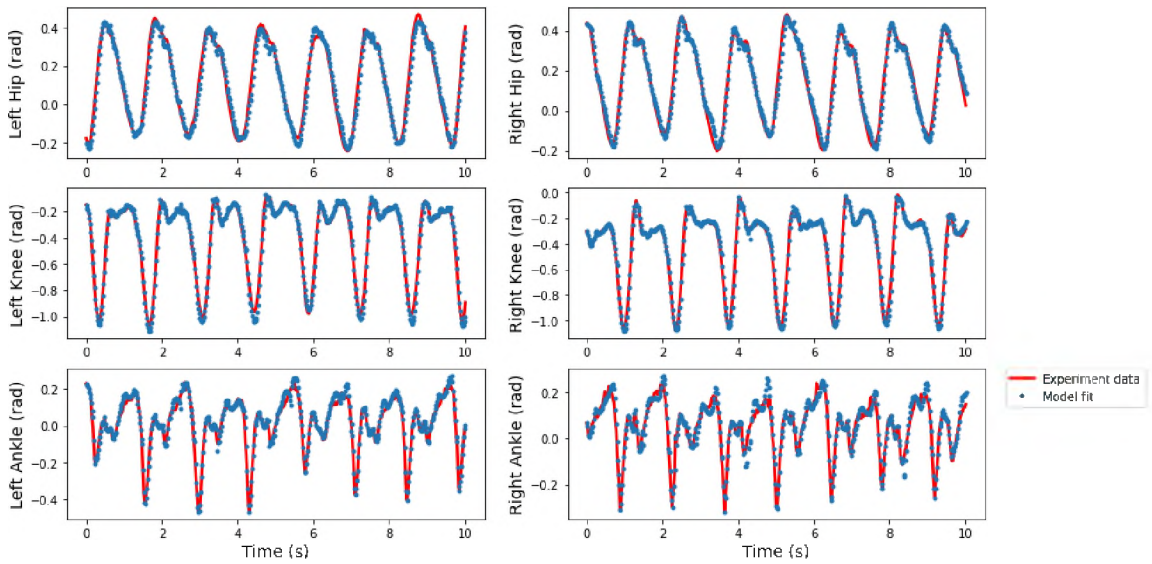

Figure 31: The identified joint trajectories of male participant 5 at walking speed 1.2m/s. The red solid line is the experimental trajectories, and the blue dash line is the identified trajectories. Note how the model replicates the variation in peak hip flexion angle at the end of stance, which is strongly related to foot placement.

difference between male and female participants.

Controller actions during one swing period are shown in Figure 33, depicting the motion of the seven-link gait model with the swing path and planned foot trajectory throughout a swing motion. This shows that the swing leg successfully follows the generated swing path. More importantly, the desired foot placement calculated by the identified step controller is not a fixed point on the ground but keeps changing based on the participant's pelvis motion throughout the swing phase. For instance, at t = 0.24 second, there is a large change of the desired foot location due to the belt speed perturbation.

The ten optimizations with different initial guesses often found similar results from the same data, suggesting that a global optimum was found. Optimizations were repeated using a 20-second and a different 10-second data segment, from the same experimental condition, and similar results were found. Details can be found in appendix D.3 and D.4.

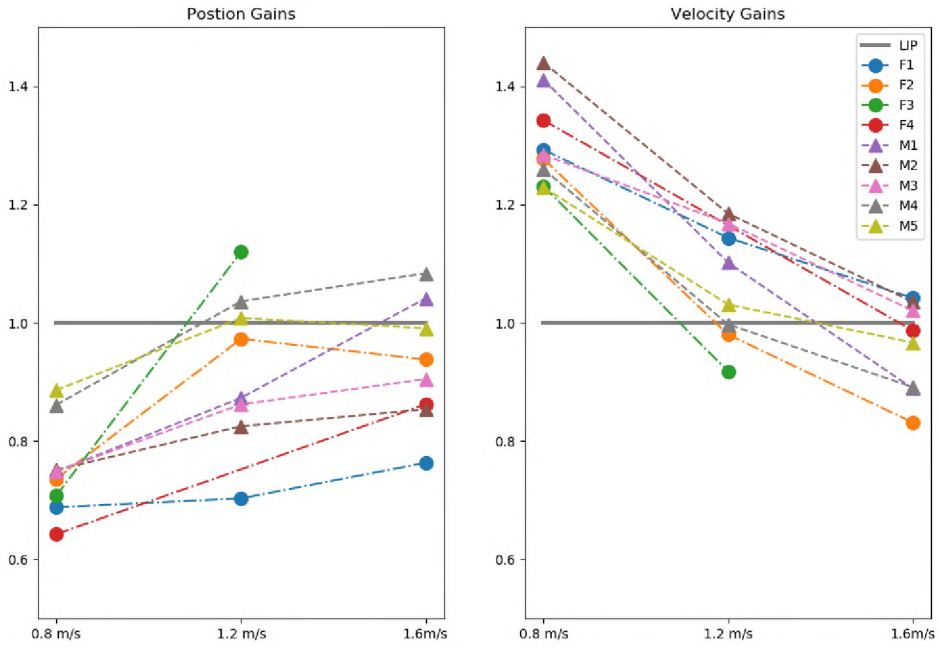

Figure 32: The identified foot placement gains in the foot placement controller. The position and the velocity gains are showing in the subplot left and right, respectively. Female subjects are marked with solid circle and male subjects are marked with solid triangles. Identified gains in one participant are connected by dash lines.

6.4 Discussion

In this study, control gains in a step controller based on capture theory were identified from human responses to continuous mechanical perturbations during walking. In general, both identified position gains and velocity gains were close to the capture theory, which suggested that our approach is valid and could find reasonable step controllers from walking data. For the highest speed (1.6m/s), both the averaged position gain (0.93) and the averaged velocity gains (0.96) are slightly lower than one, which confirmed the conservative property of the capture point. However, results of other walking speed did not support this. It should be noted that our controller predicted the location of swing ankle joint instead of the center of pressure (CoP) using feedback from position and velocity of the pelvis (hip) rather than the CoM, so not directly comparable to a controller based on capture theory and

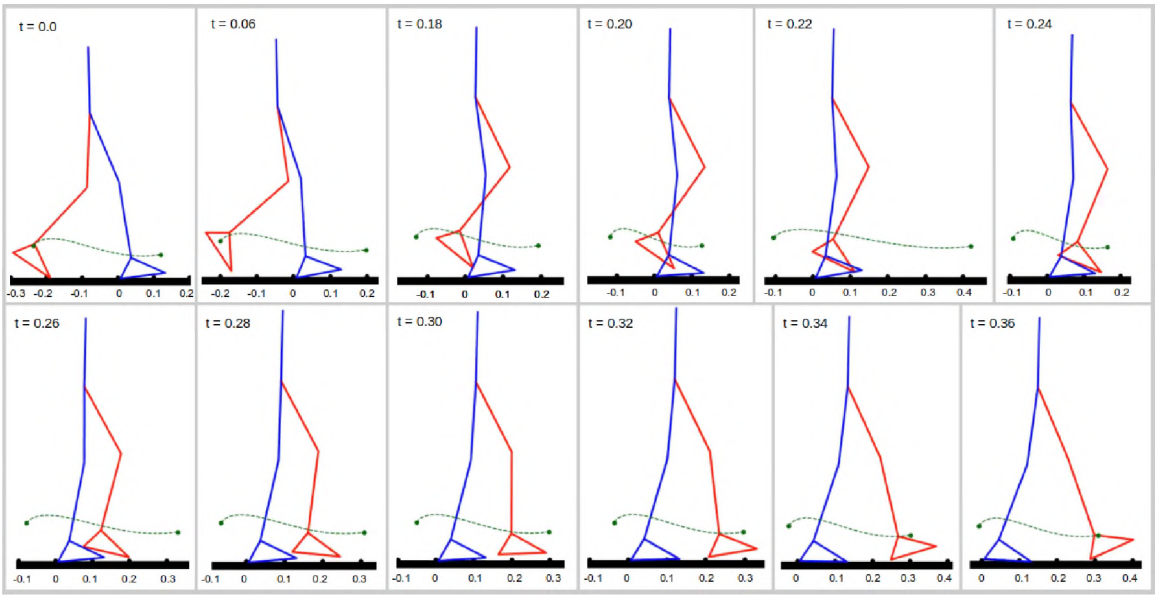

Figure 33: Stick plots of one swing motion. The red leg is the swing leg, and the blue leg is the stance leg. The green dashed line is the swing path based on the identified step strategy algorithm. The beginning and ending two green points are the start swing and end swing points.

a LIP model. The identified step control gains depend on walking speed, which is not predicted by capture theory. This suggests that humans may use a single nonlinear feedback controller or more feedback paths for foot placement control, instead of the linear control law from the capture theory. This difference may come from the simplification of the LIP model that capture theory used. By doing simultaneous trajectory optimizations on three velocities, our approach can be extended towards identification of parameters in a single nonlinear control law.

Wang and Srinivasan (2014) obtained phase dependent control gains, while our results show that one set of step strategy control gains can explain the step length changes in the perturbed walking data [13]. One possible reason is that they studied the relationship between the walking state of a specific phase and the foot landing position, which ignores the changes that happened after the studied phase.

The indirect identification approach prevents results that are biased towards the inverse plant dynamics [12] but requires a model of plant dynamics, so that the closed loop system can be simulated. Our gait dynamics model was a simple planar representation of the

human body and may have affected the results. In the present study, we believe this is justified because the control laws are also very simple: linear without time delay. Identification of a more realistic control system, with a more realistic gait dynamics model, will require more state variables and controller parameters, and tracking experimental data of longer duration. This is a straightforward extension of our approach, but beyond the current capabilities of computational methods for trajectory optimization.

Potential applications of our approach are twofold. First, the identified parameters may provide clinically relevant information about an individual's balance control system during walking. Although currently based on simple models, underlying neural mechanisms are represented in the results. Second, bipedal robots can use the identified control laws to better mimic human responses to perturbations. For this application, it is helpful that a robot-like gait dynamics model was used. This guarantees that the identified controller can produce human-like responses in a robot that is close enough to the gait dynamics model. In fact, human-like responses can even be elicited in a distinctly non-human system, using our approach for identifying a controller for such a non-human plant.

Reproducing the joint motion is better than just studying the foot placement. Foot placement only happens once per gait cycle which is accumulated results of all the previous changes or perturbation in the swing. It is impossible to decompose the final foot placement information into multiple individual contributors. In contrast, the joint motion is continuous information which includes all the adjustments of the desired foot location. It was shown that the shape of the swing phase is relatively consistent although the step lengths and swing duration lengths are different. Therefore, changes in the desired foot location will directly affect the swing leg joint motion by shortening or stretching the swing path. Through kinematics, the swing leg hip and knee joint angles are directly affected by the changes of the swing path.

The duration of the swing phase was not an optimized parameter in the step strategy identification. We predefined the stance and swing periods for each gait cycle based on

the experimental data. In principle, these durations could be optimized but this would dramatically increase the complexity of the trajectory optimization problems, which may no longer be solvable. Since the goal of the identification was to reproduce the human joint motions, fixing the swing period will automatically guarantee that the swing period is the same as experimental data once a solution is found. We therefore do not think that the results were affected by this simplification of the problem.

The gains in local tracking controllers for the hip and knee joints were also optimized in the step strategy identifications. However, these values are not the main concerns in this study. In humanoid robots, the local tracking controller is usually designed based on the specific structure of the robot hardware and our identified gains cannot provide a good reference. Also, methods other than PD control could be used to achieve the local joint tracking. However, we found that it was better to optimize these gains in our identification work rather than pre-selecting the values, because it allowed closer tracking of experimental data.

This study is not perfect due to several simplifications. First of all, the estimated foot placement from the identified step controller was the ankle joint position, which does not account for the center of pressure (CoP) changes in the feedback control. However, the CoP changes were included in the closed-loop gait system by allowing the motion of ankle joint tracking the experimental data. Incorporation of CoP in the step controller identification is possible since the nonlinear gait model we used has the potential of calculating the CoP. This will be included in future work. Future work will also include control of mediolateral foot placement, which requires a 3d gait model but will use the same methods and approach that was presented in this study.

6.5 Conclusion

In this study, step controllers that have a similar feedback structure as the capture theory were successfully identified from walking experiment data. Identification results suggested

that a controller based on capture theory was able to explain human responses to perturbations during walking, although humans had lower position feedback gains and higher velocity feedback gains. Furthermore, the human feedback gains were dependent on walking speeds, suggesting that the humans use nonlinear controllers or more feedback signals, such as acceleration of the pelvis, to choose their foot placements in perturbed walking.

6.6 REFERENCES

[1] M. A. Townsend, "Biped gait stabilization via foot placement," *Journal of Biomechanics*, vol. 18, no. 1, pp. 21–38, 1985.

[2] J. J. Kuffner, S. Kagami, K. Nishiwaki, M. Inaba, and H. Inoue, "Dynamically-stable motion planning for humanoid robots," *Autonomous Robots*, vol. 12, no. 1, pp. 105–118, 2002.

[3] B. Stephens, "Humanoid push recovery," in *Humanoid Robots, 2007 7th IEEE-RAS International Conference on*, pp. 589–595, IEEE, 2007.

[4] J. Pratt, J. Carff, S. Drakunov, and A. Goswami, "Capture point: A step toward humanoid push recovery," in *Humanoid Robots, 2006 6th IEEE-RAS International Conference on*, pp. 200–207, IEEE, 2006.

[5] S. Kajita, F. Kanehiro, K. Kaneko, K. Yokoi, and H. Hirukawa, "The 3d linear inverted pendulum mode: A simple modeling for a biped walking pattern generation," in *Proceedings 2001 IEEE/RSJ International Conference on Intelligent Robots and Systems. Expanding the Societal Role of Robotics in the the Next Millennium (Cat. No. 01CH37180)*, vol. 1, pp. 239–246, IEEE, 2001.

[6] J. Pratt, T. Koolen, T. De Boer, J. Rebula, S. Cotton, J. Carff, M. Johnson, and P. Neuhaus, "Capturability-based analysis and control of legged locomotion, part 2:

Application to m2v2, a lower-body humanoid," *The International Journal of Robotics Research*, vol. 31, no. 10, pp. 1117–1133, 2012.

[7] T. Koolen, T. De Boer, J. Rebula, A. Goswami, and J. Pratt, "Capturability-based analysis and control of legged locomotion, part 1: Theory and application to three simple gait models," *The International Journal of Robotics Research*, vol. 31, no. 9, pp. 1094–1113, 2012.

[8] L. Zhang and C. Fu, "Predicting foot placement for balance through a simple model with swing leg dynamics," *Journal of Biomechanics*, vol. 77, pp. 155–162, 2018.

[9] A. D. Kuo, J. M. Donelan, and A. Ruina, "Energetic consequences of walking like an inverted pendulum: step-to-step transitions," *Exercise and Sport Sciences Reviews*, vol. 33, no. 2, pp. 88–97, 2005.

[10] A. Hof, M. Gazendam, and W. Sinke, "The condition for dynamic stability," *Journal of Biomechanics*, vol. 38, no. 1, pp. 1–8, 2005.

[11] A. L. Hof, "The 'extrapolated center of mass' concept suggests a simple control of balance in walking," *Human Movement Science*, vol. 27, no. 1, pp. 112–125, 2008.

[12] H. van der Kooij, E. van Asseldonk, and F. C. van der Helm, "Comparison of different methods to identify and quantify balance control," *Journal of Neuroscience Methods*, vol. 145, no. 1-2, pp. 175–203, 2005.

[13] Y. Wang and M. Srinivasan, "Stepping in the direction of the fall: the next foot placement can be predicted from current upper body state in steady-state walking," *Biology Letters*, vol. 10, no. 9, p. 20140405, 2014.

[14] V. Joshi and M. Srinivasan, "A controller for walking derived from how humans recover from perturbations," *Journal of the Royal Society Interface*, vol. 16, no. 157, p. 20190027, 2019.

[15] N. Seethapathi and M. Srinivasan, "Step-to-step variations in human running reveal how humans run without falling," *eLife*, vol. 8, p. e38371, 2019.

[16] J. K. Moore, S. K. Hnat, and A. J. van den Bogert, "An elaborate data set on human gait and the effect of mechanical perturbations," *PeerJ*, vol. 3, p. e918, 2015.

[17] M. Ackermann and A. J. Van den Bogert, "Optimality principles for model-based prediction of human gait," *Journal of Biomechanics*, vol. 43, no. 6, pp. 1055–1060, 2010.

[18] H. Geyer and H. Herr, "A muscle-reflex model that encodes principles of legged mechanics produces human walking dynamics and muscle activities," *IEEE Transactions on Neural Systems and Rehabilitation Engineering*, vol. 18, no. 3, pp. 263–273, 2010.

[19] D. A. Winter, *Biomechanics and motor control of human movement*. John Wiley & Sons, 2009.

[20] J. Moore and A. van den Bogert, "Human standing controller parameter identification with direct collocation," in *15th International Symposium on Computer Simulation in Biomechanics*, ISB, 2015.

[21] C. R. Hargraves and S. W. Paris, "Direct trajectory optimization using nonlinear programming and collocation," *Journal of Guidance, Control, and Dynamics*, vol. 10, no. 4, pp. 338–342, 1987.

[22] A. Wächter and L. T. Biegler, "On the implementation of an interior-point filter line-search algorithm for large-scale nonlinear programming," *Mathematical programming*, vol. 106, no. 1, pp. 25–57, 2006.

CHAPTER VII

EVALUATION OF FOOT PLACEMENT CONTROL ON A LOWER LIMB EXOSKELETON

7.1 Introduction

Lower limb exoskeletons have been developed that intend to help people with locomotor disabilities regain the ability to stand up, walk, and even run [1–4]. Even though the hardware design of current devices has become compact and elegant, crutches are always needed to keep balance. This limitation is a consequence of fixed reference trajectories used to control joint motions, lacking the ability to response to walking pattern changes and external perturbations.

Humans use the so-called "step strategy" during walking to maintain balance. The strategy involves controlling the swing leg stepping to appropriate locations. Studies have shown that healthy adults may choose their foot placement based on the position and velocity of the pelvis or the Center of Mass (CoM) [5, 6]. The Linear inverted pendulum (LIP) model has been proposed to derive a control law for foot placement [7–9]. Even though our controller identification study has shown that humans do not use the control gains predicted by the LIP model suggested to control their foot placement, humanoid robots have achieved remarkably stable walking performance, even with external perturbations, using this control structure [10]. Theoretically, this control structure also has the potential to be applied to lower limb exoskeletons to generate better balanced walking motion. However, to our knowledge, such studies have not been done yet.

We propose that the foot placement controllers identified from the previous chapter can be applied on lower limb exoskeletons and help users maintain balance during walking. To answer this, we implemented the foot placement control algorithm on an Indego exoskeleton (Parker-Hannifin Corp., Cleveland, OH) and conducted walking tests with healthy adults. Activation of six leg muscles was measured and analyzed to show the effects of the controller, compared to the passive mode of Indego.

7.2 Methods

The structure of the foot placement controller identified in previous chapter was used to control the Indego exoskeleton. Some necessary changes (described in sections below) were made to make it suitable for the Indego hardware. In addition, components in the foot placement control were personalized for each testing participant.

7.2.1 Test Procedure

Two healthy young adults (both male) were included in the walking test. The tests were conducted over two days. On the first day, participants were asked to perform normal walking without the Indego exoskeleton and then walking with the passive Indego. During normal walking, a motion capture system (Motion Analysis Crop., Rohnert Park, CA) with 27 markers was used to track participants' motion. In the walking trial with the passive Indego, leg motion was detected through the encoders in the Indego motors at the hip and knee joints. An instrumented treadmill (Motekforce Link, Amsterdam, Netherlands) was used to record the ground reaction forces. Five electromyographic (EMG) sensors were used to record leg muscle activation during walking. Motion data of the walking trial with passive Indego were used to personalize the foot placement controller for each participant: detecting the control gains in the foot placement controller and the polynomial functions for the swing path. Details can be found in Appendix E.

On the second day, participants were asked to walk with both the passive and the foot placement-controlled Indego. Motion data were recorded through the Indego's encoders. Ground reaction force data were recorded through the instrumented treadmill. Six leg muscles were measured through EMG sensors. Measured muscles are: Biceps Femoris; Gluteus Maximus; Semitendinosus; Lateral Gastrocnemius; Medium Gastrocnemius; Rectus Femoris. Each walking trial was 2.5 minutes long.

Muscle activation from each walking trial was processed (25Hz high pass filter, full-wave rectification, 6Hz low pass filter) and averaged over gait cycles [11]. EMG compar-

isons between normal walking, walking with passive Indego, and walking with the controlled Indego will be presented.

7.2.2 Foot Placement Control

In this study, the foot placement controller includes four components: the foot placement estimator, the path planning component, the inverse kinematics component, and the local proportional-derivative (PD) tracking controllers (figure 34).

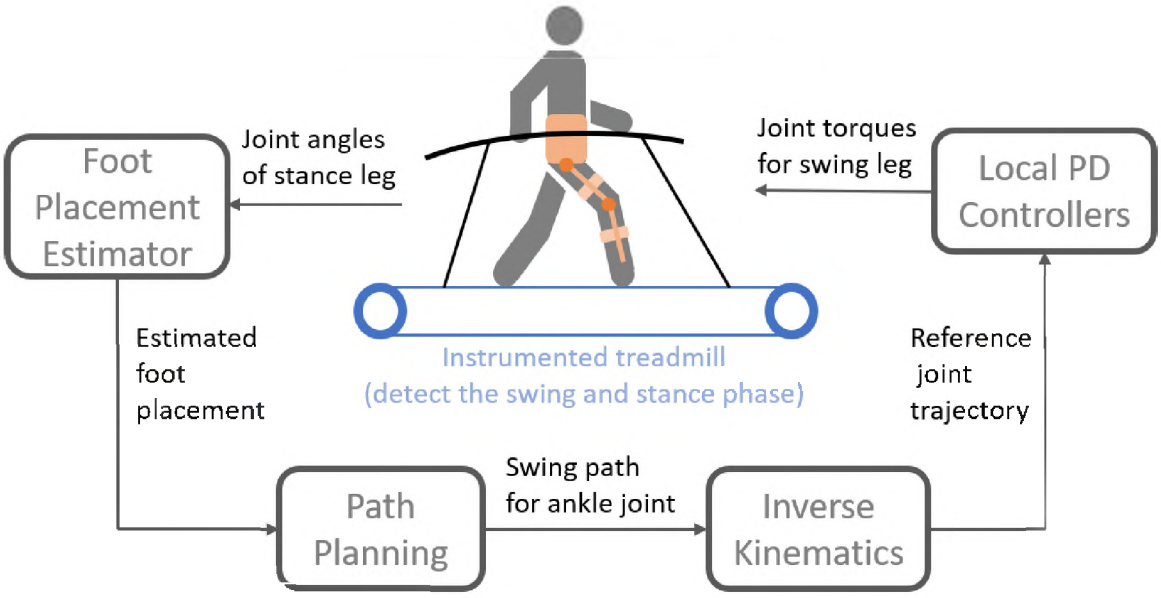

Figure 34: Structure of the foot placement control for Indego Exoskeleton.

The foot placement estimator generates a desired landing location of the swing foot based on the pelvis position and velocity relative to the stance foot (equation 7.1). The pelvis position and velocity were calculated in real time from the hip and knee joint angles and angular velocities of the stance leg, using forward kinematics.

$$\begin{aligned} x_{ifl} &= P_1 \cdot x_p + P_2 \cdot \frac{\dot{x_p}}{\omega_0} \\ x_{ifl}(\Delta t) &= x_{ifl}(0) \cdot e^{\omega_0 \cdot \Delta t} \end{aligned} \tag{7.1}$$

where, x_{ifl} is the instantaneous desired foot location in sagittal plane based on the state

feedback; x_p is the relative pelvis position to stance leg ankle position in sagittal plane; $\dot{x_p}$ is the velocity of pelvis in sagittal plane; P_1 and P_2 are the two gains applied on these two feedback signals; ω_0 is the reciprocal of the time constant of a pendulum with the leg length of human, $\omega_0 = \sqrt{g/L_{leg}}$; $x_{ifl}(\Delta t)$ is the desired foot location at the coming Δt time point; $x_{ifl}(0)$ is the current instantaneous desired foot location.

The path planning component generates paths (vertical and horizontal directions) for the swing foot based on two scaled polynomial functions. The scaling parameters are the step length and the total swing duration (Equ. 7.2). There is a difference between the path planning in this study and the identification study in Chapter VI. In this chapter, the swing paths were relative to the location of stance foot, while in the previous chapter, the swing paths were relative to the location of pelvis. In general, they are the same but for different purposes. Coefficients of the polynomial functions were calculated based on the swing motion in each participant's walking when wearing the passive Indego. Detailed information can be found in Appendix E.1 and E.3. The swing foot location at the swing time t is calculated from:

$$f(P_{sta}, P_{des}, T, t) = P_{sta} + \sum_{n=1}^{N-1} A_n \cdot (P_{des} - P_{sta}) \cdot (\frac{t}{T})^n + (1 - \sum_{n=1}^{N-1} A_n)(P_{des} - P_{sta}) \cdot (\frac{t}{T})^N \tag{7.2}$$

where, P_{sta} is the swing foot location at the beginning of swing; P_{des} is the estimated foot placement at the end of swing; T is the total swing duration; t is the current swing time frame; N is the total order of the polynomial function; A_n is the coefficient of the n^{th} order polynomial term.

An inverse kinematics module calculates the reference joint angles for the swing leg at each time frame in the swing period based on foot position. The foot position at each time frame can be calculated based on the above polynomial functions. The reference hip

and knee joint angles were calculated by solving the following nonlinear equations through Newton's method.

$$\begin{aligned} P_x &= l_{thigh} \cdot sin(\theta_h) + l_{shank} \cdot sin(\theta_h + \theta_k) \\ P_y &= -l_{thigh} \cdot cos(\theta_h) - l_{shank} \cdot cos(\theta_h + \theta_k) \end{aligned} \tag{7.3}$$

where, P_x is the desired foot position in the x direction; P_y is the desired foot position in the y direction; l_{thigh} is the length of thigh; l_{shank} is the length of shank; θ_h is the joint angle of hip; θ_k is the joint angle of knee.

Proportional-derivative (PD) controllers were used at the hip (1600 Nm/rad and 120 Nm s/rad) and knee (1200 Nm/rad and 80 Nm s/rad) joints to track the calculated reference joint angles. The gains of these two tracking controllers were set as zeros in the stance phase, which made Indego's leg fully passive in the stance phase.

7.2.3 Hardware Setup

In the hardware side, the Indego walking test includes an instrumented treadmill, a windows computer equipped with Matlab/Simulink, and the Indego itself (Fig. 35). The instrumented treadmill detects the ground reaction forces under each foot, in which the vertical force was used to determine the stance and the swing phases. The instrumented treadmill communicate with the windows computer through a data acquisition (DAQ) device (National Instruments PCI-6014). The computer communicates with the Indego through a CAN bus. The Simulink desktop real-time toolbox was used that enabled the real-time data transition between devices. The control algorithm (foot placement control) in Simulink executed with the 'external' model which compiled the entire control model into C code and sent to the Indego's micro-processor (target machine). The entire system runs at 200 Hz sampling rate.

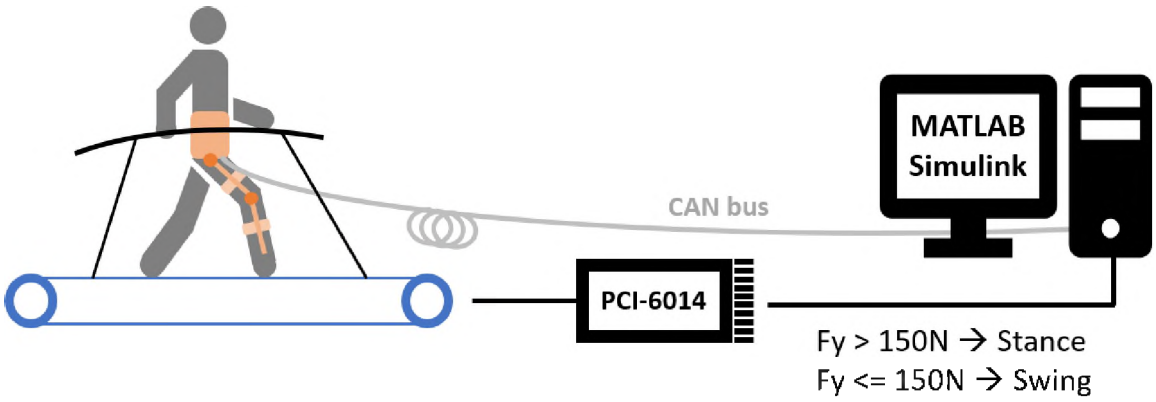

Figure 35: Hardware setting of the Indego test.

7.3 Results

Results of the walking test will be described into two parts. Result of the first day's test are described first to show the difference between normal walking and walking with passive Indego. Results of the second test day are described in the second part, which compared between walking with passive and controlled Indego.

7.3.1 Comparison Between Normal Walking and Walking with Passive Indego

In this section, the second participant's data is demonstrated. The first participant had a similar result and is shown in the appendix E.5. EMG results indicate that walking with passive Indego largely affected the activation pattern of leg muscles comparing to normal walking (Fig. 36). In five monitored muscles, walking with passive Indego shows higher activations in the phase of early stance. The function of these five muscles is to extend the hip joint and flex the knee joint. For the hip joint, higher muscle activations indicate larger efforts were needed to extend the hip joint. For the knee joint, higher muscle activations may indicate stronger co-contraction. In the phase of early swing, Gluteus Maximus and Gastrocnemius muscles have higher activations in the case of wearing passive Indego. This demonstrates that the participant tried to slow down the swing leg and tried harder to lift up the swing foot avoiding the interaction with the ground at early swing. In the late swing

phase, Biceps Femoris, Semitendinosus, and Gastrocnemius muscles all have smaller muscle activations in the walking trial with the passive Indego, shown that less efforts were used to slow down the swing leg.

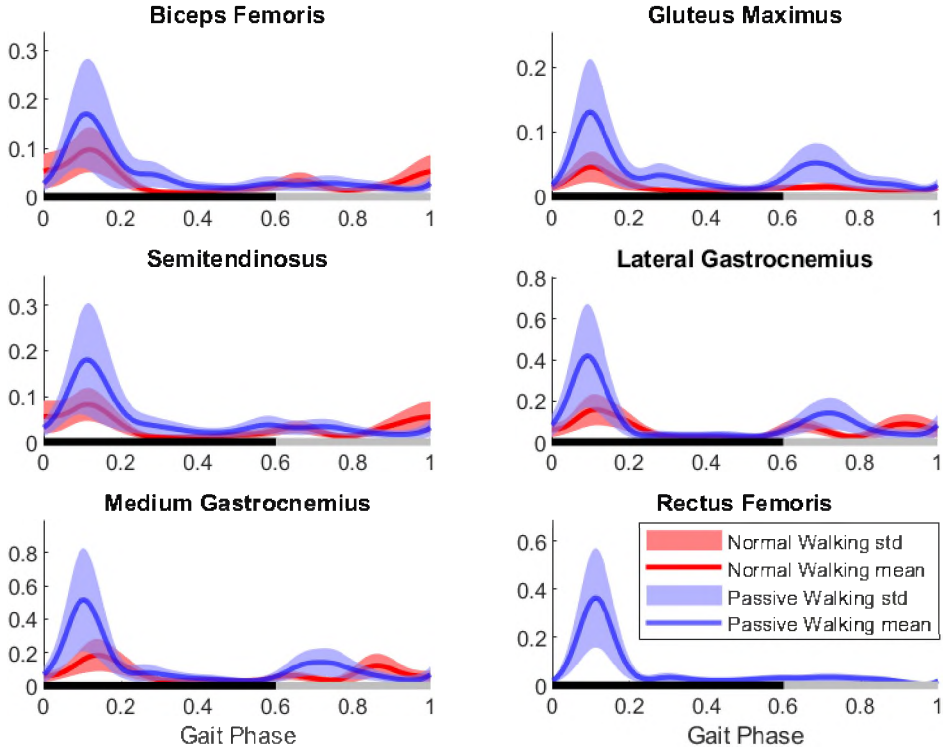

Figure 36: Activation of selected muscles in normal walking and walking wearing passive Indego. (Please note that Rectus Femoris was not recorded in the normal walking trial.)

Beside the muscle activations, motion data also showed significant difference between normal walking and walking with the passive Indego. Based on the joint motions of stance leg, pelvis position and velocity were calculated (37). Comparing to the normal walking, walking with passive Indego have much higher variation in terms of the pelvis velocity. Instead of having two peaks in the normal walking, only one larger peak exist in the early stance.

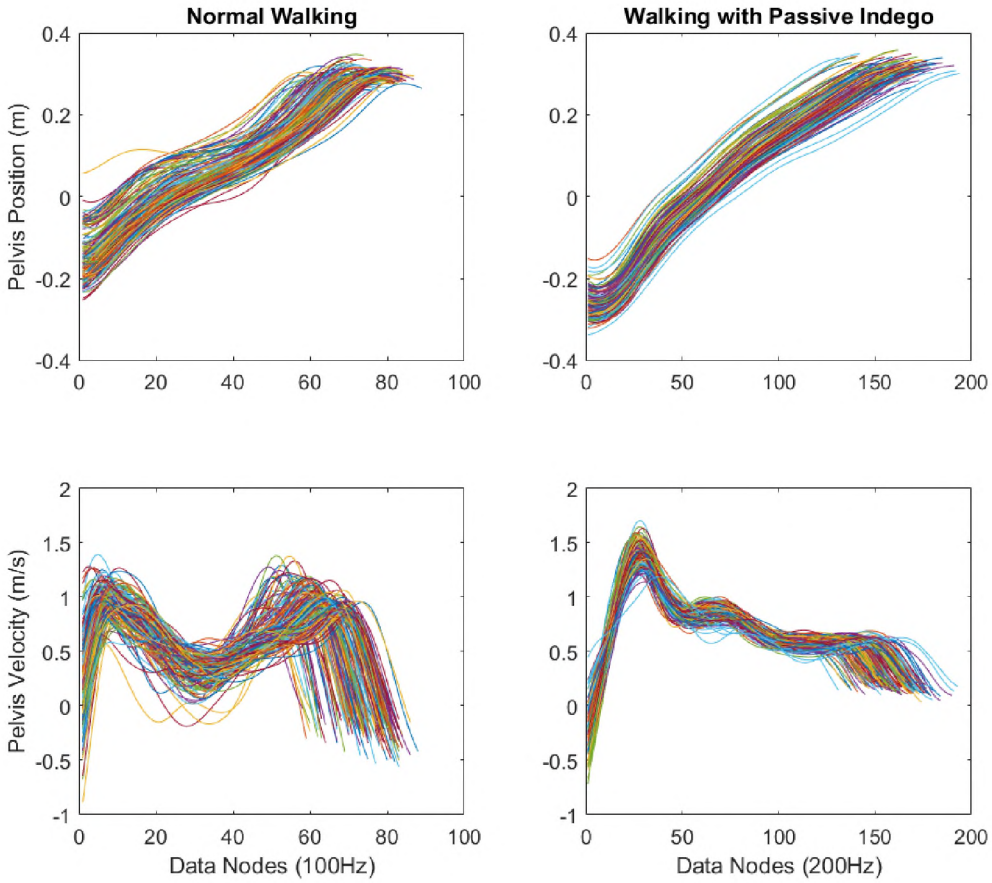

Figure 37: Pelvis position and velocity of participant two in normal walking and walking with passive Indego.

7.3.2 Comparison Between Passive and Foot Placement Controlled Indego Walking

In general, the first participant had significant higher muscle activations (yellow line indicates significant difference ($P < 0.05$) between two trials) in the walking trial with foot placement controlled Indego (blue line and area) than with the passive Indego (red line and area) during the majority of swing period (grey x axis) (Fig. 38). Biceps Femoris, Gluteus Maximus, and Semitendinosus have significant smaller muscle activations at the early swing with the foot placement-controlled Indego. Higher muscle activation in the walking trial with foot placement-controlled Indego was not expected which means that the participant was fighting with the exoskeleton.

The second participant had significant higher muscle activations in the walking trial with foot placement controlled Indego at early and middle swing phases (Fig. 39). At the late swing, smaller muscle activations of almost all six monitored muscles were recorded. These lower muscle activations indicate that the controlled exoskeleton was helping him slow down the swing leg before landing.

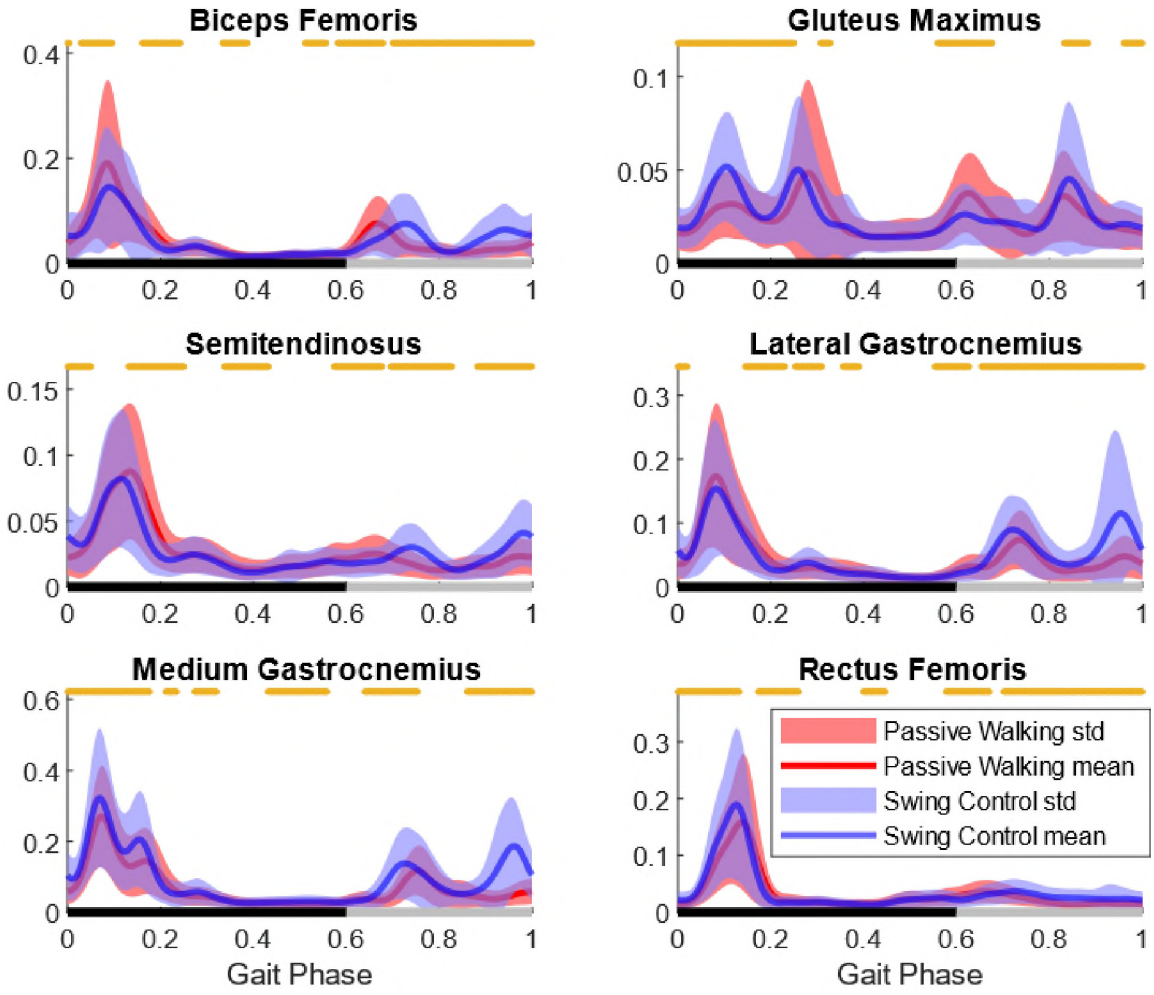

Figure 38: Difference between leg muscle activation of participant one while wearing the passive and swing controlled Indego.

7.4 Discussion

Both participants were able to keep stable walking with the foot placement controlled Indego. They all mentioned that the foot placement-controlled exoskeleton was helping them

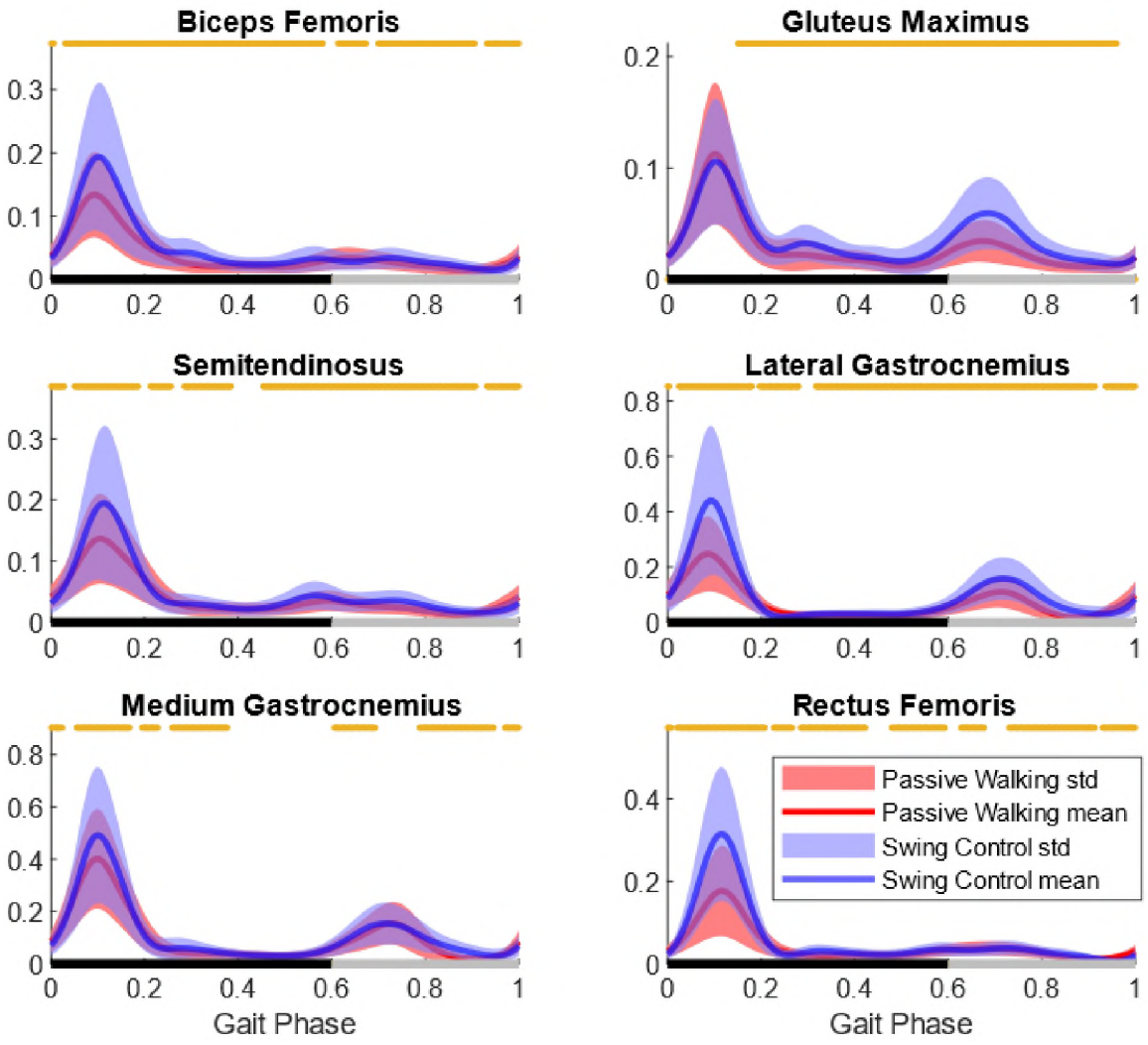

Figure 39: Difference between leg muscle activation of participant two while wearing the passive and swing controlled Indego.

to swing their legs forward which reduced around 40 % - 50% of their total efforts. However, muscle activation of these two participants does not fully support their feeling.

EMG and motion results of the passive Indego walking trial indicate that it introduced instability to the walking motion. Participants used higher co-contraction in the stance phase to perform stable walking. The passive Indego also introduced resistance to participants in the walking, which showed smaller muscle activations in the late swing phase.

EMG results of the controlled Indego walking trial did not fully support our hypothesis that the foot placement controller can reduce muscle activations in the swing phase. One

important reason is that participants didn't trust the controller and cannot fully turn off their muscles. On one hand, participant does not have sufficient time to be trained to fully turn off their leg muscles during the swing phase. On the other hand, since the Indego does not have an ankle joint, foot drop will happen if leg muscles are fully turned off in the swing phase. In the walking test, the second participant had much more significant foot drop (his foot was more frequently interacting with the treadmill belt in the middle swing) than the first participant, which turned out had lower muscle activations. In addition, since the passive Indego already worked as resisting device that slowed down the swing motion at late swing, it is hard to see a significant reduce of the muscle activations even with the foot placement control. The second participant did show some reduce of the muscle activations, which indicate that the swing controller provide more help to slow down the swing leg.

7.5 Conclusion

In this study, we implemented the foot placement controller on a lower limb exoskeleton and generated stable walking motion with healthy participants. Muscle activation results showed inconclusive effects of this controller. More studies are needed.

7.6 REFERENCES

[1] A. Chu, *Design of the Berkeley lower extremity exoskeleton (BLEEX).* PhD thesis, University of California, Berkeley, 2005.

[2] H. A. Quintero, R. J. Farris, and M. Goldfarb, "A method for the autonomous control of lower limb exoskeletons for persons with paraplegia," *Journal of Medical Devices*, vol. 6, no. 4, p. 041003, 2012.

[3] A. Esquenazi, M. Talaty, A. Packel, and M. Saulino, "The rewalk powered exoskeleton to restore ambulatory function to individuals with thoracic-level motor-complete

spinal cord injury," *American Journal of Physical Medicine & Rehabilitation*, vol. 91, no. 11, pp. 911–921, 2012.

[4] R. Griffin, T. Cobb, T. Craig, M. Daniel, N. van Dijk, J. Gines, K. Kramer, S. Shah, O. Siebinga, J. Smith, *et al.*, "Stepping forward with exoskeletons: Team ihmc's design and approach in the 2016 cybathlon," *IEEE Robotics & Automation Magazine*, vol. 24, no. 4, pp. 66–74, 2017.

[5] A. L. Hof, "The 'extrapolated center of mass' concept suggests a simple control of balance in walking," *Human Movement Science*, vol. 27, no. 1, pp. 112–125, 2008.

[6] L. Zhang and C. Fu, "Predicting foot placement for balance through a simple model with swing leg dynamics," *Journal of Biomechanics*, vol. 77, pp. 155–162, 2018.

[7] S. Kajita, F. Kanehiro, K. Kaneko, K. Yokoi, and H. Hirukawa, "The 3d linear inverted pendulum mode: A simple modeling for a biped walking pattern generation," in *Proceedings 2001 IEEE/RSJ International Conference on Intelligent Robots and Systems. Expanding the Societal Role of Robotics in the the Next Millennium (Cat. No. 01CH37180)*, vol. 1, pp. 239–246, IEEE, 2001.

[8] J. Pratt, J. Carff, S. Drakunov, and A. Goswami, "Capture point: A step toward humanoid push recovery," in *Humanoid Robots, 2006 6th IEEE-RAS International Conference on*, pp. 200–207, IEEE, 2006.

[9] T. Koolen, T. De Boer, J. Rebula, A. Goswami, and J. Pratt, "Capturability-based analysis and control of legged locomotion, part 1: Theory and application to three simple gait models," *The International Journal of Robotics Research*, vol. 31, no. 9, pp. 1094–1113, 2012.

[10] J. Pratt, T. Koolen, T. De Boer, J. Rebula, S. Cotton, J. Carff, M. Johnson, and P. Neuhaus, "Capturability-based analysis and control of legged locomotion, part 2:

Application to m2v2, a lower-body humanoid," *The International Journal of Robotics Research*, vol. 31, no. 10, pp. 1117–1133, 2012.

[11] P. Konrad, "The abc of emg," *A practical Introduction to Kinesiological Electromyography*, vol. 1, no. 2005, pp. 30–35, 2005.

PART III.

JOINT IMPEDANCE PROPERTIES

CHAPTER VIII

IDENTIFICATION OF JOINT IMPEDANCE PARAMETERS THROUGH TRAJECTORY OPTIMIZATION

8.1 Introduction

The impedance control algorithm [1, 2] has been used in controlling prosthetic legs [3–5]. Comparing to track fixed reference trajectories, it has the advantage that the soft interaction between prosthetic devices and their users can be achieved. However, implementing the impedance control on prosthetic legs isn't as straight forward as implementing on robot manipulators. One key issue is that suitable impedance parameters are not easy to find that can allow people with disabilities to regain normal and natural motions.

A common way to find suitable impedance parameters is through manually tuning on massive walking trials. In the tuning process, the quasi-stiffness and damping parameters of healthy humans' joints were normally used as a starting point to find the final appropriate parameters [6]. This process can generally achieve suitable and comfortable walking patterns for amputees, however, it requires highly skilled clinicians and is time consuming. Even though a cyber expert system [7] was developed that helped make this process easier, its tuning results were not as good as clinic experts. In addition, special lab equipment was required which may not be available in the clinic. Studies also showed that the quasi-stiffness and damping parameters are far from suitable values that can generate reasonable walking motions [3]. It is believed that the real joint impedance properties can provide better starting points for this tuning process [8].

To find the real impedance properties of human leg joints, studies have been done on walking with mechanical perturbations [9–13]. In these studies, joint impedance properties were calculated from the small variations of the joint motions and the changes in joint torques that were caused by the perturbations. As a result, these perturbations have to be applied on specific gait timing so that an averaged perturbation effects can be achieved by averaging multiple gait cycles. In addition, these perturbation devices must also provide information, such as ground reaction forces, to calculate joint torques. Finally, they should not affect participants' walking pattern when perturbation was not applied. Due to these critical requirements, only the ankle joint was studied using this approach so far

[11]. Trajectory optimization [14, 15] has the potential to identify the impedance properties of humans leg joints directly from walking data that was randomly perturbed by just belt speed. Since a simulation model is included in the trajectory optimization, it only requires the joint motion information which does not rely on specific perturbation devices. However, to our knowledge, this approach has not been validated yet.

Thus, in this study, we propose that the trajectory optimization can identify leg joints' impedance properties from randomly perturbed walking data. Two parts of work were done here. Through synthetic data, we first inspected whether sensor noise and model errors will affect the accuracy of identifying impedance properties through trajectory optimization. Then, a pilot study was done that identified the ankle joint impedance properties from perturbed walking data of two participants at two walking speeds.

8.2 Validation of the Trajectory Optimization on Identifying Joint Impedance Properties

8.2.1 Methods

The synthetic data was generated through an optimization process. It was based on a seven-link 2 dimensional gait model [15]. While generating the data, the knee and ankle joints in the model's left leg were controlled by two four-phases impedance controllers, respectively. The other joints were driven by open-loop torques. In addition, the walking data was generated under random (belt speed) perturbations [16] at an averaging walking speed of 1.2 m/s.

Ten seconds of stable walking motion which satisfied these conditions was found through trajectory optimization. Parameters of the impedance controller were optimized in this process, because it is very hard to achieve ten seconds stable walking under external perturbation with predefined control parameters. In the trajectory optimization, one participant's walking motion from a published data-set [16] was used as the reference motion for the gait model. This helped find reasonable results and reduced the computation time.

The four-phase impedance control includes two components: the periodic baseline torques and the proportional-derivative (PD) tracking controller. The periodic baseline torques is the same in gait cycles, which represents the average joint torques of the normal walking. In perturbed walking, durations of the gait cycles might be different. Accounting for this, the baseline torques were time-scaled to the gait duration of each gait cycle in the reference walking motion which is perturbed. The PD tracking controller tracked the averaged normal walking motion (unperturbed) of the same participant (equation 8.3.1). The tracking controller was defined as a four-phases control in each gait cycle. Two control gains were included in each walking phase. Four phases were predefined based on the information of the reference motion: early stance, late stance, early swing, and late swing [3] (figure 46).

$$\tau_i = \tau_i^b + K_p^j \cdot (\theta_i^m - \theta_i) + K_d^j \cdot (\dot{\theta}_i^m - \dot{\theta}_i)$$

where, τ_i represents the impedance controlled joint torque at the i^{th} data node; τ_i^b represents the baseline torque at the i^{th} data node; K_p^j is the proportional gain of the j^{th} phase of the gait cycle; K_d^j is the derivative gains of the j^{th} phase of the gait cycle; θ_i^m represents the joint angle at the i^{th} data node of the normal walking motion; θ_i represents the joint angle at the i^{th} data node of the optimized motion.

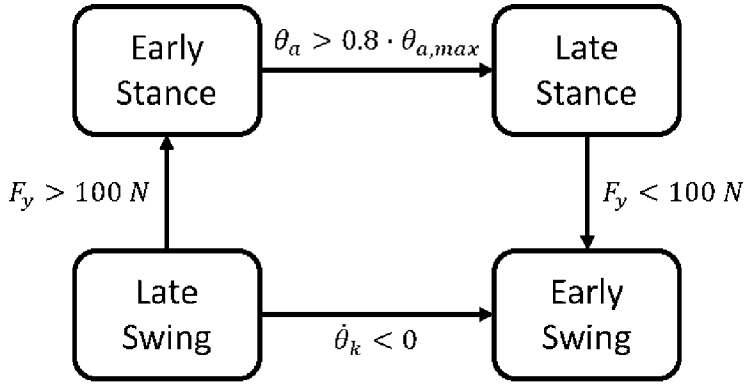

Figure 40: Four phase finite state controller for walking.

In the trajectory optimization, tracking the reference walking motion was not the only

thing in the objective function. Other components were included to make the optimized motion reasonable:

1. Track the reference motion:

$$\mathrm{F}_{tm} = \frac{\sum_{i=1}^{N}(\theta_i^m - \theta_i)^2}{N}$$

2. Smooth joint motion:

$$\mathrm{F}_{sm} = \frac{\sum_{i=1}^{N-1}(\frac{\theta_{i+1} - \theta_i}{\Delta t})^2}{N}$$

3. Smooth joint torques:

$$\mathrm{F}_{st} = \frac{\sum_{i=1}^{N-1}(\frac{\tau_{open,i+1} - \tau_{open,i}}{\Delta t})^2}{N} + \frac{\sum_{i=1}^{N-1}(\frac{\tau_{baseline,i+1} - \tau_{baseline,i}}{\Delta t})^2}{N}$$

4. Minimize the impedance control terms:

$$\tau_{imp} = K_p \cdot (\theta^m - \theta) + K_d \cdot (\dot{\theta}^m - \dot{\theta})$$
$$\mathrm{F}_{mt} = \frac{\sum_{i=1}^{N-1}(\tau_{imp})^2}{N}$$

5. Periodicity of the baseline torques:

$$\mathrm{F}_{pt} = (\tau_{baseline,1} - \tau_{baseline,N})^2$$

Five weights were setup to multiple these five components to adjust their impacts inside the overall objective function. These weights were manually tuned based on the optimization results. Weight values that used to generate the simulated motion data are:

Table VIII: Weights of the objective components.

Weights	W_{tm}	W_{sm}	W_{st}	W_{mt}	W_{pt}
Value	100.0	$5e-3$	$1e-5$	$1e-7$	$1e-1$

In the trajectory optimization, optimizing variables were: the joint motions and velocities; the baseline torques; PD gains in the tracking controllers. The reference joint motion was used as the initial guess for the optimizing joint motion. The averaged joint torques of the participant's normal walking data was used as the initial guess for the baseline torques.

Initial guess of the impedance control parameters (PD gains) were randomly selected between the lower and upper bounds. The lower bounds were set as zero for all control parameters. The upper bounds were shown in table IX, which are five times of the estimated impedance parameters in previous studies [3, 9]. Ten optimizations were conducted and the result with the lowest objective function was selected as the simulation data.

Table IX: Upper bounds for the optimizing impedance parameters.

Phase	Knee		Ankle	
	Kp (Nm/rad)	Kd ($Nm \cdot s/rad$)	Kp (Nm/rad)	Kd ($Nm \cdot s/rad$)
1	450	1.5	750	3.6
2	600	6	1500	3.0
3	30	3	150	5.1
4	30	6	150	4.2

Impedance controller identifications were applied on the simulated motion data through the trajectory optimization method. This is to check whether the correct impedance values can be found. These identifications were conducted in four different conditions. The goal is to examine the effect of the each condition on the identified impedance control parameters.

- The first test condition is to identify the impedance control parameters from the pure simulated data. The goal is to check if trajectory optimization can find the correct control gains directly from the simulated data. For identification, the same objective function in generating the simulation data was used. The only difference is to replace the reference motion with the simulated motion. The simulated motion data was used as the initial guess for the optimizing motion. Initial guess for the impedance control parameters were randomly selected between the lower and upper bounds which are the same as the setup in generating the simulation data. Ten optimizations were conducted and that optimizing result that has the closest fit with the simulation data was selected.

- The second test is to identify the impedance control parameters from the simulated data with sensor noise. The goal is to check the effect of sensor noise on the accuracy

of the identified impedance parameters. The same objective function as in generating the simulation data was used here. The only difference of this study from the first situation is that six sensor noise signals were added to the the six joint (left/right hip, knee, and ankle) motions of the simulated data. These sensor noises were designed as pink noises. Their power spectrum was based on the noise level in human quiet standing trials [17]. Ten instances of these sensor noises were generated in ten impedance control parameter identifications, respectively. In each identification with one instance of sensor noises, ten optimizations were conducted with random initial guesses of the identified impedance parameters. The optimization result that has the closest fit with the simulation data was selected from these ten optimizations.

- The third test is to check whether the change of dynamic parameter of the gait model largely affects the identifying impedance parameters. Therefore, impedance control parameters were identified on the simulated data with the adjusted gait model where its dynamic parameters were slightly changed. These changed parameters include segment mass, inertia, and center of mass location of each segment. Segment length was not changed, since it can be accurately measured. In total, 13 dynamic parameters (left and right leg were assumed symmetric) were randomly changed within 90% and 110% of its original value (used to generate simulated data). Ten instances of this random change were generated in ten impedance control parameter identifications, respectively. In each identification, these 13 parameters were randomly changed. In each identification problem with one instance of the parameter adjustment, ten optimizations were conducted with random initial guesses of the identified impedance parameters. the Optimization result that has the closest fit with the simulation data was selected from these ten optimizations.

- The fourth test is to check the effects of foot size in the gait model on the identified impedance control parameters. Thus, impedance control parameters were identified

on the simulated data with the gait model that the foot size were slightly changed. These changed parameters include foot height, the horizontal length from ankle joint to toe, and the horizontal length from ankle joint to heel. These three parameters (left and right foot were assumed symmetric) were randomly changed within 90% and 110% of its original value (used to generate simulated data). Ten instances of this random change were generated in ten impedance control parameter identifications, respectively. In each identification, these three parameters were randomly changed. In each identification problem with one instance of the parameter adjustment, ten optimizations were conducted with random initial guesses of the identified impedance parameters. The optimization result that has the closest fit with the simulation data was selected from these ten optimizations.

8.2.2 Results

This work aims to validate the ability of the trajectory optimization method for identifying correct impedance properties of human leg joints. Figure 41 shows the reference motion and the generated simulation data. The bottom two subplots are the left and right vertical ground reaction forces (GRF) from the reference motion data. Four walking phases were divided (marked with different color) based the ankle and knee joint motions as well as the vertical GRF. Overall, the generated walking motion was close to the reference motion, but with some differences at peaks. Variations among gait cycles existed in the generated motion data, even though not as large as the reference data. Joint motions in the generated data were smooth in general, except the right ankle motion.

Figure 42 shows the joint motions that were controlled by impedance controllers and the corresponding baseline motions which is the averaged gait data in normal walking. The generated motion data was close to the baseline motion, which indicates that the PD tracking controller is only response for the small variations of the generated joint motions that were away from the baseline joint motions, instead of the entire joint torques.

The optimized impedance control gains are shown in table X. There are two gains for the knee and ankle joint in each phase of the impedance control. Most of these parameters were located between the lower and upper bounds, except one derivative gain (at knee joint in phase 4) hit the upper bound and two derivative gains (at ankle joint in phase 1 and 2) hit the lower bounds. The proportional (stiffness) gains of the knee joint were less than the proportional gains at the ankle joint in all phases. In the knee joint, proportional gains had similar values among all four phases. In the ankle joint, the proportional gains in the two stance phases were significantly larger than the gains that in the two swing phases.

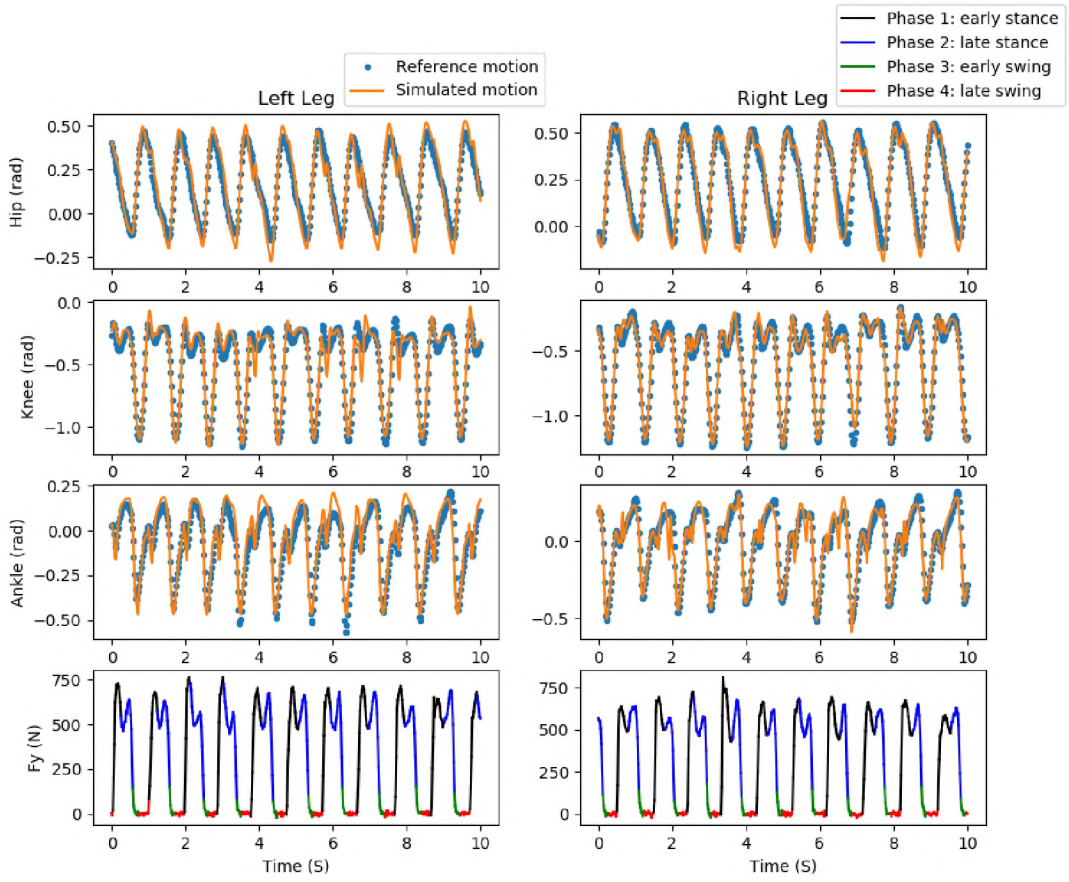

Figure 41: Comparison between the reference motion and the generated motion data.

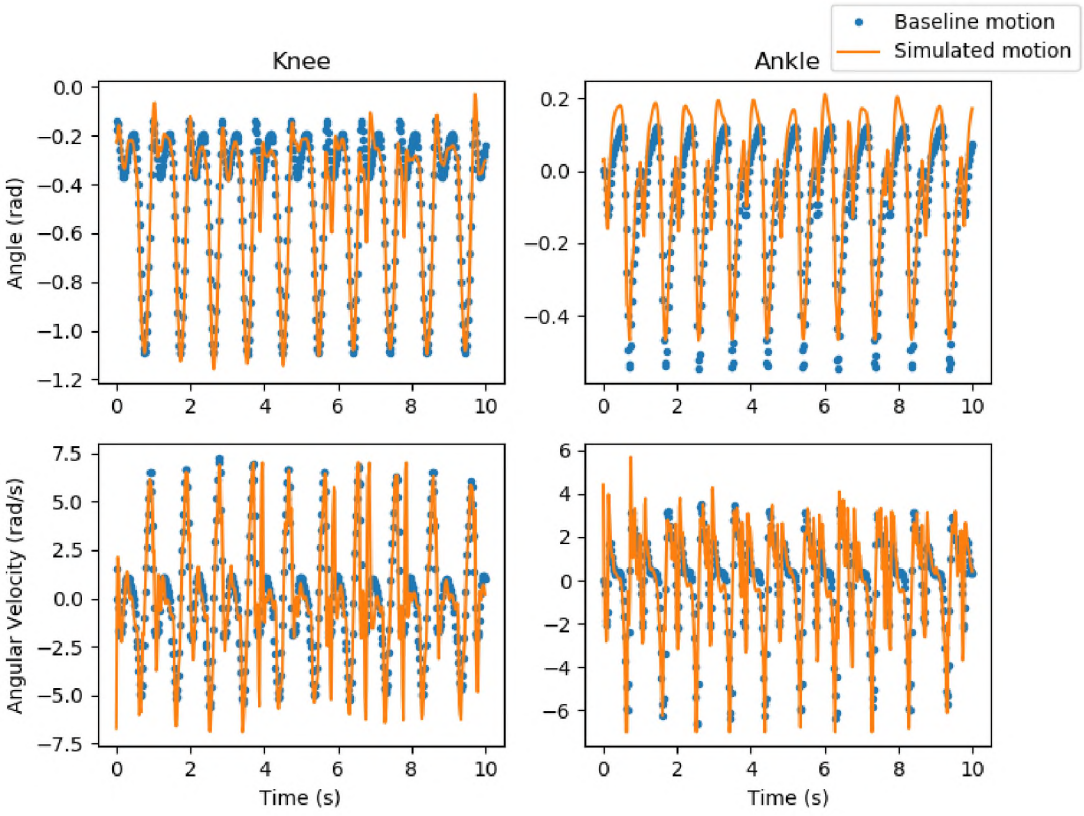

Figure 42: Comparison between the baseline joint motions and the generated joint motions

Table X: Optimized impedance parameters of the generated simulation data.

Phase	Knee		Ankle	
	Kp (Nm/rad)	Kd ($Nm \cdot s/rad$)	Kp (Nm/rad)	Kd ($Nm \cdot s/rad$)
1	13.788	1.250	440.650	0.0
2	6.977	0.481	361.956	0.0
3	12.515	0.011	147.408	4.063
4	10.932	6.000	15.795	0.073

Impedance parameter identifications were conducted on four situations to check the effects of different factors. Results of the identifications are shown in figure 43 and 44. The first bar in each subplot shows the true impedance parameter that generated the synthetic data. The other four bars are the identified impedance control gains in four situations. In the first situation, only one best result was selected from ten optimizations, therefore, there is no standard variation shown in the plot. In the other situations, ten instances of

corresponding changes were made and ten best results were selected in ten identifications with these changes. The heights of these bars indicate the averaged value of these ten best results, and the vertical black lines represent their standard deviation. In general, the identified impedance parameters are different from the true value, even in the first situation where no changes were made. However, the absolute errors between them was not large. In the knee joint, the absolute errors of the proportional gains in all situations were less than 9 Nm/rad (Table XI). The error of derivative gains were less than 0.3 Nms/rad (Table XI). In the ankle joint, even though the absolute errors of the identified proportional gains at the first and second gait phase were large, relative errors of them were relatively small (no more than 11,05%) (Table XII). Absolute errors of other identified parameters were small. The only exception is the derivative gain in the third walking phase, where the absolute error reached to around 3.5 Nms/rad and the relative error reached to around 90%. The identified baseline torques in all four situations were also close to baseline torques that generated the synthetic data.

Comparing between identification situations, the fourth situation (foot size change) caused the largest standard deviations in both knee and ankle joints.

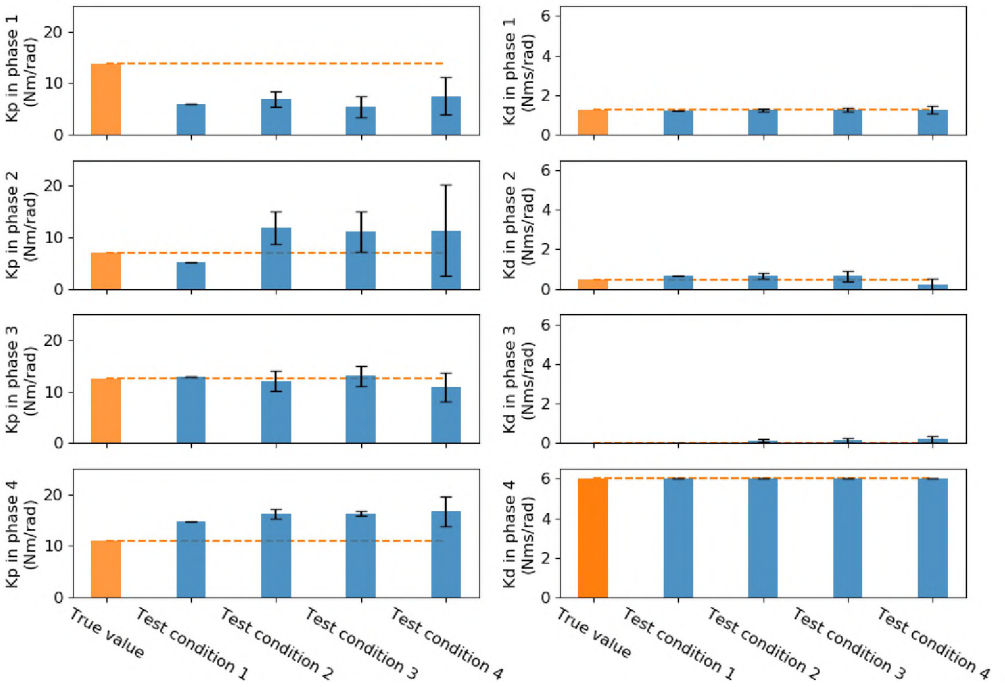

Figure 43: Identified impedance control parameters of the knee joint among four test conditions. Test condition 1 had perfect data and model. Test condition 2 had perfect model but noisy data. Test condition 3 had perfect data but adjusted model that changed dynamic properties. Test condition 4 had perfect data but adjusted model that changed foot size.

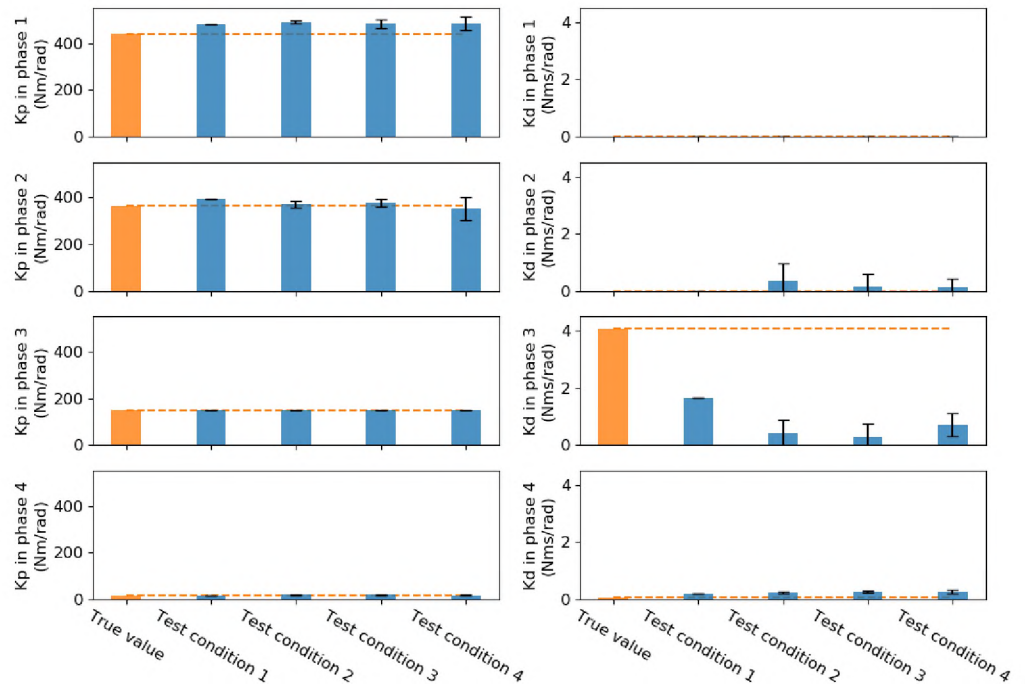

Figure 44: Identified impedance control parameters of the ankle joint among four situations. Test condition 1 had perfect data and model. Test condition 2 had perfect model but noisy data. Test condition 3 had perfect data but adjusted model that changed dynamic properties. Test condition 4 had perfect data but adjusted model that changed foot size.

Table XI: Absolute and relative error of identified impedance parameters in the knee joint.

Test conditions	Phase 1		Phase 2	
	Kp (Nm/rad)	Kd ($Nm \cdot s/rad$)	Kp (Nm/rad)	Kd ($Nm \cdot s/rad$)
1	7.86 (57.02%)	0.05 (4.17%)	1.73 (24.81%)	0.18 (38.30%)
2	6.85 (49.68%)	0.01 (0.81%)	4.93 (70.66%)	0.18 (37.23%)
3	8.36 (60.64%)	0.01 (0.97%)	4.14 (59.37%)	0.16 (32.87%)
4	6.26 (45.44%)	0.01 (0.64%)	4.40 (63.10%)	0.26 (53.62%)
	Phase 3		Phase 4	
	Kp (Nm/rad)	Kd ($Nm \cdot s/rad$)	Kp (Nm/rad)	Kd ($Nm \cdot s/rad$)
1	0.36 (2.87 %)	0.01 (133.53%)	3.80 (34.72%)	0.00 (0.00%)
2	0.48 (3.79%)	0.11 (1031.15%)	5.33 (48.78%)	0.00 (0.00%)
3	0.52 (4.15%)	0.13 (1251.1%)	5.36 (49.06%)	0.00 (0.00%)
4	1.57 (12.56%)	0.17 (1631.26%)	5.79 (52.93%)	0.00 (0.00%)

Table XII: Absolute and relative error of identified impedance parameters in the ankle joint.

Test conditions	Phase 1		Phase 2	
	Kp (Nm/rad)	Kd ($Nm \cdot s/rad$)	Kp (Nm/rad)	Kd ($Nm \cdot s/rad$)
1	40.38 (9.16%)	0.00 (100%)	31.33 (8.65%)	0.00 (99.97%)
2	48.62 (11.03%)	0.00 (568.53%)	8.44 (2.33%)	0.36 (1000+%)
3	42.30 (9.60%)	0.00 (25.27%)	14.68 (4.06%)	0.16 (1000+%)
4	43.47 (9.87%)	0.00 (27.95%)	8.83 (2.44%)	0.11 (1000+%)
	Phase 3		Phase 4	
	Kp (Nm/rad)	Kd ($Nm \cdot s/rad$)	Kp (Nm/rad)	Kd ($Nm \cdot s/rad$)
1	2.59 (1.75 %)	2.42 (59.58%)	0.91 (5.79%)	0.12 (165.26%)
2	2.59 (1.76%)	3.67 (90.22%)	3.26 (20.64%)	0.18 (240.06%)
3	2.59 (1.76%)	3.79 (93.27%)	3.05 (19.33%)	0.20 (275.41%)
4	2.58 (1.75%)	3.34 (82.31%)	1.88 (11.93%)	0.20 (271.53%)

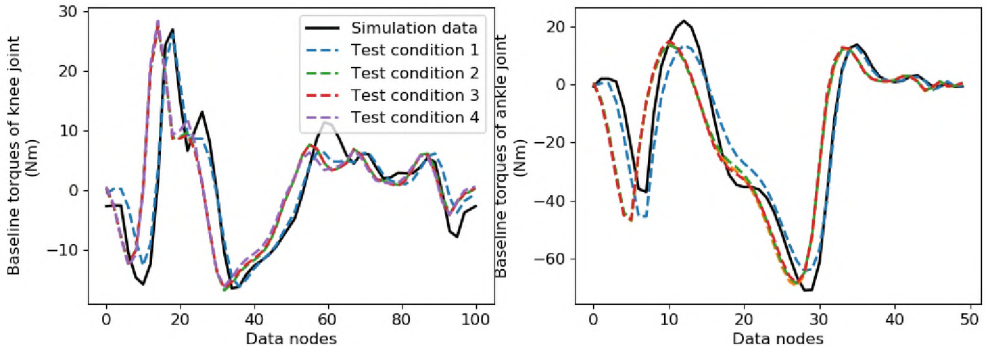

Figure 45: Identified baseline torques of the knee and ankle joints among four test conditions. Test condition 1 had perfect data and model. Test condition 2 had perfect model but noisy data. Test condition 3 had perfect data but adjusted model that changed dynamic properties. Test condition 4 had perfect data but adjusted model that changed foot size.

8.2.3 Discussion

The goal was to check whether the trajectory optimization can extract correct impedance parameters from the simulated data where the impedance control parameters were known. Results of the identifications in four different test conditions indicated that the trajectory optimization approach can identify relative close impedance parameters from just the joint motion data.

Identification in the first test condition (perfect data and model) find close but not the same impedance parameters that generated the simulation data. This did not fit our expec-

tation. In the first condition, the same gait model and pure simulated data were used in the trajectory optimization. We expected that the trajectory optimization will find the same impedance parameters that generated the simulation data. The main reason this did not happen is that the objective function included multiple components, not only the tracking part. The minimum of the objective function when generating the simulation data was not the minimum when the simulated motion was the tracking target. A new minimum of the objective function caused a different set of impedance parameters. On the other hand, we don't want to only tracking the motion. Other components in the objective function can make the identified motion more realistic. For instance, the component to smooth joint torques can avoid the rapid torque changes which cannot happen in a real human walking.

If the identified impedance parameters in test condition one was used as the comparison reference for the other three conditions, the absolute and relative errors, due to the sensor noise, model parameter changes, and foot size changes, would be much smaller. This comparison is valid, since they all converged to similar minimums. In test condition one, nothing related to the gait model or the simulated motion data was changed. The other three test conditions changed one factor of the gait model or the simulated data, respectively. Therefore, the differences in identified results between test condition one and the other three conditions indicate the effects of these change factor.

The optimized ankle joint proportional gains that generated the simulation data were slightly larger than previous identification studies [9]. To our knowledge, no studies have been done to identify the knee joint stiffness while walking. However, the optimized knee joint proportional gains were smaller than the manually tuned stiffness of a transfemoral prosthetic leg [3]. We suspect that these might because the improper weights on the objective function components. For instance, a large weight on the component that minimize the torques generated by the impedance controller may reduce the identified values of impedance parameters. This is our future study direction: to check how the weight changes on the objective components affect the identified impedance parameters.

8.3 Identification of the Ankle Joint Impedance Properties from Real Experimental Data

8.3.1 Methods

This pilot study was to identify impedance control parameters of ankle joint from the randomly perturbed walking data [16] through the trajectory optimization approach. One, two, and four-phases impedance controllers were identified from five seconds experimental data of one participant at 1.2 m/s walking speed. In addition, one-phase impedance controllers of ankle joint were identified for two participants at two walking speeds (0.8 m/s and 1.2 m/s).

The impedance control structure was slightly changed comparing to the impedance controller in the synthetic study: the zero joint position was used as the reference motion, instead of the averaged normal walking motion:

$$\tau_i = \tau_i^b + K_p^j \cdot (0 - \theta_i) + K_d^j \cdot (0 - \dot{\theta}_i)$$

The objective function here is simpler than the objective function used in the synthetic study. It only included the motion tracking component and the toque smoothing component. Ten optimizations were included in each identification problem to eliminate local minimums. Optimizing result that has the best fit with the experimental joint motions was selected from these ten optimizations as the best result.

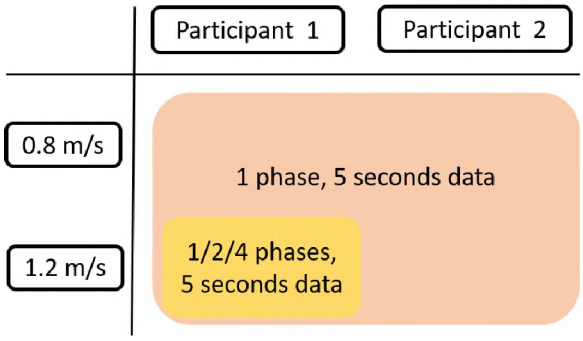

Figure 46: Identifications on experimental data.

8.3.2 Results

Figure 47 shows the identified results of participant 2 at walking speed of 1.2 m/s. One, two, and four-phases impedance controllers were identified from five seconds experimental data. The identified proportional gains in stance phases were larger than in the swing phases. The early stance stiffness is much higher than the late stance and the swing phases. The identified joint motions and the experimental data are shown in figure 48. The identified joint motions that with different phase impedance controllers were close to the experimental data. The left ankle (controlled by the identified impedance controllers) was able to generate the variations between gait cycle.

One phase impedance controllers were identified from two participants at two walking speeds (Figure 49). In general, participant two had slightly higher proportional gains than participant one in both speeds. Also, at faster walking speed, the proportional gains were higher. The derivative gains were almost zero.

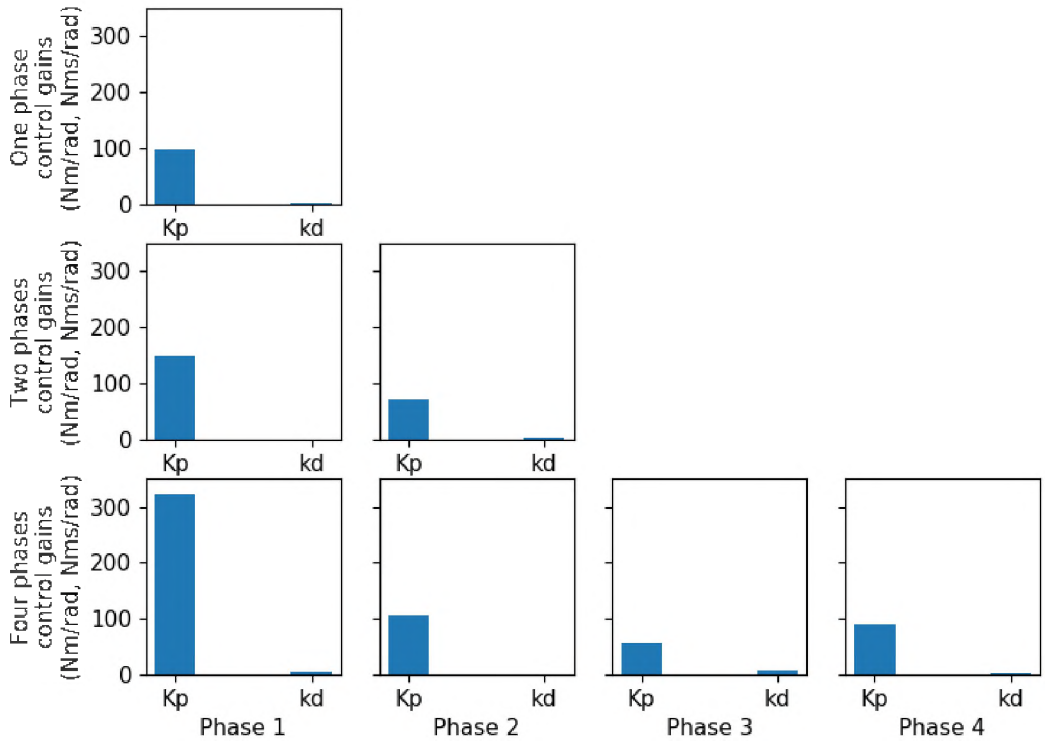

Figure 47: Impedance control parameters that identified for the ankle joint with different control structures.

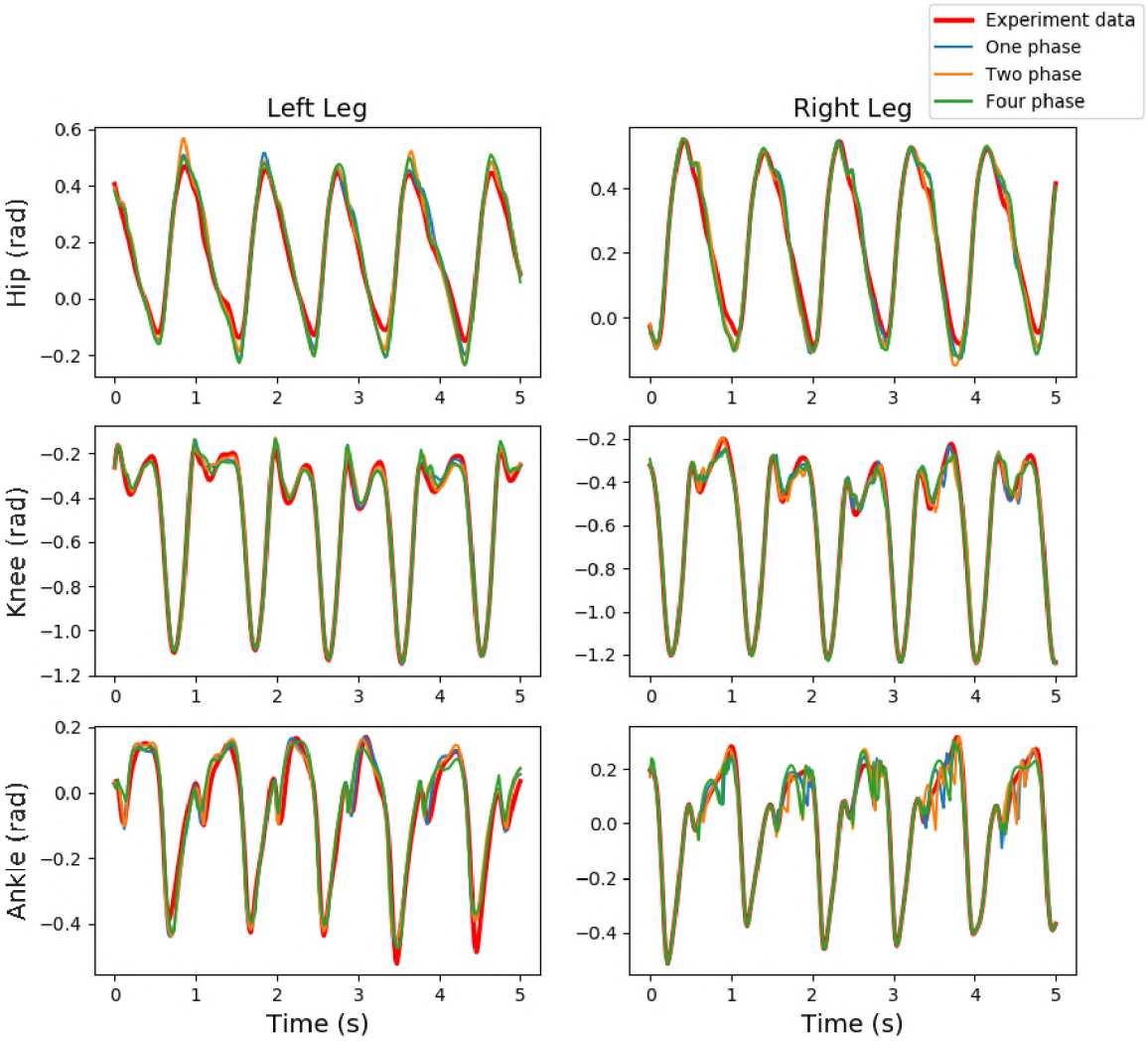

Figure 48: Motion that identified for the ankle joint with different control structures.

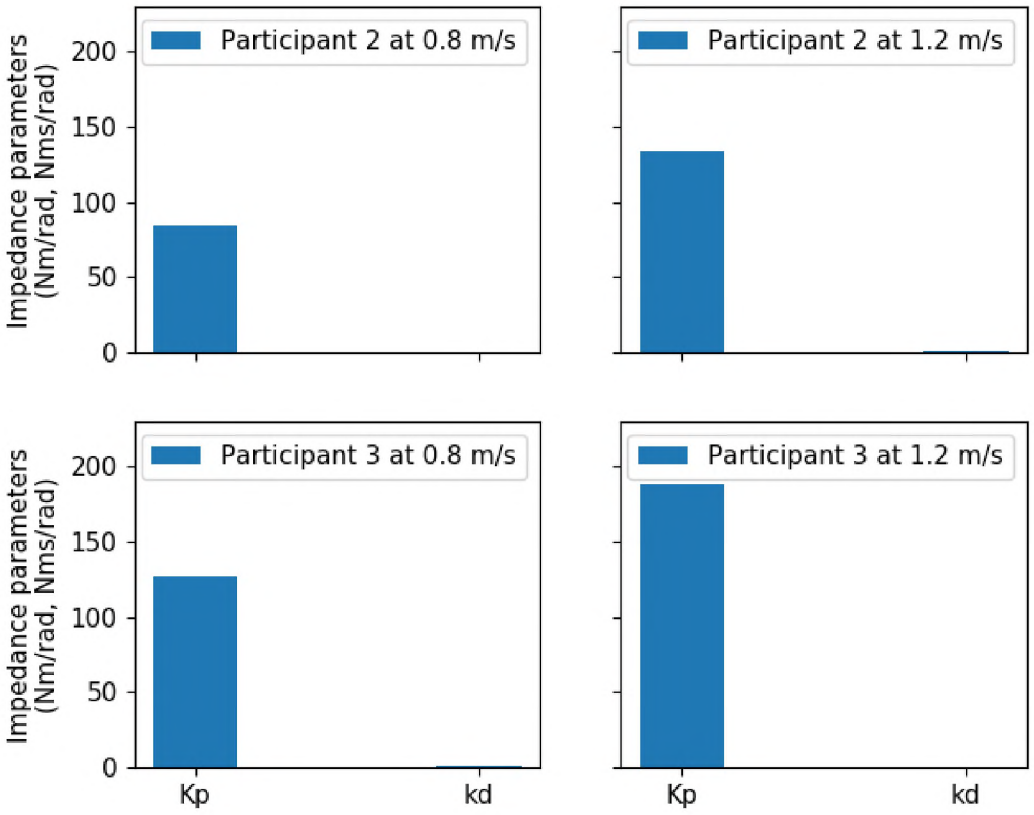

Figure 49: One-phase impedance control parameters of the ankle joint that were identified of two participants at two walking speeds.

8.3.3 Discussion

The identified proportional gains of the ankle joint are close to previous identification studies [9, 11]. One difference lies in the change direction of the identified stiffness. Rouse et. al. showed that the stiffness of ankle joint keeps increasing from the early stance to late stance, while, our results showed the opposite trend. One possible reason might be the changes that were made to the impedance control structure: using zero joint angle and the reference motion, instead of the normal walking motion. This can be examined in our further studies.

These identified impedance parameters were consistent between different participants

at at different walking speed. Also, parameters in different phases impedance controllers showed consistency. This may indicate that the trajectory optimization approach is robust in identifying the impedance properties. However, this needs to be examined by doing identification work on more participants' data.

8.4 Conclusion

In this work, the trajectory optimization approach was validated on identifying the joint impedance parameters through the synthetic study. Results indicated that it can identify relative accurate impedance parameters by only using the motion data. In addition, the this approach was used to identify impedance controllers that with different structures on two participants' perturbed walking data. Consistency results were got which indicates the robustness of this identification approach.

8.5 REFERENCES

[1] N. Hogan, "Impedance control: An approach to manipulation: Part i—theory," 1985.

[2] N. Hogan, "Impedance control: An approach to manipulation: Part ii—implementation," 1985.

[3] F. Sup, A. Bohara, and M. Goldfarb, "Design and control of a powered transfemoral prosthesis," *The International Journal of Robotics Research*, vol. 27, no. 2, pp. 263–273, 2008.

[4] A. F. Azocar, L. M. Mooney, L. J. Hargrove, and E. J. Rouse, "Design and characterization of an open-source robotic leg prosthesis," in *2018 7th IEEE International Conference on Biomedical Robotics and Biomechatronics (Biorob)*, pp. 111–118, IEEE, 2018.

[5] N. Aghasadeghi, H. Zhao, L. J. Hargrove, A. D. Ames, E. J. Perreault, and T. Bretl, "Learning impedance controller parameters for lower-limb prostheses," in *2013*

IEEE/RSJ International Conference on Intelligent Robots and Systems, pp. 4268–4274, IEEE, 2013.

[6] F. Sup, A. Bohara, and M. Goldfarb, "Design and control of a powered knee and ankle prosthesis," in *Proceedings 2007 IEEE International Conference on Robotics and Automation*, pp. 4134–4139, IEEE, 2007.

[7] H. Huang, D. L. Crouch, M. Liu, G. S. Sawicki, and D. Wang, "A cyber expert system for auto-tuning powered prosthesis impedance control parameters," *Annals of Biomedical Engineering*, vol. 44, no. 5, pp. 1613–1624, 2016.

[8] E. J. Rouse, R. D. Gregg, L. J. Hargrove, and J. W. Sensinger, "The difference between stiffness and quasi-stiffness in the context of biomechanical modeling," *IEEE Transactions on Biomedical Engineering*, vol. 60, no. 2, pp. 562–568, 2013.

[9] E. J. Rouse, L. J. Hargrove, E. J. Perreault, and T. A. Kuiken, "Estimation of human ankle impedance during the stance phase of walking," *IEEE Transactions on Neural Systems and Rehabilitation Engineering*, vol. 22, no. 4, pp. 870–878, 2014.

[10] A. L. Shorter and E. J. Rouse, "Mechanical impedance of the ankle during the terminal stance phase of walking," *IEEE Transactions on Neural Systems and Rehabilitation Engineering*, vol. 26, no. 1, pp. 135–143, 2017.

[11] H. Lee, E. J. Rouse, and H. I. Krebs, "Summary of human ankle mechanical impedance during walking," *IEEE journal of Translational Engineering in Health and Medicine*, vol. 4, pp. 1–7, 2016.

[12] H. Lee and N. Hogan, "Time-varying ankle mechanical impedance during human locomotion," *IEEE Transactions on Neural Systems and Rehabilitation Engineering*, vol. 23, no. 5, pp. 755–764, 2015.

[13] H. Lee, H. I. Krebs, and N. Hogan, "Linear time-varying identification of ankle mechanical impedance during human walking," in *ASME 2012 5th Annual Dynamic Systems and Control Conference joint with the JSME 2012 11th Motion and Vibration Conference*, pp. 753–758, American Society of Mechanical Engineers, 2012.

[14] A. J. van den Bogert, D. Blana, and D. Heinrich, "Implicit methods for efficient musculoskeletal simulation and optimal control," *Procedia Iutam*, vol. 2, pp. 297–316, 2011.

[15] M. Ackermann and A. J. Van den Bogert, "Optimality principles for model-based prediction of human gait," *Journal of Biomechanics*, vol. 43, no. 6, pp. 1055–1060, 2010.

[16] J. K. Moore, S. K. Hnat, and A. J. van den Bogert, "An elaborate data set on human gait and the effect of mechanical perturbations," *PeerJ*, vol. 3, p. e918, 2015.

[17] A. D. Goodworth and R. J. Peterka, "Identifying mechanisms of stance control: a single stimulus multiple output model-fit approach," *Journal of Neuroscience Methods*, vol. 296, pp. 44–56, 2018.

PART IV.

CONCLUSION

CHAPTER IX

Conclusion

Understanding how humans control their movements can inspire the control of powered exoskeletons and prostheses for better performance. The method of trajectory optimization with direct collocation has the potential to extract generalized and realistic motion controllers from long duration movement data without requiring extensive measurement equipment. Therefore, this dissertation validated and applied this method on extracting the feedback motion controllers of two types of human movements. Three aims were defined:

- **Aim 1:** Identify postural feedback controllers for human standing balance.
- **Aim 2:** Identify step strategy controllers for human walking.
- **Aim 3:** Identify joint impedance properties for human walking.

In chapter III, the human standing balance experiment was conducted on eight young adults. Movement data (optical motion capture data and ground reaction forces) was recorded in both the quiet and perturbed standing balance trials. The raw and processed experimental data, including joint angles and torques, was publicly shared on Zenodo. In chapter IV, a stochastic trajectory optimization approach was proposed. It was suggested that this approach can help find practically stable controllers in the identification process, which was not guaranteed in past motion controller identification studies [1–3]. In chapter V, the trajectory optimization approach was validated on simulated standing balance data to demonstrate that it can extract the correct postural control parameters. Then, five types of postural feedback controllers, from simple linear to complex nonlinear, were identified on the standing balance data-set from chapter III. Results indicated that a nonlinear controller with multiple time delay paths can best explain the balance control of those young adults.

In chapter VI, step strategy controllers were successfully identified on perturbed walking motions from a published data-set [4]. It was shown that young adults use nonlinear feedback controllers or more feedback inputs to estimate their foot placements, instead of the linear control suggested by the linear inverted pendulum model. In chapter VII, the step

strategy control was applied on a power exoskeleton (Indego, Parker-Hannifin, Cleveland, US) to control its leg swing motion. Walking tests with two healthy participants did not show a clear conclusion, but suggested that the step controller was trying to help decelerate the swing motion at the late swing phase.

Finally, in chapter VIII, the trajectory optimization was used to identify the joint impedance properties. Results of the synthetic study showed that relatively close impedance parameters that used to generate the synthetic data can be identified from just joint angle data. Then, a preliminary identification study was done identified the ankle joint impedance properties of two participants at two walking speeds and showed consistent results.

9.1 Future Perspective

The complex motion controllers that can explain long duration movements under random perturbation conditions preferable, compared to the simple controllers that can only explain specific short motions, since they can make assistive devices smarter in handing complex conditions. The studies in this dissertation explored a method that can help achieve this goal. Even though the trajectory optimization with direct collocation can identify complex nonlinear controllers from long duration motion data, limitations exist that prevented us getting more promising results. The identification of human movement control will be more useful if these limitations can be overcome in future studies.

A main limitation is that, in all identification studies in this dissertation, the identified results were limited by the predefined structures of the identifying controllers. Although the parameters in these predefined controllers can be optimized, their control properties cannot beyond the defined control structure. For instance, a predefined linear feedback controller can never generate a nonlinear relationship with any control gains. We have tried to define and identify more general nonlinear controllers, such as neural network controllers. However, the size (hidden layers and nodes) of them cannot be very large, for two reasons. First, large size neural network controllers can largely increase the computation time. Second,

we don't want to have over-fitting. Another drawback of the neural network controllers is that it is hard to interpret the physical meanings of the optimized weights.

One possible way to solve this issue is to describe motion controllers as lookup tables, in which the discrete data nodes describe the relationship between the control inputs and outputs. The motion controller identification can be defined to identify these discrete data nodes. Taking the foot placement controller as an example, the control structure of it was defined that the desired foot placement is proportional to pelvis position and velocity and the proportional gains were constant. To break this control structure, we can just assume that the relationship between the desired foot placement and the pelvis position and velocity is a 2 dimensional lookup table. Value between the discrete data nodes can be calculated using linear or spline interpolation. Theoretically, this lookup table can describe any type of controllers, including linear and nonlinear. Comparing to the neural network controllers, the physical meaning of the lookup table controllers can also be easily interpreted. One difficulty of this idea is to make sure that the lookup table controller is continuous and the continuous derivative can be obtained, because this is required for the gradient-based trajectory optimization approach.

The second limitation is that some of the identified controllers in this dissertation will need to be adjusted before applying to assistive devices, such as exoskeletons and prostheses. One main reason is that these controllers are torque controllers which are strongly correlated with the dynamic property of the studying target. The dynamic property of human with exoskeleton or amputee with prosthesis is different from the dynamic property of healthy humans. Therefore, the controllers identified from healthy human movements cannot be directly used to control these devices. One way to solve this issue is to include assistive devices inside the identification process. This requires accurate dynamic models of these assistive devices, which are not extremely hard to get. The dynamic properties of them can either be identified from operation data or calculated from the design files. Considering that controller identification could become an integral part of the controller design

of assistive devices as computer power increases, accurate dynamic properties of the user will be needed also.

9.2 REFERENCES

[1] S. Park, F. B. Horak, and A. D. Kuo, "Postural feedback responses scale with biomechanical constraints in human standing," *Experimental Brain Research*, vol. 154, no. 4, pp. 417–427, 2004.

[2] A. D. Goodworth and R. J. Peterka, "Identifying mechanisms of stance control: a single stimulus multiple output model-fit approach," *Journal of Neuroscience Methods*, vol. 296, pp. 44–56, 2018.

[3] H. Wang and A. J. van den Bogert, "Identification of the human postural control system through stochastic trajectory optimization," *Journal of Neuroscience Methods*, p. 108580, 2020.

[4] J. K. Moore, S. K. Hnat, and A. J. van den Bogert, "An elaborate data set on human gait and the effect of mechanical perturbations," *PeerJ*, vol. 3, p. e918, 2015.

APPENDIX A: Human Standing Balance Model

The system model of human standing balance includes two components: human body dynamic model and the postural feedback controller (figure 20). The human body was simplified to a two-link pendulum in the standing balance tasks. Its standing plate is a movable base where the displacement perturbation was applied. The dynamic equation of the human model is:

$$\begin{bmatrix} (I_L + I_T + d_L^2 \cdot m_L + m_T \cdot (d_T^2 + 2 d_T l_L cos(\theta_h) + l_L^2)) & (I_T + d_T \cdot m_T \cdot (d_T + l_L cos(\theta_h))) \\ (I_T + d_T m_T \cdot (d_T + l_L \cdot cos(\theta_h))) & (I_T + d_T^2 \cdot m_T) \end{bmatrix} \begin{bmatrix} \ddot{\theta}_a \\ \ddot{\theta}_h \end{bmatrix}$$
$$+ \begin{bmatrix} d_T \cdot l_L \cdot m_T \cdot \dot{\theta_a}^2 sin(\theta_h) - d_T l_L \cdot m_T \cdot (\dot{\theta_a} + \dot{\theta_h})^2 \cdot sin(\theta_h) \\ d_T \cdot l_L \cdot m_T \cdot \dot{\theta_a}^2 \cdot sin(\theta_h) \end{bmatrix}$$
$$+ \begin{bmatrix} -d_L \cdot g m_L sin(\theta_a) - d_T \cdot g \cdot m_T \cdot sin(\theta_a + \theta_h) \\ -d_T \cdot g \cdot m_T \cdot sin(\theta_a + \theta_h) \end{bmatrix}$$
$$+ \begin{bmatrix} d_L \cdot m_L \cdot cos(\theta_a) + d_T \cdot m_T \cdot cos(\theta_a + \theta_h) + l_L \cdot m_T \cdot cos(\theta_a) \\ d_T \cdot m_T \cdot cos(\theta_a + \theta_h) \end{bmatrix} \cdot a$$
$$= \begin{bmatrix} \tau_a \\ \tau_h \end{bmatrix} \tag{1}$$

where. θ_a and θ_h represent the ankle and hip joint angles, respectively; l_L represents the length of leg; m_L and m_T represent the masses of leg and trunk; d_L and d_T represent the center of mass location in leg and trunk; τ_a and τ_h represent the joint torques at ankle and hip joints; g is the gravity; a is the acceleration of the standing plate due to external perturbation.

In the identification study, the joint torque τ_a and τ_h were assumed to be generated by state feedback controllers:

$$\begin{bmatrix} \tau_a \\ \tau_h \end{bmatrix} = \begin{bmatrix} f_a(\theta_a, \theta_h, \dot{\theta_a}, \dot{\theta_h}, P_a) \\ f_h(\theta_a, \theta_h, \dot{\theta_a}, \dot{\theta_h}, P_h) \end{bmatrix} \tag{2}$$

where, f_a and f_h are the control equations of the ankle and hip joints; P_a and P_h represent the control gains inside the ankle and hip controllers.

By putting the state feedback controller into the equation 1, the closed-loop dynamic model of the human standing balance system can be described in the format:

$$M(q) \cdot \ddot{q} + C(q, \dot{q}) + G(q) + D(q, a) - F(q, \dot{q}, P) = 0 \tag{3}$$

where, $q = [\theta_a, \theta_h]$ includes the joint angles of the system; $M(q)$ is the mass matrix; $C(q, \dot{q})$ is the col force term; $G(q)$ is the gravity term; $D(q, a)$ is the joint torque term that caused by mechanical perturbation; $F(q, \dot{q}, P)$ is the joint state feedback control term.

In trajectory optimizations, this dynamic equation was implemented as a equality constraint. A more generalized format of the system dynamics can be wrote as:

$$f(x, \dot{(x)}, P, a) = 0 \tag{4}$$

where $x = [q, \dot{q}]$ represents the system state.

APPENDIX B: Identified Control Gains in Stochastic Trajectory Optimization

This appendix includes the gains and eigenvalue distributions of identified controllers in both deterministic and stochastic environments.

Identified control gains of PD and FPD control structures are shown in table XIII and XIV. Weights of neural network controller is not shown here, since they do not have a realistic meaning. Eigenvalue distributions of the identified PD and FPD controllers are shown in table XV and XVI. Eigenvalues are calculated at the neutral pose (standing straight) which is close to the close-loop system equilibrium point. The eigenvalues of the neural network controllers are not shown either, since eigenvalue at one point does demonstrate stability for nonlinear systems. All proportional gains Kp shown below have a unit of Nm/rad. All derivative gains Kd shown blow have a unit of Nm $\cdot s/rad. All reference angles$ ref $have a unit of rad. In the Table II (FPD controllers), foot$ xy $after$ Kp and means a proportional gain that use the feedback information of hip to the control target of ankle. Experimental data, identification code, and related results were included in a public GitHub repository `https://github.com/HuaweiWang/Stochastic_Paper`.

Table XIII: Identified control parameters in the PD control structure.

	DET	STO2	STO3	STO4
$Kp_{,ankle}$	883.80 $\pm$ 0.08	766.04 $\pm$ 0.00	972.25 $\pm$ 1.84	970.91 $\pm$ 1.52
$Kd_{,ankle}$	18.33 $\pm$ 0.01	20.33 $\pm$ 0.00	29.68 $\pm$ 1.25	30.23 $\pm$ 1.12
$Kp_{,hip}$	222.05 $\pm$ 0.01	224.24 $\pm$ 0.00	236.58 $\pm$ 0.57	236.94 $\pm$ 0.58
$Kd_{,hip}$	8.99 $\pm$ 0.00	7.84 $\pm$ 0.00	10.57 $\pm$ 0.03	10.56 $\pm$ 0.03
$Ref_{,ankle}$	0.0014 $\pm$ 0.00	0.0026 $\pm$ 0.00	0.0007 $\pm$ 0.00	0.0007 $\pm$ 0.00
$Ref_{,hip}$	-0.0005 $\pm$ 0.00	-0.0006 $\pm$ 0.00	-0.0015 $\pm$ 0.00	-0.0016 $\pm$ 0.00

Table XIV: Identified control gains in the FPD control structure.

	DET	STO2	STO3	STO4
$Kp_{,aa}$	341.49 ± 0.57	431.78 ± 5.17	454.75 ± 37.77	453.08 ± 34.30
$Kp_{,ah}$	412.23 ± 0.47	336.78 ± 4.23	318.62 ± 28.74	322.54 ± 27.21
$Kd_{,aa}$	68.84 ± 0.10	59.35 ± 0.85	55.29 ± 5.58	56.30 ± 4.86
$Kd_{,ah}$	47.65 ± 0.06	49.07 ± 0.45	50.18 ± 0.89	49.48 ± 0.87
$Kp_{,ha}$	-105.74 ± 0.19	-81.13 ± 2.12	-74.46 ± 11.64	-73.15 ± 10.04
$Kp_{,hh}$	364.04 ± 0.16	339.79 ± 1.24	334.14 ± 9.25	335.36 ± 8.71
$Kd_{,ha}$	19.93 ± 0.04	17.29 ± 0.31	16.15 ± 1.74	16.29 ± 1.44
$Kd_{,hh}$	23.44 ± 0.02	24.09 ± 0.20	24.50 ± 0.34	24.19 ± 0.33
$Ref_{,ankle}$	-0.0005 ± 0.00	0.0000 ± 0.00	0.0000 ± 0.00	0.0000 ± 0.00
$Ref_{,hip}$	-0.0052 ± 0.00	-0.0047 ± 0.00	-0.0046 ± 0.00	-0.0047 ± 0.00

Table XV: Eigenvalue distribution of identified best PD controllers. The best controllers were those with the lowest RMS in each identification problem.

	DET	STO2	STO3	STO4
$Eig1$	-2.344 + 8.717i	-2.151 + 8.529i	-2.940 + 9.115i	-2.949 + 9.118i
$Eig2$	-2.344 -8.717i	-2.151 - 8.529i	-2.940 - 9.115i	-2.949 - 9.118i
$Eig3$	-0.987	-1.273	-0.181 + 0.046i	-0.181 + 0.046i
$Eig4$	0.715	1.032	-0.181 - 0.046i	-0.181 - 0.046i

Table XVI: Eigenvalue distribution of identified best FPD controllers. The best controllers were those with the lowest RMS in each identification problem.

	DET	STO2	STO3	STO4
$Eig1$	-2.097 + 8.550i	-2.092 + 8.539i	-2.091 + 8.535i	-2.083 + 8.529i
$Eig2$	-2.097 - 8.550i	-2.092 - 8.539i	-2.091 - 8.535i	-2.083 - 8.529i
$Eig3$	-1.020	-0.991	-0.981	-0.967
$Eig4$	-0.053	-0.062	-0.061	-0.073

APPENDIX C: Supplementary Materials of the Postural Controller Identification

C.1: Motion Fit of Six Identified Controllers

Motion fit of the identified six types of controllers of participant 3. Top two subplots are the external stimulus signal (standing platform translation). Left subplots are the ankle joint motion fit. Right subplots are the hip joint motion fit. It is clear that the fit got better with the complex increase of the controller types.

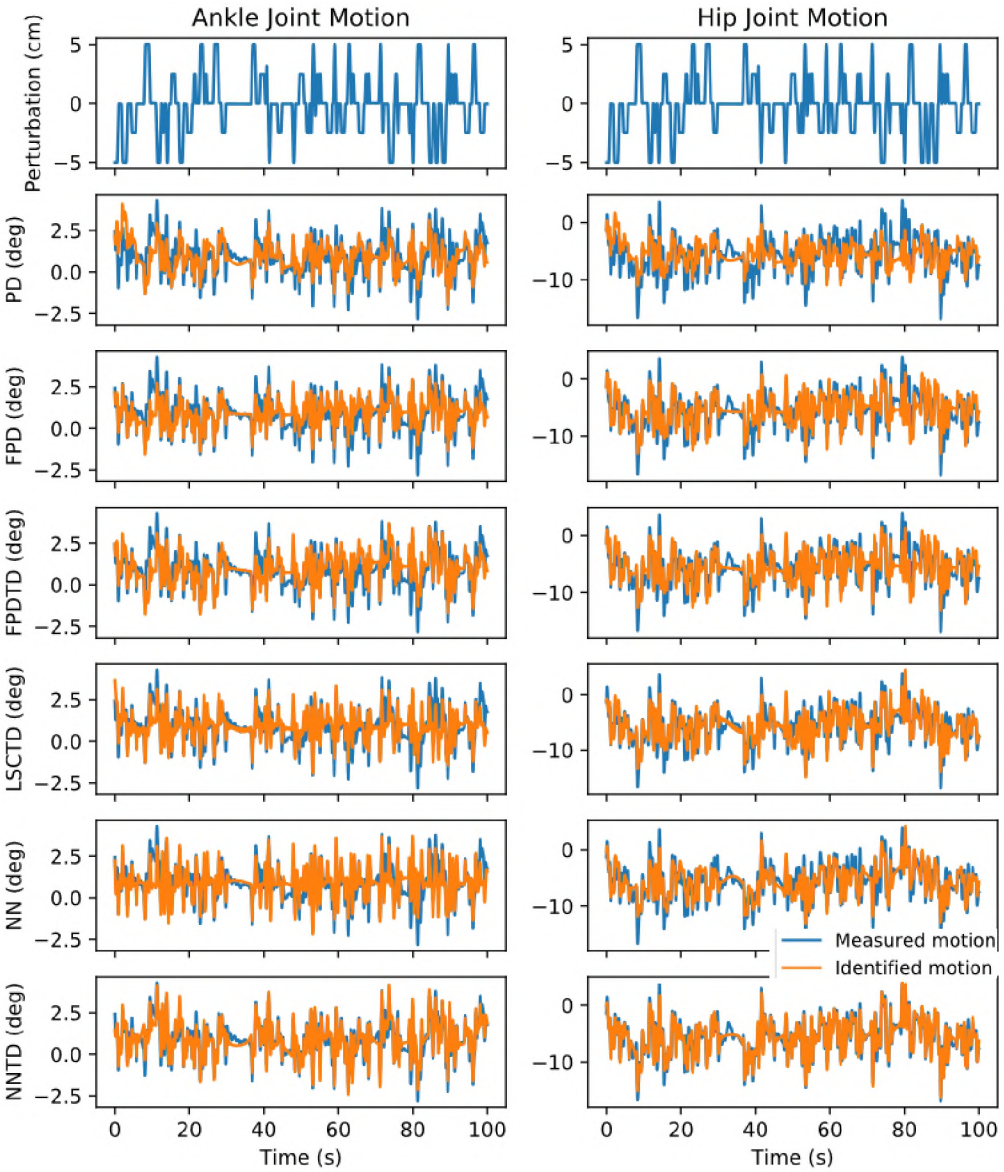

Figure 50: Motion fit of identified six types of controllers of participant 3.

C.2: Eigenvalue Distribution of the identified PD and FPD Controllers

The eigenvalue analysis of the identified PD and FPD controllers are shown in figure 51 and 52, respectively.

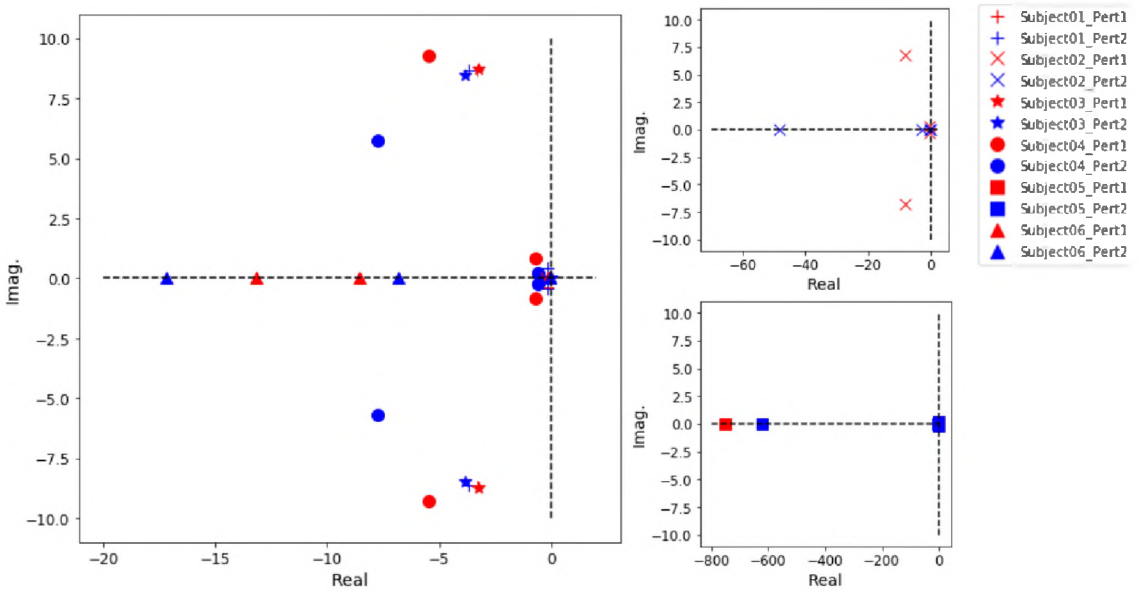

Figure 51: Eigenvalue analysis of the identified PD controllers.

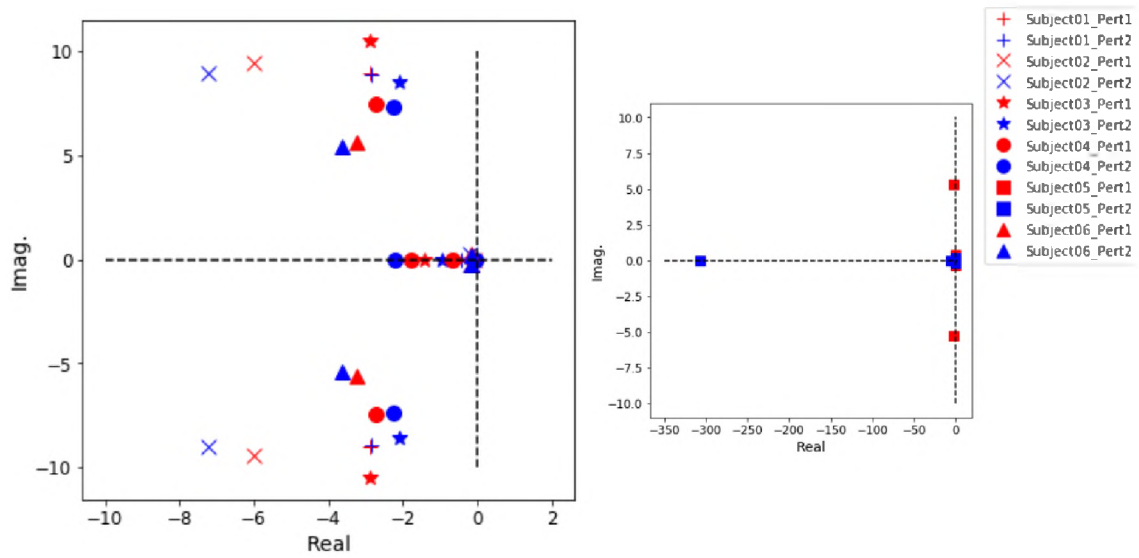

Figure 52: Eigenvalue analysis of the identified FPD controllers.

APPENDIX D: Supplementary Materials of the Foot Placement Identification

The appendix contains the following sections:

- **Section D.1**: lists the dynamic equations of the nonlinear gait model described in Figure 1 of the main manuscript.
- **Section D.2**: provides the information about the normalized polynomial function for the swing phase generator
- **Section D.3**: gives information of the similarity of the identified step control gains among ten optimizations.
- **Section D.4**: provides information of the cross-check.

D.1: Dynamic Equation of the Gait Model

The model used in the foot placement study is a two dimensional seven-link gait model (figure 29), which has been used in many gait studies [1-2]. The dynamic equation of this seven-link gait model was generated using Kane's method through AUTOLEV [3]. The dynamic equation is in the format of general robotics: $M(q) \cdot q + C(q, \dot{q}) \cdot \dot{q} + G(q) = T_{joint} + T_{grf}$, where $q = [x, y, \theta_{trunk}, \theta_{Lhip}, \theta_{Lknee}, \theta_{Lankle}, \theta_{Rhip}, \theta_{Rknee}, \theta_{Rankle}]^T$ represents motion variables of the gait model, including pelvis motion and joint angles; $M(q)$ represents the mass matrix of the gait model and is a function of motion variables q; $C(q, \dot{q})$ represents the Coriolis matrix and is a function of motion variables q and velocity variables $\dot{q}$; $G(q)$ represents the gravity matrix and is a function of motion variables q; T_{joint} represents the external joint torques and T_{grf} represents the effect of ground reaction force applied on the gait model.

The contact model between the gait model and ground is modeled as a nonlinear spring-damper system in the vertical direction [2]. In the horizontal direction, a Coulomb friction

model smoothed by a logistic function was included. The effect of speed perturbation in this gait model is modeled as relative speed changes in the contact model. In each foot, there are two contact points (heel and toe). The vertical and horizontal contact forces are calculated:

$$
\begin{aligned}
F_y &= K_p \cdot d \cdot (1 - K_d \cdot \dot{d}) \\
F_x &= -C_{friction} \cdot F_y \cdot \frac{2}{(1 + e^{\frac{-(v_x - v_{ground})}{v_0}}} - 1
\end{aligned}
\tag{5}
$$

where, F_y is the vertical contact force; F_x is the horizontal contact force; K_p is the stiffness of the ground; $d = \frac{\sqrt{(y^2+\sigma^2)}-y}{2}$ is the constraint vertical position of contact point, which limited that valuable vertical ground reaction force only exist when contact point interact with ground; σ is a small number which controls the smoothness of the constraint vertical position; K_d is the damping property of the ground; $\dot{d}$ is the constraint vertical velocity of the contact point; $C_{friction}$ is the horizontal friction coefficient of the ground; v_x is the horizontal velocity of the contact point; v_{ground} is the horizontal velocity of the ground; v_0 is the parameter which determines how large the difference between contact point velocity and ground velocity when friction force appears.

The contact model was modeled with continuous functions in which gradients always exist. This guaranteed that the plant model in loop optimization can be solved by gradient-based method. Considering that ground contact forces are functions of the position and velocity of contact point which are functions of the gait model state, the dynamic equation of the gait model with ground contact can be written in the format of $M(q)\ddot{q} + C(q,\dot{q})q + G(q) - E(q,\dot{q},v_{ground}) = \tau_{joint}$. In which the contact model is included in the $E(q,\dot{q},v_{ground})$ component.

The step controller identified in this study is a state feedback controller which has the format of $\tau_{joint} = f(P,q,\dot{q})$, in which P represents control parameters. Combine this state

feedback controller with gait model and contact model, the dynamic equation of the closed-loop system can be written as $M(q)\ddot{q} + C(q,\dot{q})\dot{q} + G(q) - E(q,\dot{q},v_{ground}) - f(P,q,\dot{q}) = 0$. In simplification, it can be written in the format of: $F(q,\dot{q},\ddot{q},P,v_{ground}) = 0$.

D.2: Normalized Polynomial Function for the Swing Foot

The swing foot trajectory is described as normalized polynomial functions in both vertical and horizontal directions. The coefficients of the polynomial functions were optimized to fit with the swing paths in the experimental data. For each participant at one walking speed, swing paths from over 500 gait cycles were used to optimize the coefficients. An example swing path from one participant at one walking speed is shown in figure 53. The swing path is relative motion which is relative to the pelvis point.

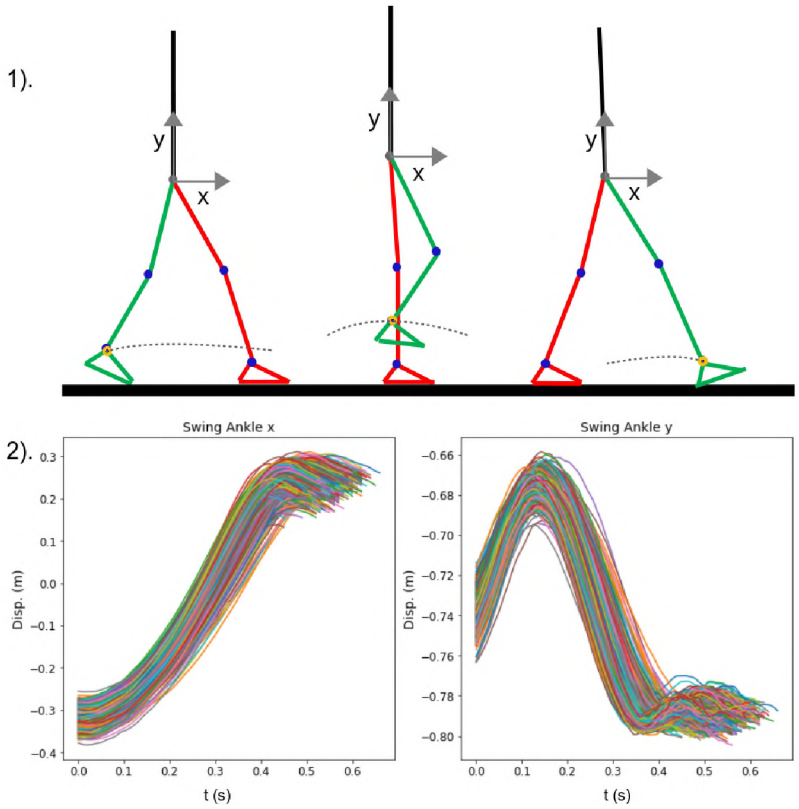

Figure 53: Swing trajectories from the experimental data. Subplot 1) shows the swing trajectory in the swing phase. It starts at the swing starting position and finishing at the touch down point. Subplot 2) shows the swing trajectory shape in the x and y directions over 500 gait cycles. The swing path of the ankle joint is relative to the pelvis position

The optimization problem of the polynomial coefficients is regular optimization problem which is defined in follow:

$$\begin{aligned} &\text{Find coefficients: } A_n \\ &\text{To minimize the objective function: } obj = \sum_{i=1}^{M} \int_{t=0}^{T_i} (f^i_{data}(t) - f^i_{polynomial}(A_n, t))^2 \cdot dt \\ &\text{Subject to: } f^i_{polynomial}(A_n, 0) = f^i_{data}(0), fori = 1, 2, ..., M \\ &\qquad\qquad f^i_{polynomial}(A_n, T) = f^i_{data}(T), fori = 1, 2, ..., M \end{aligned} \tag{6}$$

where, A_n represents coefficients of the polynomial function; M represents the total number of the experimental swing paths; $f^i_{path}(t)$ represents the i^{th} experimental swing path; T_i represents the swing time length for the i^{th} experimental swing path; $f^i_{polynomial}(A_n, t) = \sum_{n=1}^{N} A_n \cdot (f^i_{path}(T) - f^i_{path}(0)) \cdot (\frac{t}{T_i})^n$ represents the path generated by the normalized polynomial function for the i^{th} experimental swing path with the coefficients A_n;

Constraints of the optimization guaranteed that the normalized polynomial function starting and ending with the same values as experimental swing paths. The optimization problem is solved by using the minimize function in python scipy.optimize package [4]. Different orders of the polynomial functions, from first and sixth, were optimized to find the number of orders that holds the best fit. Based on the fitting results, fifth order polynomials are selected for both x and y directions of the swing path. Root-mean-square errors for the different orders of the normalized polynomial functions with experimental data and one example of the swing path fit are shown in figure 54.

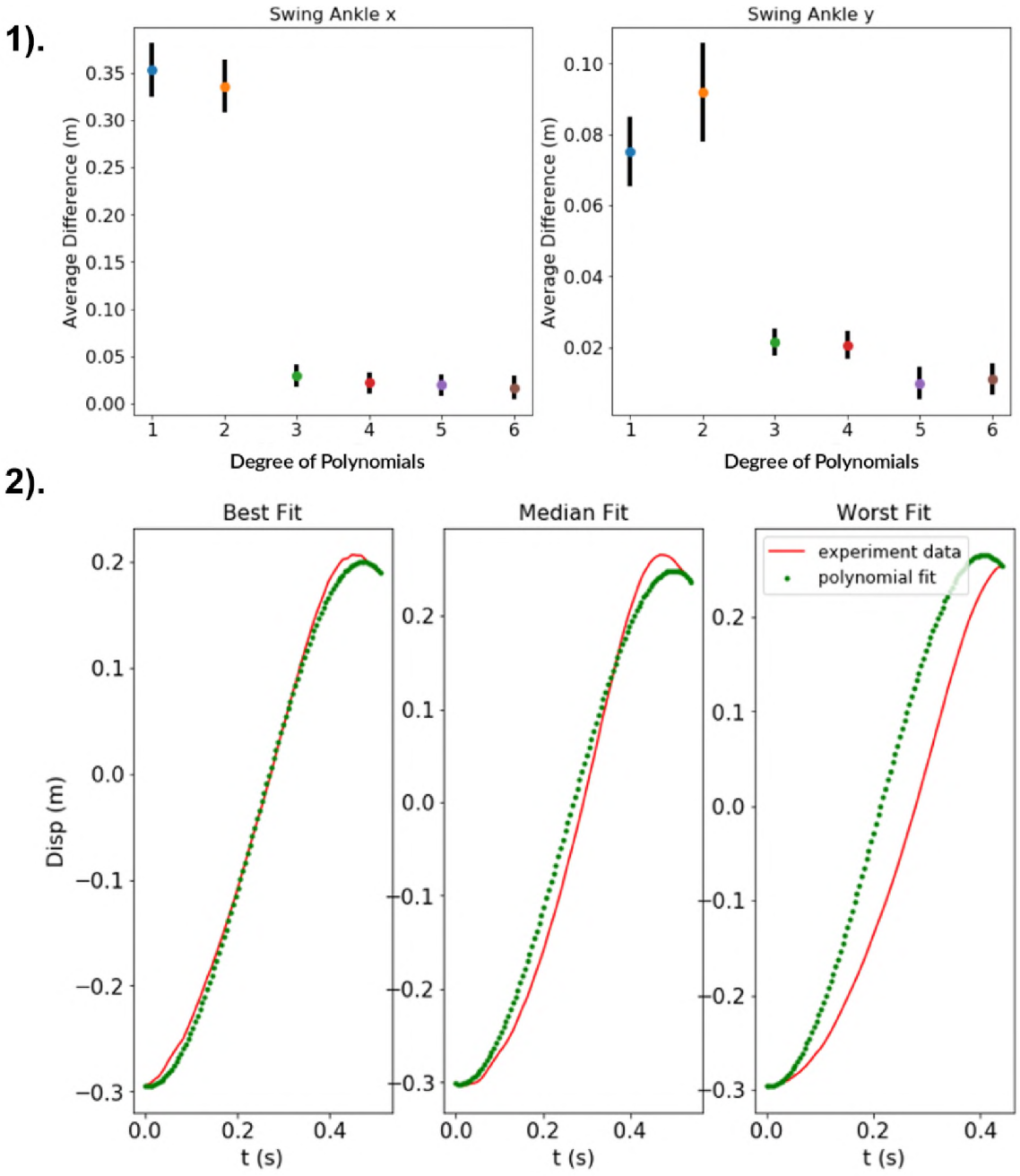

Figure 54: Fits between the optimized polynomial functions and the experimental swing paths. Subplot 1) shows the means and standard deviation of the difference between the polynomial functions and experimental data. The fit improves as the degree of polynomial functions increases. Subplot 2) shows one example of the fit for one optimized polynomial function. In which, the best, median, and worst fits in over 500 experimental swing trajectories are shown.

D.3: Similarity of the Identified Control Gains among Ten Optimizations

To increase the confidence that the identified step strategies are not a bad local optimum

result, the number of results similar to the best result out of the ten optimizations were counted in each identification problem (table XVII). The similar best results were defined within 5% variation when comparing the root-mean-square (RMS) of the difference between the identified trajectories and the experimental data. In most identification problems, the similar best results were found more than once, which suggests that the identified step controllers are more likely not the bad local solutions. The standard deviation of the control gains in the corresponding best similar results are shown in table XVIII and table XIX. In general, they are around or less than 5%, which means that the identified step strategies among the similar best fits are similar. This, in another aspect, suggests that the identified step controllers are good results.

Table XVII: The number of similar best results in each identification problem. In most of the identification problems, similar best results were found more than once. Only six out of twenty-seven identification problems found one similar best result. There are two identification problems which were not successful in finding feasible results.

Speed	M1	M2	M3	M4	M5	F1	F2	F3	F4
0.8 m/s	7	5	5	1	1	4	2	2	1
1.2 m/s	4	2	3	9	3	4	8	2	0
1.6 m/s	7	2	1	8	2	2	1	0	1

Table XVIII: The standard deviation of the similar best results as a percentage of the averaged position feedback gains. For the identification problems which have no solution, or only one best result, there is no standard deviation and 'N/A' was wrote.

Speed	M1	M2	M3	M4	M5	F1	F2	F3	F4
0.8 m/s	2.34%	2.44%	3.56%	N/A	N/A	5.34%	4.21%	2.47%	N/A
1.2 m/s	0.69%	0.45%	3.80%	2.56%	1.17%	3.39%	1.66%	1.58%	N/A
1.6 m/s	1.73%	1.82%	N/A	1.53%	0.16%	0.43%	N/A	N/A	N/A%

Table XIX: The standard deviation of the similar best results as a percentage of the averaged velocity feedback gains. For the identification problems which have no solution, or only one best result, there is no standard deviation and 'N/A' was wrote.

Speed	M1	M2	M3	M4	M5	F1	F2	F3	F4
0.8 m/s	0.69%	0.71%	0.67%	N/A	N/A	0.14%	0.13%	0.49%	N/A
1.2 m/s	0.45%	0.54%	1.93%	1.97%	1.68%	0.30%	1.62%	1.81%	N/A
1.6 m/s	0.60%	0.34%	N/A	1.29%	0.30%	0.65%	N/A	N/A	N/A%

D.4: Cross Check of the Identified Control Gains

To make sure that ten seconds experimental data is sufficient to identify the two feedback gains in the step controllers, cross check of the identified control gains was done. Beside the ten seconds perturbed walking data used in the identification in the main manuscript, we also identified the step strategy on another ten- and twenty-seconds perturbed walking data, which did not show significant differences with the results on the ten seconds data (figure 55). Using a significance level of $\alpha = 0.05$, one-way ANOVA tests showed that there is no significant difference between the three periods. Tests on the gains of different speeds showed that there is significant difference between three speeds. Since joint motion is the reproducing target in this research, instead of the foot placement, ten seconds perturbed walking data contains enough information for identifying the two feedback gains.

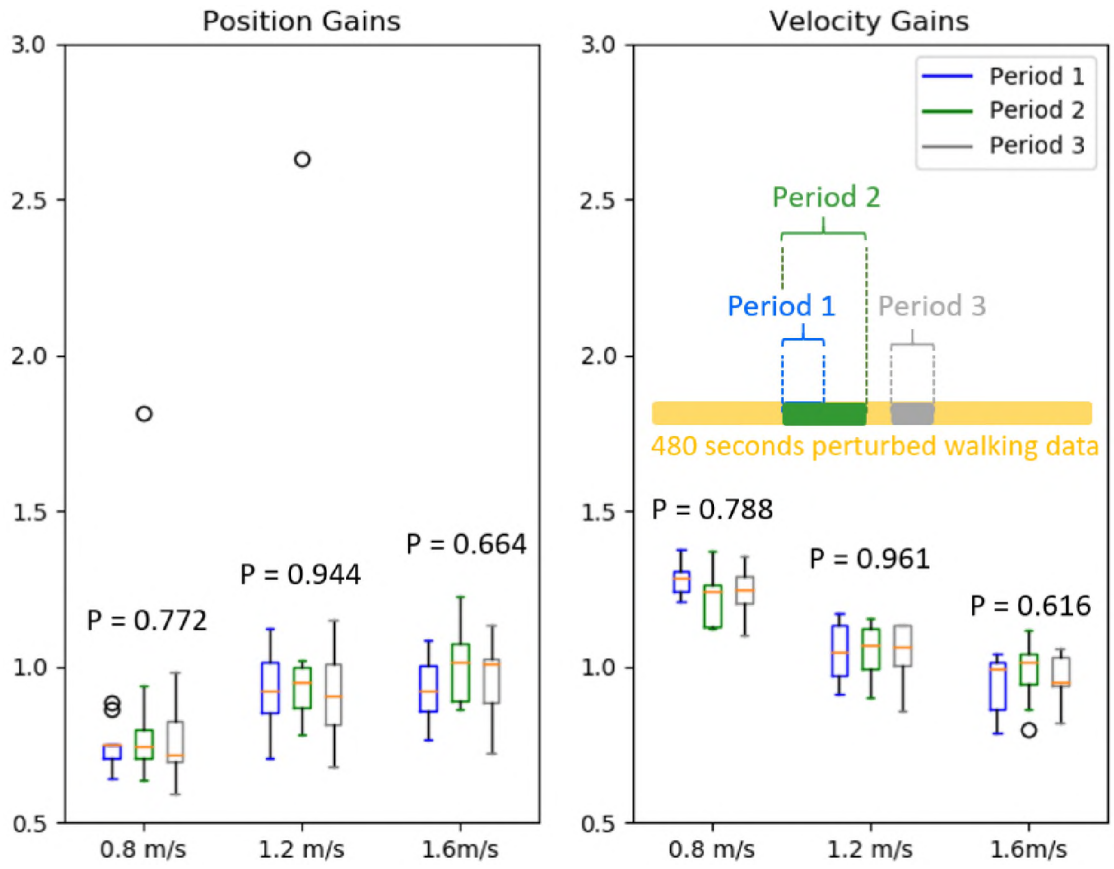

Figure 55: Comparison of the identified control gains among three periods of experimental data. In which, period 1 is the 10 seconds experimental data mentioned in the Result section; period 2 is the 20 seconds experimental data which includes the period 1 data; period 3 is another 10 seconds experimental data away from the period 1 and 2. One-way ANOVA tests show that there is no significant difference of the identified control gains ($P > 0.05$) among the three data periods. Two-way ANOVA tests indicate that there is significant difference of the identified control gains ($P = 0.015 < 0.05$ for position gain, $P = 0.00878 < 0.05$ for velocity gains) among the three speeds.

Reference

[1]. Geyer, H. and Herr, H., 2010. A muscle-reflex model that encodes principles of legged mechanics produces human walking dynamics and muscle activities. *IEEE Transactions on neural systems and rehabilitation engineering*, 18(3), pp.263-273.

[2]. Ackermann, M. and Van den Bogert, A.J., 2010. Optimality principles for model-based prediction of human gait. *Journal of biomechanics*, 43(6), pp.1055-1060.

[3]. Levinson, D.A. and Kane, T.R., 1990. AUTOLEV—a new approach to multibody

dynamics. In Multibody systems handbook (pp. 81-102). *Springer*, Berlin, Heidelberg.

[4]. Jones, E., Oliphant, T. and Peterson, P., 2001. SciPy: Open source scientific tools for Python. *http://www.scipy.org/*

[5]. Kelly, M., 2017. An introduction to trajectory optimization: How to do your own direct collocation. *SIAM Review*, 59(4), pp.849-904.

[6]. Wächter, A. and Biegler, L.T., 2006. On the implementation of an interior-point filter line-search algorithm for large-scale nonlinear programming. *Mathematical programming*, 106(1), pp.25-57.

APPENDIX E: Supplementary Materials of the Indego Test

E.1: Swing Path Polynomial Function of Participant One

Recorded data of the walking with the passive Indego exoskeleton on the first day was used to personalize the foot placement estimator and the path planning components.

Two scaled polynomial functions were used to describe participant's swing motion in x and y direction, respectively. Coefficients of each polynomial function were optimized to minimize the difference between its output and the swing motion data. Taking participant two as an example, the optimized polynomial functions are:

$$f_x(P_{sta,x}, P_{des,x}, T_s, t) = P_{sta,x} + 0.1795 \cdot (P_{des,x} - P_{sta,x}) \cdot (\frac{t}{T_s}) + 2.4645 \cdot (P_{des,x} - P_{sta,x}) \cdot (\frac{t}{T_s})^2 - 1.6440 \cdot (P_{des,x} - P_{sta,x}) \cdot (\frac{t}{T_s})^3 \quad (7)$$

$$f_y(P_{sta,y}, P_{des,y}, T_s, t) = P_{sta,y} - 26.8977 \cdot (P_{des,y} - P_{sta,y}) \cdot (\frac{t}{T_s}) - 73.8179 \cdot (P_{des,y} - P_{sta,y}) \cdot (\frac{t}{T_s})^2 - 65.9014 \cdot (P_{des,y} - P_{sta,y}) \cdot (\frac{t}{T_s})^3 + 19.4716 \cdot (P_{des,y} - P_{sta,y}) \cdot (\frac{t}{T_s})^4 + 0.5186 \cdot (P_{des,y} - P_{sta,y}) \cdot (\frac{t}{T_s})^5 \quad (8)$$

where, $P_{sta,x}$ and $P_{sta,y}$ are the swing foot locations in x and y directions at the starting swing time; $P_{des,x}$ and $P_{des,y}$ are the estimated foot locations in x and y directions at the ending swing time; T_s is the total swing time (0.6 second); t is the current swing time point;

Third order polynomial function was used to describe the swing motion in the x direction. Fifth order polynomial function was used to describe the swing motion in the y

direction. With the optimized coefficients, x direction polynomial function was able to describe the second participant's swing motion roughly good (figure 56).

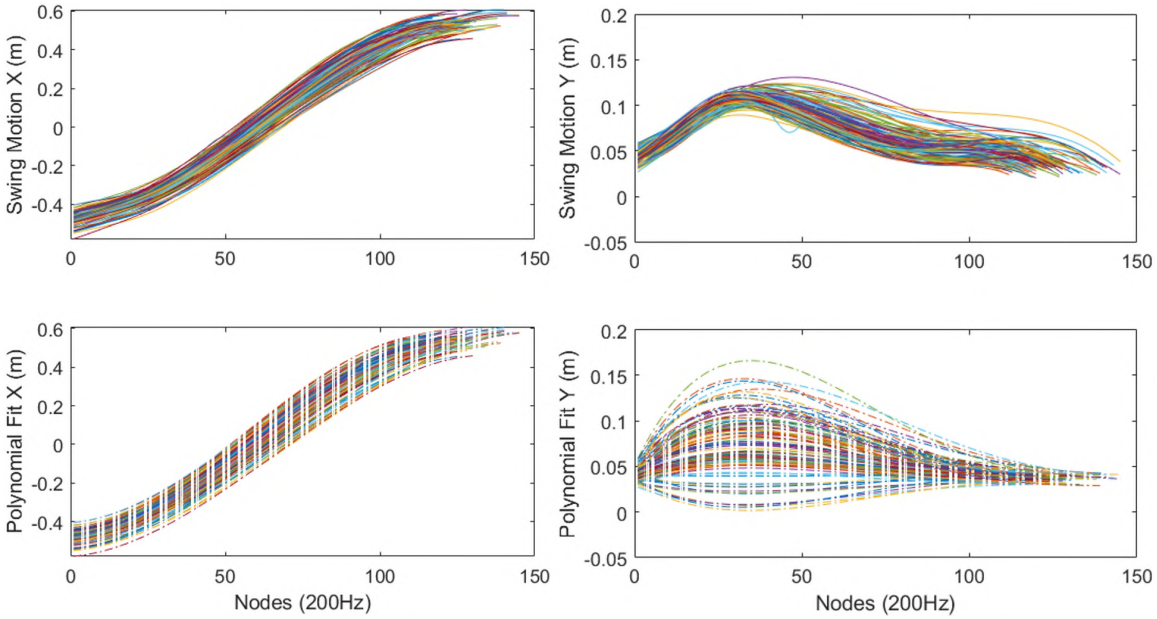

Figure 56: Polynomial fit of the swing motion in the x and y direction, respectively.

E.2: The Foot Placement Control Gains of Participant One

With the optimized polynomial functions, gains inside the foot placement estimator was manually tuned to make the swing path smooth and reach the actual landing location in the walking data (figure 57). For the second participant, gains that multiple to pelvis position and velocity (equation 7.1) were both set as 1.4.

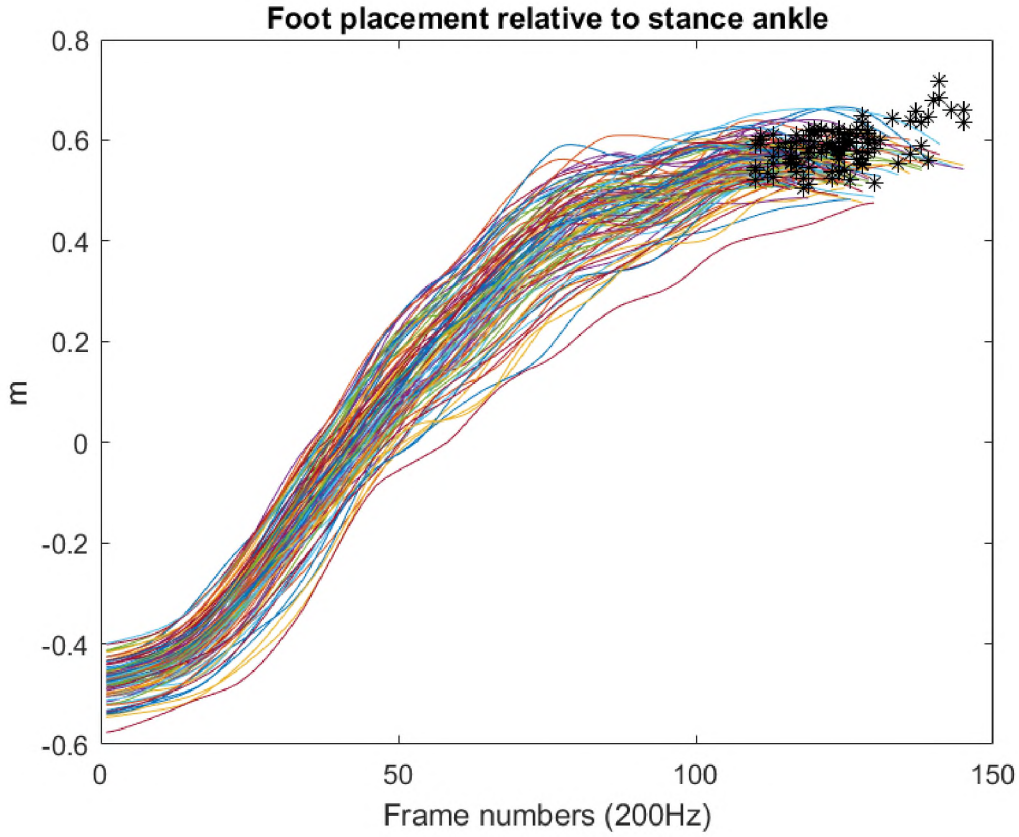

Figure 57: Estimated swing motion with selected foot placement control gains of participant one.

E.3: Swing Path Polynomial Function of Participant Two

Recorded data of the walking with the passive Indego exoskeleton on the first day was used to personalize the foot placement estimator and the path planning components.

Two scaled polynomial functions were used to describe participant's swing motion in x and y direction, respectively. Coefficients of each polynomial function were optimized to minimize the difference between its output and the swing motion data. Taking participant two as an example, the optimized polynomial functions are:

$$f_x(P_{sta,x}, P_{des,x}, T_s, t) = P_{sta,x} + 0.3836 \cdot (P_{des,x} - P_{sta,x}) \cdot (\frac{t}{T_s}) + 1.6011 \cdot (P_{des,x} - P_{sta,x}) \cdot (\frac{t}{T_s})^2 - 0.9847 \cdot (P_{des,x} - P_{sta,x}) \cdot (\frac{t}{T_s})^3 \quad (9)$$

$$f_y(P_{sta,y}, P_{des,y}, T_s, t) = P_{sta,y} - 4.8123 \cdot (P_{des,y} - P_{sta,y}) \cdot (\frac{t}{T_s})$$
$$- 19.2268 \cdot (P_{des,y} - P_{sta,y}) \cdot (\frac{t}{T_s})^2 + 107.6261 \cdot (P_{des,y} - P_{sta,y}) \cdot (\frac{t}{T_s})^3$$
$$- 138.1750 \cdot (P_{des,y} - P_{sta,y}) \cdot (\frac{t}{T_s})^4 + 55.5880 \cdot (P_{des,y} - P_{sta,y}) \cdot (\frac{t}{T_s})^5 \quad (10)$$

where, $P_{sta,x}$ and $P_{sta,y}$ are the swing foot locations in x and y directions at the starting swing time; $P_{des,x}$ and $P_{des,y}$ are the estimated foot locations in x and y directions at the ending swing time; T_s is the total swing time (0.6 second); t is the current swing time point;

Third order polynomial function was used to describe the swing motion in the x direction. Fifth order polynomial function was used to describe the swing motion in the y direction. With the optimized coefficients, these two polynomial functions are able to describe the second participant's swing motion roughly good (58).

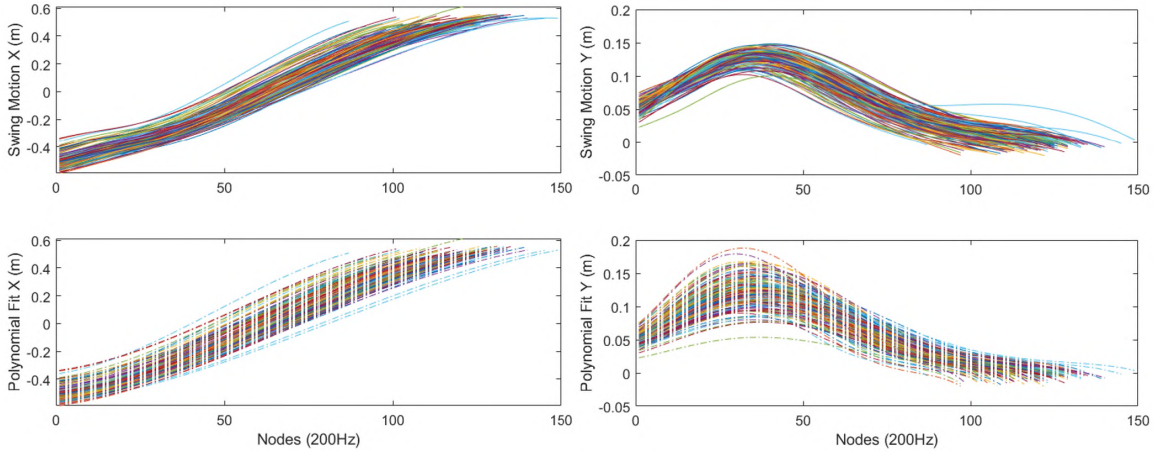

Figure 58: Polynomial fit of the swing motion in the x and y direction, respectively.

E.4: The Foot Placement Control Gains of Participant Two

With the optimized polynomial functions, gains inside the foot placement estimator was manually tuned to make the swing path smooth and reach the actual landing location in the walking data (Fig. 59). For the second participant, gains that multiple to pelvis position

and velocity (Equ. 7.1) were both set as 1.2.

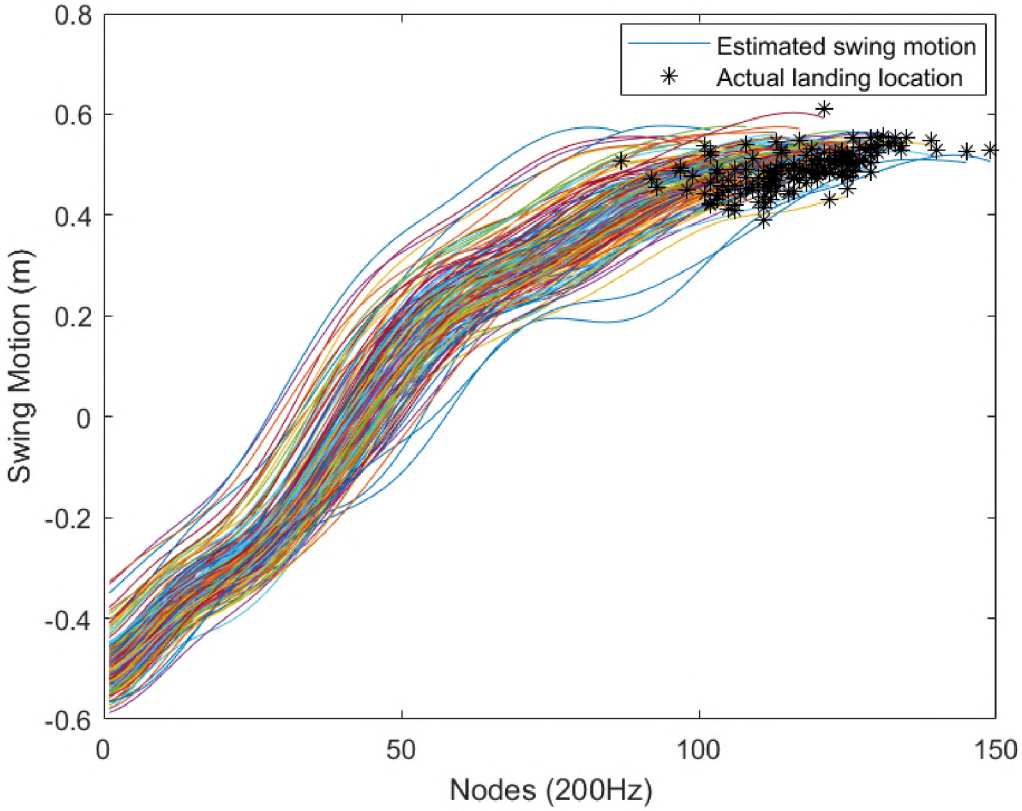

Figure 59: Estimated swing motion with selected foot placement control gains of participant two.

E.5: Test Data of Participant One

Muscle activation of normal walking and walking with passive Indego was shown in figure 60. From these three muscles that were monitored in both conditions, it is clear the passive Indego largely affected the pattern of muscle activations, which is similar to participant two.

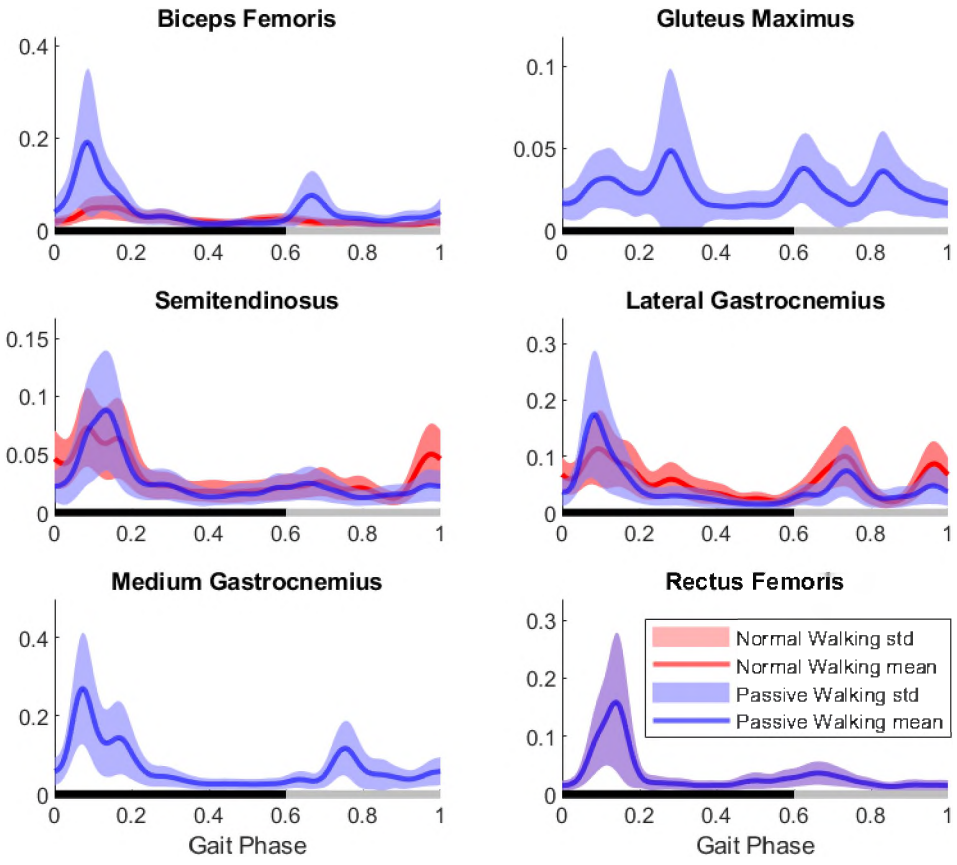

Figure 60: Activation of selected muscles in normal walking and walking wearing passive Indego of participant one. (Please note that Gluteus Maximums, Medium Gastrocnemius, Rectus Femoris were not recorded in the normal walking trial.)

APPENDIX F: Code and Data for this Dissertation

Code used in this dissertation was organized in a public repository on GitHub: `https://github.com/HuaweiWang/Dissertation_Work`.

Data used in this dissertation was uploaded in a public project on Zenodo. The data can be accessed by searching the project number (3767611) on Zenodo.

Merging the code folders and data folders together, theoretically, you can reproduce all the results in this dissertation. Feel free to contact me (huawei.wang.buaa@gmail.com), if you faced issues using this code. I am happy to help you make it work as well as to improve the code repository.